

**IMPACTS OF METEOROLOGICAL PARAMETERS ON SHORT-TERM
METHANE EMISSIONS AND EMISSION MEASUREMENTS FROM
LANDFILLS**

By

Madjid Delkash

A dissertation submitted to the Faculty of the University of Delaware in partial fulfillment of the requirements for the degree of Doctor of Philosophy in Civil Engineering

Summer 2021

© 2021 Madjid Delkash
All Rights Reserved

**IMPACTS OF METEOROLOGICAL PARAMETERS ON SHORT-TERM
METHANE EMISSIONS AND EMISSION MEASUREMENTS FROM
LANDFILLS**

By

Madjid Delkash

Approved: _____
Jack A. Puleo, Ph.D.
Chair of the Department of Civil and Environmental Engineering

Approved: _____
Levi T. Thompson, Ph.D.
Dean of the College of Engineering

Approved: _____
Louis F. Rossi, Ph.D.
Vice Provost for Graduate and Professional Education and
Dean of the Graduate College

I certify that I have read this dissertation and that in my opinion it meets the academic and professional standard required by the University as a dissertation for the degree of Doctor of Philosophy.

Signed: _____
Paul T. Imhoff, Ph.D.
Professor in charge of dissertation

I certify that I have read this dissertation and that in my opinion it meets the academic and professional standard required by the University as a dissertation for the degree of Doctor of Philosophy.

Signed: _____
Daniel K. Cha, Ph.D.
Member of dissertation committee

I certify that I have read this dissertation and that in my opinion it meets the academic and professional standard required by the University as a dissertation for the degree of Doctor of Philosophy.

Signed: _____
David R. Legates, Ph.D.
Member of dissertation committee

I certify that I have read this dissertation and that in my opinion it meets the academic and professional standard required by the University as a dissertation for the degree of Doctor of Philosophy.

Signed: _____
Fotini K. Chow, Ph.D.
Member of dissertation committee

ACKNOWLEDGMENTS

I wholeheartedly appreciate my life advisor, Paul Imhoff, who taught me beyond environmental engineering, taught me to be a better human being for this planet. I acknowledge financial support from the Environmental Research and Education Foundation for this project. I am grateful to Li-COR Bioscience and Dr. Liukang Xu for sharing their Eddy Covariance data from the Southeastern US landfill, and Mr. Roger Green from Waste Management and Dr. Eben Thoma from USEPA for sharing the TDM data from the Southeastern US landfill. Mr. Roger Green provided significant guidance in understanding previous EC and TDM measurements at the Southern US landfill.

TABLE OF CONTENTS

LIST OF TABLES.....	viii
LIST OF FIGURES	x
ABSTRACT.....	xv

Chapter

1	SIGNIFICANCE AND OUTLINE.....	1
2	SHORT-TERM METHANE EMISSIONS DEPENDENCY ON WIND	6
2.1	Introduction.....	6
2.2	Materials and Methods.....	10
2.2.1	Site Description.....	10
2.2.2	Field Emissions Measurements.....	11
2.2.3	Atmospheric Dispersion Modeling	14
2.3	Results and Discussion	19
2.3.1	Field Emissions Measurements.....	19
2.3.2	Comparison of Atmospheric Dispersion Model to Field Data	21
2.3.3	Travel Time.....	24
2.3.4	Testing Hypothesis 1: Homogeneous but Transient Emissions...26	
2.3.5	Testing Hypothesis 2: Heterogeneous but Steady Emissions	32
2.3.6	Testing Hypothesis 3: Misalignment of Tracer	35
2.3.7	Field Emission Correlation with Wind	38
2.4	Conclusions.....	42
3	DIURNAL LANDFILL METHANE FLUX PATTERNS ACROSS DIFFERENT SEASONS AT A LANDFILL IN SOUTHEASTERN US	45
3.1	Introduction.....	45
3.2	Theory	47
3.3	Material and Methods	51
3.3.1	Site Description.....	51
3.3.2	Methane Flux Measurements.....	53

3.3.3	Time Periods of Investigation.....	54
3.3.4	EC Data Filtering.....	57
3.3.5	Correlations Between Methane Flux and Meteorological Parameters.....	59
3.3.6	Statistical Tests for Significance of Correlations.....	62
3.4	Results.....	62
3.4.1	Meteorological Parameter Dependency.....	62
3.4.2	Pressure-Induced Flux.....	65
3.4.3	Wind-Induced Flux.....	68
3.4.4	Buoyancy-induced flux.....	71
3.5	Implications.....	75
3.5.1	Validity of WRF Methane Flux Equation.....	75
3.5.2	Diurnal Variations of Methane Flux.....	77
3.5.3	Preferred Times of Day for Measurement.....	82
3.6	Conclusions.....	85
4	DEPENDENCY OF THE TRACER DISPEPRSION METHOD ACCURACY ON ENVIRONMENTAL PARAMETERS FOR LANDFILL GAS EMISSION ESTIMATION.....	86
4.1	Introduction.....	86
4.2	Method.....	91
4.2.1	Tracer Dispersion Method.....	91
4.2.2	TDM Field Deployments.....	92
4.2.3	Meteorological Parameters.....	93
4.2.4	Methane Emission Quantification.....	94
4.2.5	Method Quality Indicators.....	96
4.2.5.1	Correlation of plumes.....	96
4.2.5.2	Distinguishing signal from noise.....	96
4.2.5.3	Emission Rate Difference.....	97
4.2.6	Correlation Analysis.....	98
4.3	Results and discussion.....	105
4.3.1	TDM Mobile Approach.....	105
4.3.1.1	Wind speed.....	107

4.3.1.2	Wind direction standard deviation	111
4.3.1.3	Diurnal variations of the filtering parameters.....	113
4.3.1.4	Seasonal variations of the TDM filtering parameters.	116
4.3.2	TDM Stationary Approach	119
4.3.3	Comparison between the mobile and stationary approaches	120
4.4	Implications and Conclusions	122
5	FUTURE WORK.....	126
6	REFERENCES	130

Appendix

A.	SHORT-TERM METHANE EMISSIONS DEPENDENCY ON WIND.....	138
B.	DIRNAL LANDFILL METHANE FLUX PATTERNS ACROSS DIFFERENT SEASONS AT A LANDFILL IN SOUTHEASTERN US	142
C.	DEPENDENCY OF THE TRACER DISPERSION METHOD ACCURACY ON ENVIRONMENTAL PARAMETERS FOR LANDFILL GAS EMISSION ESTIMATION	155
D.	PUBLICATION LIST	175
E.	PRESENTATION LIST	176
F.	PERMISSION FROM PUBLISHERS	177

LIST OF TABLES

Table 2.1	Linear regression of normalized methane emission versus normalized wind speed for three simulation pairs with and without data filtering.36
Table 3.1	Correlation coefficients between the meteorological parameters (P = atmospheric pressure; T = air temperature; u = shear velocity; dP/dt= temporal variations of atmospheric pressure) for different measurement periods. The standard errors of the daily-average correlation coefficients are shown with \pm values.....63
Table 3.2	Correlation coefficient of each meteorological parameter with methane flux under different atmospheric conditions and time periods. The N is the number of days during each period that have either unstable or neutral atmospheric conditions. Fraction is the fraction of measurement days in the 7 or 8 day period where $R > 0.5$. Note that R is only calculated if at least six data points are available.66
Table 3.3	Diurnal variations of methane flux in the studied periods: June 2012, December 2012, and February 2013.....78
Table 4.1	Case studies: Measurement locations and emissions data102
Table 4.2	Description of the Pearson correlation coefficients between TDM filtering parameters and meteorological parameters.....104
Table C.1	Definition of ASI155
Table C.2	Correlation coefficients between the meteorological parameters.....157
Table C.3	Results of Pearson correlations of Case I for different meteorological parameter classifications. The description about classification is found above. The selected classifications are highlighted.159

Table C.4	Pearson correlations between filtering parameter and the investigated meteorological parameter for the two selected classifications in Case study I: 011 corresponds to lower wind direction variations and turbulence intensity, and wind speed is the investigated parameter; 201 corresponds to higher wind speeds and lower turbulence intensity, and WDS is the investigated parameter. The selected pairs are highlighted.	160
-----------	---	-----

LIST OF FIGURES

Figure 2.1	Aerial view of Sandtown Landfill (Sandtown, DE) illustrating emissions locations for simulations (CF1, CF2, VF1, VF2 and 3Pts) and tracers in field test. The downwind gas sampling location is also shown where measurements were taken at 2.5 and 85 m AGL.....	11
Figure 2.2	Field methane emissions (equation (2.1)) from individual concentrations at 2.5 (orange) and 85 m AGL (blue) at downwind measurement location (Figure 2.1). Each elevation had seven measurement periods. Measured methane emissions were zero when gas concentrations were below background; gaps between measurements correspond to switching sampling tubing between 2.5 and 85 m heights.....	20
Figure 2.3	Times-series of observed and modeled surface wind speed (top) and direction (bottom). Solid lines are model results from the 25 m grid; dash-dotted lines are observations from surface station	23
Figure 2.4	Normalized tracer concentration at downwind measurement location (see Figure 2.1). Blue solid and red dashed lines are for model (3Pts) and field data, respectively, at 2.5 and 85 m AGL. Gaps between field data correspond to switching sample tubing between 2.5 and 85 m heights. Gaps between field data correspond to switching sample tubing between 2.5 and 85 m heights.	23
Figure 2.5	Travel time from landfill to downwind measurement location at 2.5 m AGL during the 2-h field test. Travel time varies with wind conditions and was computed at different temporal resolutions using CF1 simulation.....	25
Figure 2.6	Numerical simulation output. Normalized actual emissions (VF2) and 2 s downwind emissions measurements (VF2/CF1) versus time at 2.5 m AGL with no travel time correction.....	27
Figure 2.7	Normalized emissions calculated with TDM using 1-min data from simulation pair VF2/CF1 at 2.5 and 85 m AGL at measurement location in Figure 1. Emissions plotted versus normalized wind speed on landfill surface with no data filtering. 95% confidence intervals on individual data points are so small as not to be visible.....	30

Figure 2.8	Same as Figure 2.7 except using data filtering: R^2 and second derivative of wind velocity criteria.....	31
Figure 2.9	Normalized emissions calculated with TDM using 1-min data from simulation pair VF1/CF1 at 2.5 and 85 m AGL at measurement location in Figure 2.1. Emissions plotted versus normalized wind speed on landfill surface with data filtering: R^2 and second derivative of wind velocity criteria. 95% confidence intervals on individual data points are so small as not to be visible.....	34
Figure 2.10	Normalized emissions calculated with TDM using 1-min data from simulation pair CF1/3Pts at 2.5 and 85 m AGL at measurement location in Figure 2.1. Emissions plotted versus normalized wind speed on landfill surface with data filtering: R^2 and second derivative of wind velocity criteria. 95% confidence intervals on individual data points are so small as not to be visible.....	37
Figure 2.11	Normalized emissions calculated with TDM using 1-min field data at 2.5 and 85 m AGL at measurement location in Figure 2.1. Emissions plotted versus normalized wind speed on landfill surface with data filtering: R^2 and second derivative of wind velocity criteria.	40
Figure 3.1	Topography of the landfill at the nearest date to each test period. The date of surveying is shown bottom left of each map. The EC tower location is displayed by yellow triangle.	52
Figure 3.2	Temporal variations of daily-averaged T obtained from EC tower.....	54
Figure 3.3	Temporal variations of daily-averaged volumetric soil moisture (at 10 cm depth) between June 2012 and February 2013 measured at three nearest weather stations (each about 47 km distance from the landfill). The black boxes indicate the three studied periods.	55
Figure 3.4	Daily average volumetric water content at 10 cm depth between June 2012 and February 2013 measured at three nearest weather stations (each about 47 km distance from the landfill).	56

Figure 3.5	Scheme of field measurements. The EC tower is shown with a yellow triangle. (a) Illustration of the 90° filter for wind direction. The transparent rectangle shows the area of focus in the other figures. Locations of $x50$ are within blue shaded regions for (b) June 2012; (c) December 2012; and (d) February 2013. The blue arrows indicate the distance between the EC tower location and $x50$ locations, while white numbers are Julian days associated with the EC measurements that occur in each blue region. The error tolerance of these illustrations is less than 10 m.....	58
Figure 3.6	Temporal variations of the normalized 30-min averaged meteorological parameter $X_i - X_{min}X_{max} - X_{min}$ between June 19 and 25, 2012. Air pressure is detrended.....	64
Figure 3.7	Temporal variations of methane flux measured by the EC tower versus $u * u$ under neutral atmosphere for February 2013.	70
Figure 3.8	Variations of methane flux measured by the EC tower with T under unstable atmosphere for June 2012.....	73
Figure 3.9	Temporal variations of TDM flux versus T for March 8, 2013.....	75
Figure 3.10	Examples of diurnal flux variations measured by the TDM at the Southeastern US landfill. The dataset is filtered with $R^2 > 0.8$ between methane and tracer concentrations. The days are categorized into two plots to clearly display diurnal variations. The data with lower emissions in 2012 are depicted in the left plot and the higher emission data during 2013 are shown in the right plot.	80
Figure 3.11	Normalized variations of the weekly-averaged flux measured by the EC tower during the three measurement periods. Black dashed line shows the average of normalized flux measured by the EC tower during each period. Blue shading displays the measurement window typical for TDM measurements at this landfill. Dashed red lines are the average of all data within each blue area, and the average percent errors of diurnal methane flux estimates using TDM measurements only during the blue shading periods are indicated in red.	84
Figure 4.1	Google Earth image of the landfill with the three roads used for mobile deployments. The white and yellow areas indicate tracer gas and methane plumes, respectively. The yellow and white dashed lines represent the margins of the methane and tracer gas plumes. The black area on the landfill indicates the approximate locations of tracer gas releases. The blue arrow indicates predominant wind direction.....	101

Figure 4.2	Variations of the R^2 TDM filtering parameter versus wind speed when WDS and TI are low ($<$ mean) for the four defined case studies.	109
Figure 4.3	Variations of the acetylene (the tracer gas) signal to noise ratio (SN_A) versus wind speed when WDS and TI are small ($<$ mean) for the defined case studies.	110
Figure 4.4	Variations of the R^2 filtering parameter versus circular wind direction variations standard deviation (WDS) for high wind speed ($>$ mean) and low TI ($<$ mean) for the four defined case studies.....	113
Figure 4.5	Hourly averaged TDM filtering or meteorological parameters for Case study IV data: a) R^2 , b) ERD, c) wind speed, and d) WDS. The blue highlight areas in plots (a) and (b) indicate the conditions when the TDM has reliable data. The wind speed and WDS variations during seven days between February 10 th and 16 th 2013 are available and shown in this figure.....	115
Figure 4.6	Seasonal variations of the R^2 filtering parameter obtained using mobile TDM data and seasonal variations of WDS, wind speed and TI.....	118
Figure 4.7	Dependency of the R^2 filtering parameter on a) wind speed and b) WDS for TDM data collected with the stationary approach.	120
Figure 4.8	Comparison of the R^2 filtering parameter for stationary and mobile approaches on dates when both TDM methods were applied.	121
Figure 4.9	Variation of the R^2 filtering parameter versus wind speed for TDM data grouped into 3-4 day periods. Data of group is averaged and shown as a single data point. The bars indicate one standard deviation.....	124
Figure B.1	Schematic of resistance layers that methane passes through from bottom of landfills into the atmosphere. Black arrows indicate methane emissions, which can move directly from topsoils into the atmosphere or go through plants. Scales are not considered in this schematic.	145
Figure B.2	Impacts of atmospheric stability on near surface gas fluxes. Top - neutral atmosphere, Bottom - unstable atmosphere. The orange arrow indicates sensible heat radiation, white arrow wind speed, blue arrow methane flux from surface, black vortex the turbulence. The dashed line is the Monin-Obukhov length L and the instrument on the right is the EC tower.	150

Figure C.1 Weekly averaged wind speeds a) the week in June 2012, and b) the week in February 2013. Weekly averaged Monin Obukhov Length, L for c) the week in June 2012, and d) the week in February 2013. The red dashed lines separate different atmospheric stability conditions.....174

ABSTRACT

Landfills are an important anthropogenic source of greenhouse gas emissions, accounting for about 18% of anthropogenic methane emissions. With growing regulatory interest in greenhouse gas emissions and the development of fast and accurate gas sampling tools, an increasing number of landfill methane emissions measurements have been reported. Data from these studies indicate significant short-term variability, the cause of which is unknown. It is hypothesized that short-term (within a day) variations of landfill emissions are associated with temporal fluctuations of some atmospheric parameters. Atmospheric modeling supports the hypothesis that short-term emission variations would lead to short-term variations of downwind measurements.

Because methane emissions may vary within short periods (~ a few hours), understanding the mechanisms driving emission variations will help to understand their temporal variability. A long-term data set of eddy covariance (EC) measurements from a Southeastern US landfill was examined to determine the influence of atmospheric conditions on methane emissions and their diurnal variation. The results indicate that surface methane flux significantly varies with wind shear velocity when the atmosphere is neutral. Under unstable atmospheric conditions, air temperature has the best correlation with methane flux, which was corroborated with an independent dataset of

tracer dilution method (TDM) measurements for similar measurement periods. These field data support the formulation of interface flux employed recently in the Weather Research Forecasting model for landfill gas emissions. The EC data display diurnal flux variations for this landfill (daytime fluxes up to 23 times greater than nighttime fluxes). Flux measurements from this landfill between 12 pm and 6 pm might overestimate diurnal-average fluxes up to 73%. Therefore, the best measurement times representing diurnally averaged fluxes for this landfill are before noon (~11 am) and in the evening (~5 pm).

Among current methane emission measurement methods, the TDM is believed best for quantifying the whole-landfill methane emissions. However, not all the collected data are reliable. The level of data reliability depends on landfill topography, properties of downwind measurements (e.g. distance to downwind roads and alignment compared to landfill), gas tracer setup (number of tracer bottles and their locations compared to high methane emission spots), and meteorological conditions (wind direction, wind speed, and atmospheric stability). Therefore, data filtering techniques have been proposed for removing unreliable data. Statistical analyses were conducted between previously established data filtering criteria and meteorological parameters to

determine the meteorological conditions and time of day when the most accurate TDM data may be collected. Using the data collected from the Southeastern US landfill as a test case, results indicate that the rate of passing the TDM filtering criteria increases as wind speed increases and as the circular standard deviation of the wind direction decreases. Comparison between the mobile and stationary TDM approaches indicates that the stationary approach is more sensitive to the atmospheric conditions, with 64% of stationary data passing the filtering criteria when wind speed is greater than 5 m/s and the standard deviation of circular wind direction is less than 0.4. About 65% of the data obtained by the mobile approach pass these filtering criteria when circular wind direction standard deviations are less than 0.5 with no wind speed limitation. This study showed that measurements during early morning and late evening are more susceptible to error because of atmospheric stability conditions at this landfill. Moreover, the measurements during colder seasons were more accurate than results in warmer seasons for this landfill, because of higher frequency of unstable atmosphere during warmer seasons. At the Southeastern US landfill, the best times of day to collect the most accurate and reliable data are ~ 11 am and ~ 4 pm. Interestingly, conducting TDM

measurements at these times leads not only to high data accuracy, but also data that are most representative of daily emissions.

Chapter 1

SIGNIFICANCE AND OUTLINE

Anaerobic biological decomposition of buried organic waste in landfills generates methane (55% of the landfill gas) and carbon dioxide (45%). The generated methane that is neither collected nor oxidized in landfill covers is emitted into the atmosphere. Landfills are considered to be an important source of anthropogenic methane emissions (Scheehle et al. 2006). Although landfills contribute about 3-4% of annual global warming (Bogner et al. 2008), emission reduction potentials have not been thoroughly explored and are still a topic of study (International Solid Waste Association 2009). Some practices that have been utilized to mitigate emissions include 1) stimulating microbial methane oxidation in landfill covers; 2) installing gas collection systems, which remove methane and carbon dioxide via a network of collection wells; 3) implementing management procedures such as in situ aerobic degradation (Spokas et al. 2011; Bogner et al. 1997; Scheutz et al. 2009); and 4) waste reduction (Meidiana and Gamse 2011). These measures are not able to completely prevent emissions into the atmosphere. To develop or evaluate measures to control emissions and to estimate emissions for greenhouse gas inventories, it is necessary to quantify methane emissions from individual landfills. Emission measurements help to assess the importance of greenhouse gas emissions from landfills, and may be used to evaluate the effectiveness of proposed remedies (Perera et al. 2002).

Several methods quantifying landfill methane emissions have been developed over the past two decades for annual emission inventories. These methods include flux chambers (Metcalf and Farquhar, 1987), the tracer dilution method (Czepiel et al., 1996), inverse plume modeling (Flesch et al., 2004), and micrometeorological eddy-covariance (Laurila et al., 2005). Among these methods, the tracer dispersion method (TDM) is known as the most promising method for quantifying whole-landfill methane emissions (Galle et al., 2001). The United States Environmental Protection Agency (US EPA) has included this method in Category C as “other test method” (OTM) 33B as a reliable approach to estimate gas emissions from large sources.

In the TDM methodology, methane emission is estimated by releasing a tracer gas at a fixed and known rate from a location coincident with the methane source and measuring both methane and the tracer gas concentrations far enough downwind such that the gas plumes are well-mixed. In this situation, emissions of both methane and the tracer may be treated as point sources (Mønster et al., 2014; Foster-Witting et al., 2015; Taylor et al., 2016, Mønster et al., 2019). The TDM is conducted during a few hours to estimate emissions from the whole landfill. With the past decade advancement of fast and accurate gas sampling, TDM is able to quantify short-term emission variations. This dissertation assesses the magnitude of these short-term variations in measurements from landfills, their relationship to atmospheric and soil conditions, and their influence on determination of average daily emission rates with limited TDM data. From this effort, the preferred time of day to achieve the most accurate and most representative methane emission estimates from TDM data is determined at one landfill.

Chapter 2 presents a field experiment at the Sandtown Landfill, Delaware, and an atmospheric model of gas emissions from that site to assess the relationship between atmospheric conditions and gas plume transport. This is the first application of an atmospheric dispersion model to a landfill for understanding gas transport patterns. The field measurements show that landfill methane emissions depend upon wind conditions. The measured emission variations during this field test might be due to 1) actual temporal variations of emissions, 2) temporal variability of surface wind speeds affecting whole landfill emissions, 3) spatial variability of fixed emissions sources, and/or 4) misaligned locations of tracer gas release and methane emissions. The atmospheric model provides a reasonable match to measured wind speed and direction on the landfill surface and measured downwind tracer concentrations.

In Chapter 3, the dependency of diurnal landfill methane emissions on meteorological parameters under different atmospheric stability conditions is examined to 1) understand which meteorological parameter has the most significant effect on methane emissions under each atmospheric stability condition, 2) assess the reasonableness of the interface flux equation found in atmospheric models of landfill gas emissions, and 3) determine the preferred time for conducting short-term emission measurements for diurnal-average methane emissions. Using a combination of eddy covariance (EC) and TDM field data from a Southeastern US landfill, the diurnal emission variability was determined to be due to the influence of air temperature and wind speed under unstable and neutral atmospheric conditions, respectively. This is the first report about the impact of meteorological parameters on methane emissions under different atmospheric stability

conditions. The information in Chapter 3 may play an important role in understanding gas emissions from landfills and improving the efficiency of gas collection systems and landfill covers. If meteorological parameters can alter diurnal methane emissions from landfills, then field measurements conducted under particular air temperature and wind speed conditions may not be representative of emissions at other times.

In Chapter 4, the importance of conducting TDM under favorable atmospheric conditions is discussed. The TDM is a costly and technologically-complicated method to quantify emissions (Oonk, 2010), and a significant portion (up to 96%) of the collected data may be unreliable. Therefore, statistical analyses are employed in Chapter 4 to investigate the dependency of the data filtering criteria, which are used to discard inaccurate data, on metrological parameters. The aim of Chapter 4 is to determine the optimal atmospheric conditions for accurate TDM measurements. It was found that TDM measurements are more reliable during winter time compared to summer time because of higher sustained wind speeds. Moreover, avoiding TDM measurements during early morning and late evening would increase data reliability. A simple desktop task prior to field measurements would save resources and lead to more reliable data.

Finally, in Chapter 5, the directions for future research on landfill methane emission quantification, mitigation and estimation are discussed. Contribution of this dissertation to the literature is:

- First study presents that wind causes short-term methane emission variations from the whole landfill.

- First study that explains how wind speed and air temperature affects diurnal emission variations under different atmospheric conditions.
- First study reveals that afternoon short-term emission measurements might be erroneous (up to 73%). This finding challenges current annual emission inventories.
- First study suggests preferred times of day to conducted measurements for this inland landfill are before noon (~ 11 am) and afternoon (~ 4 pm) (both diurnal-average wise and meeting filtering criteria wise).

Chapter 2

SHORT-TERM METHANE EMISSIONS DEPENDENCY ON WIND

This chapter is the paper entitled “Short-term Landfill Methane Emissions Dependency on Wind”, published in the *Waste Management* journal in 2016.

2.1 Introduction

Methane (CH₄) from biological decomposition of buried waste in landfills is considered an important source of anthropogenic CH₄ emissions (Scheehle et al., 2006). Measurement of CH₄ emissions is useful for evaluating landfill gas control measures and improving estimates of CH₄ emissions for greenhouse gas inventories. CH₄ emissions from landfills are not constant, with annual changes associated with aging of waste (Foster-Wittig et al., 2015) or changes in the composition of landfilled materials (Weitz et al., 2002, Allen et al., 1997), and seasonal variations due to changes in temperature and moisture content of cover soils that affect gas transport and methane oxidation (Wang et al., 2011, Chanton and Liptay, 2000, Stern et al., 2007).

Short-term emissions variations due to weather have also been reported. Czepiel et al. (2003) measured whole-landfill CH₄ emissions using the tracer dilution method (TDM) and found CH₄ emissions increased by a factor of five when barometric pressure dropped approximately 15 mbar over a 1-month period of emissions measurements. Xu et al. (2014)

measured CH₄ emissions from portions of landfill cells using the eddy covariance method and attributed a 35-fold variation in emissions to barometric pressure variations.

Over even shorter time periods, wind speed has been implicated as a factor affecting CH₄ emissions (McBain et al., 2005, Rachor et al., 2013) - as wind speed increases, gas pressures fluctuate because of atmospheric turbulence at the landfill surface causing a pumping effect that increases emissions. Numerical modeling of gas transport processes in landfill cover soils suggests that pressure pumping caused by wind turbulence may increase CH₄ emissions up to four times that of the CH₄ diffusive flux for some soil conditions (Poulsen and Moldrup, 2006). While the effect of wind speed on CH₄ emissions have been observed in flux chamber (Rachor et al., 2013) and eddy covariance (McBain et al., 2005) measurements over portions of a landfill surface, there are no data indicating variations in whole-landfill CH₄ emissions because of wind speed.

TDM, also known as the tracer correlation or dynamic plume technique, was developed to quantify whole-landfill CH₄ emissions and has seen increased use in the past several years because of improved gas measurement technology (Foster-Wittig et al., 2015, Mønster et al., 2015, Mønster et al., 2014). A tracer gas, traditionally sulfur hexafluoride (SF₆) or nitrous oxide (N₂O) but more recently acetylene (C₂H₂), is released at a known rate at multiple locations on the landfill which then mixes with CH₄ emissions from the landfill surface (Czepiel et al., 2003, Galle et al., 2001). Downwind of the source if the released tracer gas is sufficiently well mixed with emitted CH₄, the mass flux of CH₄ is calculated from the known mass flux of the tracer gas multiplied by the ratio of the CH₄ to tracer gas concentration

$$E_{CH_4} = E_T \frac{M_{CH_4} C_{CH_4}}{M_T C_T} \quad (2.1)$$

where E_{CH_4} and E_T are CH_4 and tracer emissions rates, respectively, expressed as mass flowrate (kg/min); M_{CH_4} and M_T are the molecular weights of CH_4 and tracer; and C_{CH_4} and C_T are the concentrations of CH_4 and tracer above background (ppm).

If measured at a fixed location, this concentration ratio can be averaged over time by regressing scatter plots of C_{CH_4} versus C_T to obtain the fitted slope used for the ratio C_{CH_4}/C_T in equation (2.1) (Galle et al., 2001, Börjesson et al., 2009). When measured by a moving vehicle that traverses the downwind gas plumes, similar scatter plots can be generated (Foster-Wittig et al., 2015, Mønster et al., 2014), or, more commonly, C_{CH_4} and C_T are integrated individually in space and the ratio of the two integrations are used to represent the ratio C_{CH_4}/C_T (Foster-Wittig et al., 2015, Mønster et al., 2014).

With increasing TDM applications, significant variations in measured CH_4 emissions have been reported for short measurement campaigns. For example, during measurement campaigns that ranged from 1.7 to 4.3 h, Scheutz et al. (2011) reported a coefficient of variation of CH_4 emissions up to 0.30. Similarly, in a study of nine Danish landfills where single measurement campaigns (2 to 10 h duration) were conducted at each landfill, the average coefficient of variation was 0.19 for the nine landfills with a maximum of 0.35 (Mønster et al., 2015). On the other hand, when the TDM method was tested with controlled releases of CH_4 and tracer (Mønster et al., 2014), the coefficient of variation was much smaller: for three tracer/ CH_4 release configurations and measurements at three downwind transects, the mean coefficient of variation was 0.05 with maximum of 0.15,

which occurred for the configuration with significant misalignment between CH₄ and tracer and for measurements close to the points of gas release. The cause of the increased coefficient of variation for landfill CH₄ emissions versus controlled CH₄ releases is unclear: it may be due to misalignment of tracer release and regions of CH₄ emissions, short-term variations in emissions possibly due to wind, or other factors.

The primary objective of this work is to determine if short-term variations in whole-landfill CH₄ emissions measured with TDM might be due to variations in wind speed. If wind affects whole-landfill CH₄ emissions, in some situations TDM may result in biased estimates of emissions, since TDM requires sufficient wind speed to generate well-mixed gas plumes downwind of the landfill (Foster-Wittig et al., 2015), and thus measurements are not possible under low wind speeds (Foster-Wittig et al., 2015, Galle et al., 2001). A secondary objective is to evaluate the utility of atmospheric dispersion modeling to understand the influence of atmospheric conditions on landfill emissions measurements requiring sampling of landfill gas plumes.

To accomplish these objectives, CH₄ emissions data were collected using TDM from the Sandtown Landfill in Delaware (USA) for a short-term experiment in March 2010. Correlations between wind conditions on the landfill surface and CH₄ emissions were explored with field data. An atmospheric dispersion model was developed for the site and used for three purposes: to determine the travel time of emissions from the landfill surface to a downwind measurement location; to refine data filtering techniques for TDM, since in the atmospheric model CH₄ emissions were known and could be compared with TDM results from analysis of model output; and to assess if temporal variation in emissions

determined from TDM might be caused by misalignment of tracer/CH₄ emissions locations or wind conditions. Field data and numerical model results were collected at one downwind location at two measurement heights, at the ground surface and at approximately 85 m above ground to evaluate the benefit of above ground measurements on TDM.

2.2 Materials and Methods

2.2.1 Site Description

The Sandtown Landfill has an active landfill gas collection system in all landfill cells and ongoing waste disposal activities. Area A-B (110,000 m²) in Figure 2.1 was filled with 532,000 tons of household waste from 1980 to 1988 and is now closed and equipped with a final cover. A total of 1,226,000 tons of waste were landfilled in Area C and D (170,000 m²) from 1988 to 1998 and these regions have intermediate covers. Area E (132,000 m²) is an active cell where 2 million tons of waste have been landfilled since 1999: portions of Area E have intermediate and daily cover soils. The landfill rises 40 m above the surrounding topography and is located in a coastal plain with minimal variations in ground elevation for a 100 km radius surrounding the site. The landfill is in a rural area with low traffic density and is surrounded by farms with 25 to 30 m high pine trees.

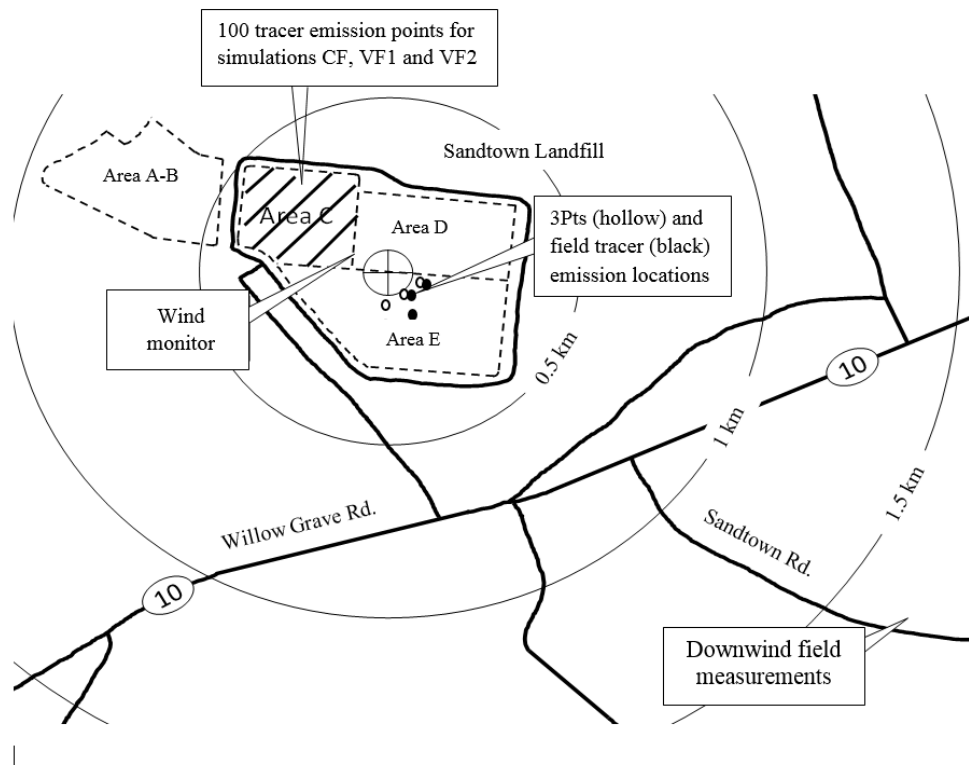


Figure 2.1 Aerial view of Sandtown Landfill (Sandtown, DE) illustrating emissions locations for simulations (CF1, CF2, VF1, VF2 and 3Pts) and tracers in field test. The downwind gas sampling location is also shown where measurements were taken at 2.5 and 85 m AGL.

2.2.2 Field Emissions Measurements

TDM was utilized to quantify CH_4 emissions from the Sandtown Landfill. Details of the method are found elsewhere (Czepiel et al., 2003, Foster-Wittig et al., 2015, Mønster et al., 2015). In this application, C_2H_2 was selected as the tracer gas (Foster-Wittig et al., 2015, Mønster et al., 2014). Three C_2H_2 gas cylinders were located on the upstream edge of the active landfill region on Area E (Figure 2.1), identified as the main CH_4 source

during preliminary ground-level atmospheric CH₄ measurements around the landfill in March 2010. The gas cylinders were arranged 70 m apart in a line perpendicular to the mean wind direction. Mass flow controllers were used to discharge C₂H₂ at a constant mass flow rate of $E_{C_2H_2} = 52.23 \text{ g C}_2\text{H}_2/\text{min}$.

C_{CH_4} and $C_{C_2H_2}$ measurements for the TDM are often obtained by making transects of the downwind gas plumes perpendicular to the mean wind direction with a vehicle-mounted gas sampling system (Czepiel et al., 2003, Börjesson et al., 2009). Downwind roadways are not, however, always located with suitable alignment for TDM measurements. For these situations, if plume meandering is adequate to cause plumes to move into and out of a fixed measurement location, stationary measurements may be used and have provided similar estimates of CH₄ emissions (Green et al., 2010). Here, all measurements were conducted at one geographic location, indicated in Figure 2.1, since road alignment was not ideal for vehicle-mounted gas sampling with the prevailing wind. Sampling along downwind roads was attempted but resulted in poor data: tracer and CH₄ plumes were either not well mixed or gas concentrations were too low for accurate measurements.

A prototype gas analyzer developed by Picarro, Inc. (Sunnyvale, CA) and based on an all-optical technique called cavity ring-down spectroscopy (CRDS) was used to measure C_{CH_4} and $C_{C_2H_2}$ (Crosson, 2008). The CRDS analyzer measures CH₄ and C₂H₂ in less than 2 s with a measurement precision (one estimated standard error) of 0.8 ppb and 0.2 ppb for

CH₄ and C₂H₂, respectively, and has been used in other TDM measurements at landfills (Foster-Wittig et al., 2015, Mønster et al., 2015).

The TDM was used to measure CH₄ emissions using data collected at 2.5 and 85 m above ground level (AGL) at the same location (*39° 01' 45" N, 74° 42' 47" W*) between 14:00 to 16:00 local time on March 6, 2010. A single stationary location was used since a large, open region was needed to launch and monitor the weather balloon used for measurements at 85 m, and a limited number of locations were available in the actively farmed land surrounding the landfill. A short measurement period was selected since changes in landfill operations or in soil temperature and barometric pressure, which are known to affect CH₄ emission, would be minor, permitting an examination of wind on emission. While it would have been desirable to examine emission variations in other 2-h periods, financial limitations prevented this. For 85 m measurements, a chloroprene weather balloon (2.4 m diameter) was inflated with helium and flown while tethered using light-weight nylon rope. Teflon tubing (1/8" ID, 3/16" OD, and 150 m long) was attached to the balloon and connected to a vacuum pump, which when operated resulted in a 22 s residence time of the air in the tubing. The balloon height was measured by the nearly vertical tubing length and ranged from 70 to 100 m, with an average height of approximately 85 m. By connecting and disconnecting the Teflon tubing to the gas analyzer alternatively every 4 to 9 minutes, measurements of C_{CH_4} and $C_{C_2H_2}$ could be made at 2.5 m AGL or 85 m AGL at the flying weather balloon.

Meteorological data were collected during the sampling period with a wind monitor (RM Young's 0513, Campbell Scientific) 2 m AGL on top of Area E, which is 40 m higher

than surrounding terrain (see Figure 2.1), and with a weather station at the base of the landfill. One-minute averaged wind speed data were recorded by the wind monitor. Average temperature and barometric pressure during measurements at the landfill base were 8 °C and 101.3 kPa, respectively.

2.2.3 Atmospheric Dispersion Modeling

Given the variability in CH₄ emissions discussed below, relationships between landfill operations, atmospheric conditions, and CH₄ emissions were explored. We postulated that downwind CH₄ and tracer concentrations obtained from ground and airborne measurements could be used to quantify temporal CH₄ emissions variations. To test this, an atmospheric dispersion model was developed that described wind conditions in the vicinity of the landfill for the 2 h TDM test. Controlled releases of CH₄ and tracer were made at different locations in the model landfill, and then forward simulations performed to predict downwind gas concentrations at 2.5 and 85 m AGL at the field measurement location shown in Figure 2.1. Simulations were performed to test three hypotheses about TDM-measured whole landfill CH₄ emissions: TDM emissions measurements will be correlated with wind speed if (1) local CH₄ emissions vary with wind speed causing wind-induced variations of whole landfill emissions, (2) if the spatial distribution of CH₄ emissions varies with wind speed but whole landfill emissions are constant, and (3) if local CH₄ emissions are constant but significantly misaligned with tracer emissions locations. In the process of testing these hypotheses, the atmospheric

dispersion model was also used to develop data filtering techniques that were then applied to field measurements.

The Advanced Regional Prediction System (ARPS) was used for simulations. ARPS was developed at the Center for Analysis and Prediction of Storms at the University of Oklahoma. It is a non-hydrostatic meso-scale and small-scale finite-difference numerical weather prediction model that runs in parallel using the message passing interface. Descriptions of the model can be found in Xue et al. (2001) with relevant details presented in Appendix A and summarized below.

Daytime atmospheric flow was simulated using ARPS for 3 h starting from 13:00 to 16:00 local time on March 6, 2010. Results from the last 2 h period were used for analysis. To resolve the local flow around the landfill, a multi-scale approach was adopted. Simulations were first performed on a 200 x 200 km² area with 2400 m horizontal resolution which covered the entire Delmarva Peninsula. Realistic initial and lateral boundary conditions were obtained from meteorological analysis data produced by the North American Mesoscale forecast system. Results from the 2400 m grid were used to drive lateral boundaries of a 150 m grid, which was then fed into a 30 m grid. Vertical grid stretching was applied to better resolve the surface layer. On the finest grid, the vertical resolution was 20 m with 5 m spacing near the surface. The land surface was represented with high resolution terrain (10 m) and land cover (30 m) data from the Delaware Solid Waste Authority and the U.S. Geological Survey.

On the 2400 m grid, ARPS was run in meso-scale mode with boundary layer parameterizations (Sun and Chang, 1986) to model the synoptic-scale flows. On the 30 m

grid a numerical tracer, representing CH₄ or C₂H₂, was released at constant or variable mass flow rate, depending on the simulation, on top of the landfill from 1400 LST onwards. Tracers were released either from the three tracer release points shown in Figure 2.1 that correspond to the location of field tracer release points, or from 100 points distributed in a spatially uniform grid covering Area C in Figure 2.1. A vertical column of model results at the field sampling location was recorded every 2 s, while 3D flow fields were output every minute. Wind velocity was also output every 2 s at 2.5 m AGL for selected locations.

Due to the fine vertical grid spacing with near surface grid-stretching, the 30 m pine trees surrounding the landfill were represented by 7 grid points in the vertical direction. The traditional representation of trees in mesoscale atmospheric models with an elevated roughness length ($z_o \sim 1$ m) was insufficient for the large-eddy simulation domain. Therefore, a canopy model was adopted to explicitly resolve the additional drag on the atmospheric flow by the trees.

The increased turbulence within the canopy layer led to more mixing of the tracer, and resulted in low, broad peaks near the surface. In general, the canopy model acted like a semi-permeable flow obstacle. An internal boundary layer formed downwind of the canopy, so that wind speed reduction was also felt above the canopy height. At the 85 m balloon height, mean wind speed was reduced by ~10% when the canopy model was on.

Four different numerical tracer release configurations were considered. Three Point (3Pts) simulation mimicked C₂H₂ release in the field tests and is described by

$$Q_{3Pts}(\vec{x}_i, t) = \frac{Q}{3}; i = 1:3 \quad (2.2)$$

where Q is the total tracer mass flux that is invariant with time. The three release points (\vec{x}_i) were in close proximity to the C_2H_2 release points for the field tests shown in Figure 2.1. For the Constant Flux 1 (CF1), Variable Flux 1 (VF1), and Variable Flux 2 (VF2) simulations, the numerical tracer was released from 100 uniformly spaced grid points in Area C in Figure 2.1. For the Constant Flux 2 (CF2) simulation, the numerical tracer was released from 89 uniformly spaced grid points in Area D in Figure 2.1. The tracer releases for CF1 and CF2 are described by

$$Q_{CF1}(\vec{x}_i, t) = \frac{Q}{100}; i = 1:100 \quad (2.3)$$

$$Q_{CF2}(\vec{x}_i, t) = \frac{0.89Q}{89}; i = 1:89 \quad (2.4)$$

where $Q_{CF1}(\vec{x}_i, t)$ and $Q_{CF2}(\vec{x}_i, t)$ are the tracer mass fluxes at location \vec{x}_i and are equal to the total mass flux divided by the 100 or 89 release points in Area C and D, respectively. Because identically sized surface grid cells were used for CH_4 emissions in CF1 and CF2 while Area D was approximately 89% of Area C, the number of release points was larger for CF1 than CF2. CF1 and CF2 simulations were used to represent either a uniform, time-invariant release of CH_4 , or release of a tracer gas in perfect alignment with the CH_4 release in simulations VF1 and VF2, where CH_4 emissions varied with wind conditions.

The numerical tracer released in simulations VF1 and VF2 was dependent on wind speed

$$V(\vec{x}_i, t) = \sqrt{u(\vec{x}_i, t)^2 + v(\vec{x}_i, t)^2 + w(\vec{x}_i, t)^2}; i = 1:100 \quad (2.5)$$

where (u, v, w) are magnitudes of wind velocity in x , y and z directions at 2.5 m AGL. Tracer release for VF1 is described by

$$Q_{VF1}(\vec{x}_i, t) = \frac{V(\vec{x}_i, t)}{\sum_{j=1}^{100} V(\vec{x}_j, t)} Q ; i = 1:100 \quad (2.6)$$

where $Q_{VF1}(\vec{x}_i, t)$ is the tracer mass flux at location \vec{x}_i and is equal to the total mass flux Q normalized by the relative wind speed at this measurement location. The summation of Q_{VF1} over all \vec{x}_i is the total CH₄ flux from Area C and was invariant with time but varied spatially at each time step depending on local wind speed.

The numerical tracer release in simulation VF2 is described by

$$Q_{VF2}(\vec{x}_i, t) = \frac{\sum_{j=1}^{100} V(\vec{x}_j, t)}{\frac{\sum_{k=1}^n (\sum_{j=1}^{100} V(\vec{x}_j, t_k))}{n}} \left(\frac{Q}{100} \right) ; i = 1:100 \quad (2.7)$$

where $Q_{VF2}(\vec{x}_i, t)$ is the tracer mass flux at location \vec{x}_i and is equal to the total mass flux Q normalized by the average relative wind speed in Area C. Here, n is the number of simulation time steps. Q_{VF2} represents CH₄ emission that is spatially uniform within Area C but varies linearly with the average Area C wind speed.

To test the three hypotheses described above, correlations between TDM-measured CH₄ emissions and wind conditions on the landfill surface were examined using simulation results. To account for the travel time for gases emitted from the landfill to the downwind measurement location (see Figure 2.1), estimates of travel time are necessary to adjust wind speeds at the landfill surface to the corresponding time of TDM-measured CH₄ emissions. The numerical technique of Deleersnijder et al. (2001) was applied to estimate the travel time T of numerical tracer gas to the downwind measurement location.

2.3 Results and Discussion

2.3.1 Field Emissions Measurements

TDM data are typically integrated in space (Mønster et al., 2015; Foster-Wittig et al., 2015; Mønster et al., 2014) or time (Börjesson et al., 2009; Galle et al., 2001) to estimate average CH₄ emissions. To illustrate the variability in raw data from the field campaign, instantaneous emission measurements determined using equation (2.1) are shown in Figure 2.2. Data alternate between measurements at 2.5 and 85 m AGL, with time gaps between data sets for switching measurement heights. When CH₄ concentrations were at or below background, CH₄ emissions were plotted as zero, although this only indicates the CH₄ plume did not intersect the measurement location at that time. Variability between individual CH₄ emissions measurements was large and was not correlated with changes in wind direction, which are shown in Figure 2.3. For example, there was no significant change in wind direction from 15:15-16:00, while emission variations during this period are similar to those from 14:15-15:15 when wind direction did change. Average measurements during some periods differed significantly: for example, mean CH₄ emissions at 85 m AGL between 14:24-14:26 was 45% smaller than mean CH₄ emissions between 14:57-14:60 and statistically different (t-Test of means, $p < 0.001$). When averaged over the entire measurement period, though, emissions measurements at 2.5 and 85 m AGL were 2330 ± 60 g and 2289 ± 46 g CH₄/min (+/- values represent 95% confidence interval), respectively. Thus, while field data indicate temporal variability in CH₄ emissions, mean measurements at the two sampling heights for the entire 2-h sampling

period were similar, differing by less than 2%. Understanding the cause of temporal variability in emissions is an objective of this work.

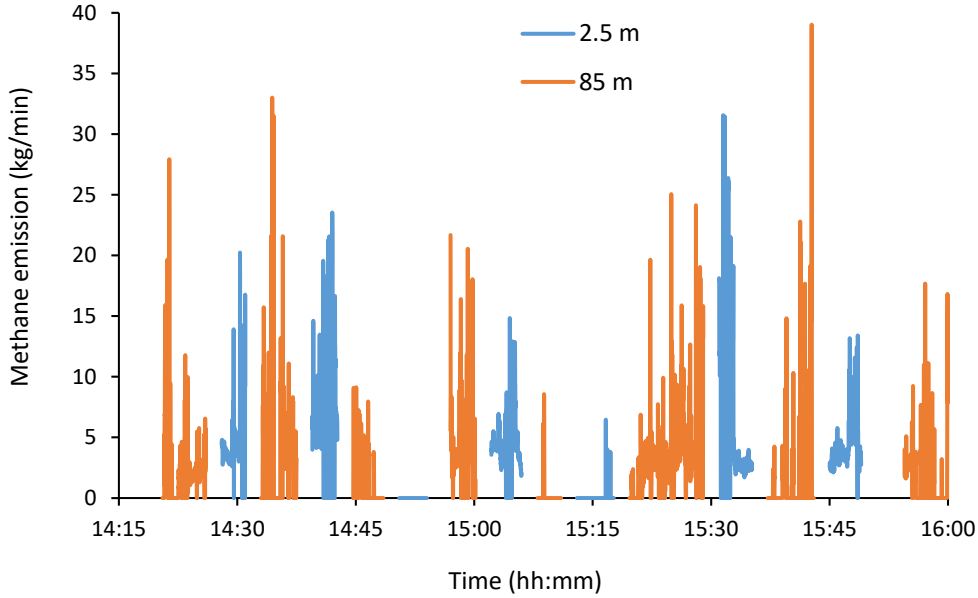


Figure 2.2 Field methane emissions (equation (2.1)) from individual concentrations at 2.5 (orange) and 85 m AGL (blue) at downwind measurement location (Figure 2.1). Each elevation had seven measurement periods. Measured methane emissions were zero when gas concentrations were below background; gaps between measurements correspond to switching sampling tubing between 2.5 and 85 m heights.

It is important to note that after subtracting background concentrations, 1.88 ppm and 0.86 ppb for C_{CH_4} and $C_{C_2H_2}$, respectively, peak C_{CH_4} and $C_{C_2H_2}$ averaged over all 1-min measurement periods were smaller at 2.5 than at 85 m AGL: $\overline{C_{CH_4}} = 258 \pm 45$ ppb and $\overline{C_{C_2H_2}} = 2.37 \pm 0.84$ ppb at 2.5 m AGL, but $\overline{C_{CH_4}} = 323 \pm 87$ ppb and $\overline{C_{C_2H_2}} =$

3.59 ± 99 ppb at 85 m AGL. Higher gas concentrations should result in more accurate emissions measurement, since the signal to noise ratio is larger (Foster-Wittig et al., 2015). During some measurement periods at 2.5 m AGL, increases in $C_{C_2H_2}$ occurred without corresponding increases in C_{CH_4} , which we attributed to ground-level sources of C_2H_2 like motor vehicles. Higher gas concentrations and the absence of unexplained increases in $C_{C_2H_2}$ at 85 m AGL suggest that emissions measurements may be more accurate at 85 than 2.5 m AGL.

2.3.2 Comparison of Atmospheric Dispersion Model to Field Data

Wind monitor data from the top of Sandtown Landfill and C_2H_2 concentration at the downwind sampling location (see Figure 2.1) were used to validate the atmospheric dispersion model. Wind speed and direction from field data and model simulations are shown in Figure 2.3 and show good agreement: model-predicted mean ($\bar{\bar{V}}$) and standard deviation (s_V) of wind speed, and the resultant mean wind direction ($\bar{\bar{\theta}}_{RV}$) on the landfill surface were $\bar{\bar{V}} = 4.5$ m/sec $s_V = 1$ m/sec and $\bar{\bar{\theta}}_{RV} = 320^\circ$, respectively, compared to measured values of $\bar{\bar{V}} = 5$ m/sec $s_V = 0.8$ m/sec and $\bar{\bar{\theta}}_{RV} = 320^\circ$, where the double overbar indicates a 2-h average of 1-min averaged wind speeds. Thus, without tuning or data assimilation the atmospheric model matched available wind data well.

Simulation 3Pts describes the release of C_2H_2 from three gas cylinders on the landfill surface. Normalized tracer concentrations ($C_N = (C - C_{min}) / (C_{max} - C_{min})$) at 2.5 and 85 m AGL for simulation 3Pts and field measurements are displayed in Figure 2.4. While the match between tracer concentrations at particular times for model and field data

is often poor, model-predicted mean ($\overline{C_N}$) and standard deviation (s_{C_N}) are similar to field measurements when data are compared over the same time intervals. At 2.5 m AGL, $\overline{C_N}=0.19$ ($s_{C_N}=0.15$) and $\overline{C_N}=0.21$ ($s_{C_N}=0.17$) for model and observation, respectively. At 85 m AGL, the match is not quite as good with $\overline{C_N}=0.12$ ($s_{C_N}=0.19$) and $\overline{C_N}=0.19$ ($s_{C_N}=0.20$) for model and observation, respectively. At 2.5 m AGL field data have sharper gradients than model simulation results, suggesting that mixing because of surface roughness was too large in the model. Field data at 2.5 m AGL may have been affected by vehicular sources of C_2H_2 too, which would have resulted in some of the data spikes. Because the atmospheric dispersion model provided a reasonable match to field wind measurements and tracer data, the model was subsequently used to estimate the travel time from the landfill and to test three hypotheses about the effect of wind on TDM measurements.

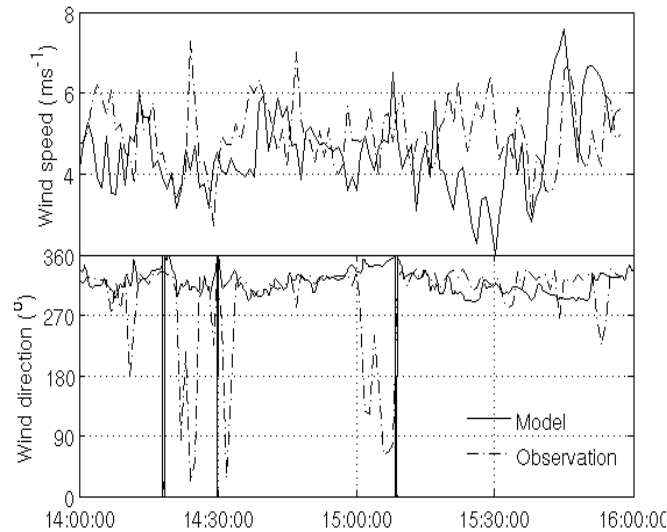


Figure 2.3 Times-series of observed and modeled surface wind speed (top) and direction (bottom). Solid lines are model results from the 25 m grid; dash-dotted lines are observations from surface station

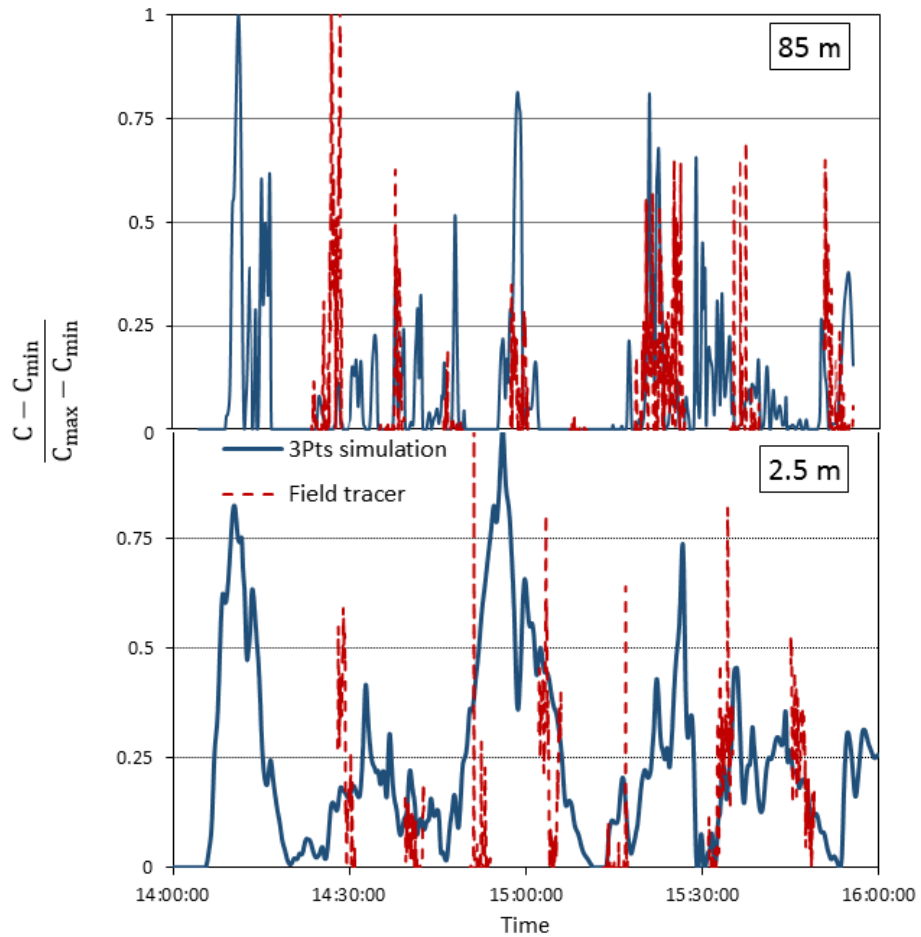


Figure 2.4 Normalized tracer concentration at downwind measurement location (see Figure 2.1). Blue solid and red dashed lines are for model (3Pts) and field data, respectively, at 2.5 and 85 m AGL. Gaps between field data correspond to switching sample tubing between 2.5 and 85 m heights. Gaps between field data correspond to switching sample tubing between 2.5 and 85 m heights.

2.3.3 Travel Time

Estimates of travel time are necessary to correlate wind speed at the landfill surface to the corresponding time of TDM-measured CH₄ emissions for testing three hypotheses about the influence of wind on CH₄ emissions. Travel times from the landfill surface to the downwind measurement location are shown in Figure 2.5. Because the wind monitor for field measurements provided only 1-min average wind data $\bar{V}(t)$, travel times were determined for four time-averaging increments (15 sec, 1, 15 and 30 min) to assess the impact of 1-min averaging on travel time calculations. Travel times ranged from approximately 5 to 16 min at the finest resolutions (15-sec and 1-min averaging increments), with minimal differences between 15-sec and 1-min wind speed averaging (see Figure 2.5). Thus, in the analyses below 1-min average wind speeds were used to compute travel times for all analyses.

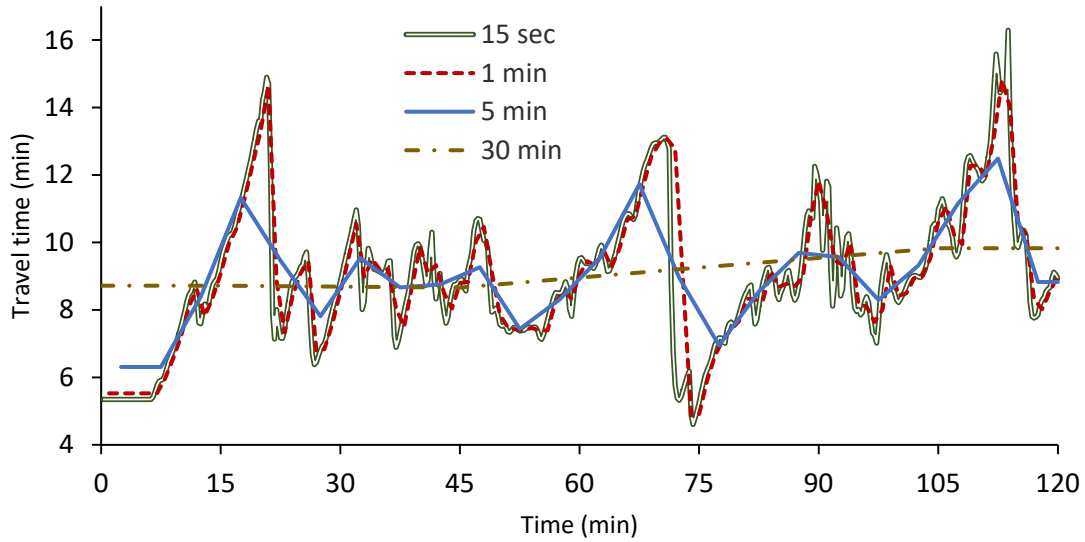


Figure 2.5 Travel time from landfill to downwind measurement location at 2.5 m AGL during the 2-h field test. Travel time varies with wind conditions and was computed at different temporal resolutions using CF1 simulation.

$\bar{V}(t)$ were determined for consecutive 1-min time increments at the landfill surface and this information propagated to the downwind measurement location by adding the travel time $T(t)$, thus providing wind speed at the downwind location to correlate with measured CH_4 emissions. However, because of variability in travel time this sometimes resulted in multivalued $\bar{V}(t + T(t))$ at the downwind location: more than one wind speed on the landfill surface affected downwind C_{CH_4} at such times. At such times downwind concentrations were influenced by emissions from at least two *different* 1-min time periods on the landfill surface. These multivalued wind speed and associated 1-min emissions data were excluded from all subsequent analyses.

2.3.4 Data Filtering and Testing Hypothesis 1: Homogeneous but Transient Emissions

Data filtering techniques were developed for TDM-measured CH₄ emissions using the atmospheric dispersion model simulations. In these simulations, CH₄ emissions are known and temporal variation of emissions with wind speed are also known and specified. Thus, the numerical model provides a convenient platform for evaluating data filtering that will later be applied to field data. Because only 1-min average wind data were available from the field, to explore relationships between CH₄ emissions and wind speed emissions data were grouped into consecutive 1-min intervals for simulations too, which facilitated comparison between the simulation and field results.

To develop the data filtering methods, data without any filtering were first considered. To illustrate the procedure, consider simulation pair VF2/CF1 where VF2 represents time-varying CH₄ emissions that are linearly related to wind speed (equation (2.7)), while CF1 represents a constant tracer emission that is perfectly aligned with CH₄ emissions (equation (2.3)) from Area C at Sandtown Landfill. The purpose of this comparison is to determine the role of wind speed on TDM-measured CH₄ emissions, by comparing to a tracer that is perfectly aligned but not wind dependent. The 2 s numerical simulation data showing variable CH₄ emissions at the landfill surface and corresponding downwind VF2/CF1 emissions measurement at 2.5 m are shown in Figure 2.6. Downwind measurements lag emissions on the landfill surface because of gas plume transit. The 2 s downwind VF2/CF1 measurements are less variable than actual emissions because of

atmospheric mixing, which smooths the peaks and valleys of actual emissions at the landfill surface.

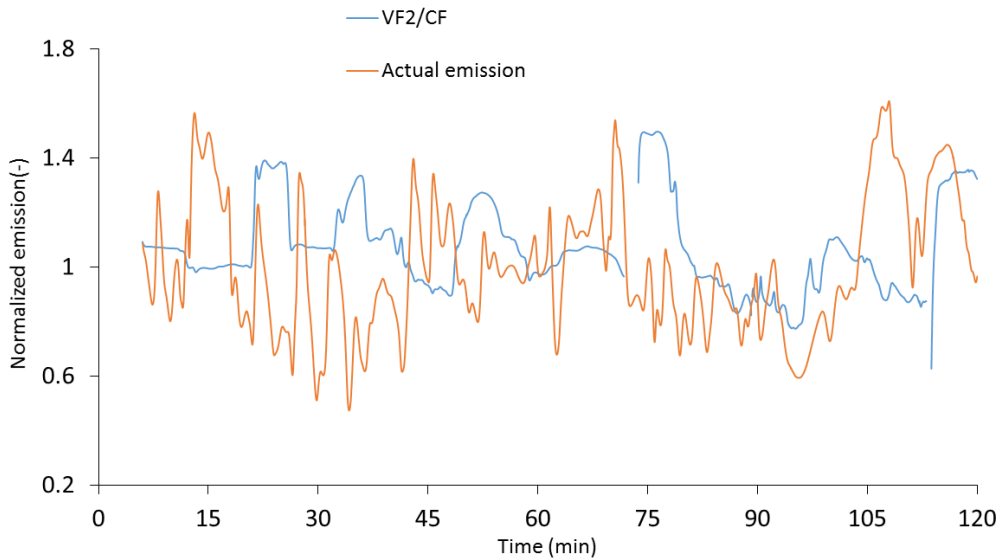


Figure 2.6 Numerical simulation output. Normalized actual emissions (VF2) and 2 s downwind emissions measurements (VF2/CF1) versus time at 2.5 m AGL with no travel time correction.

The 2 s data were grouped into consecutive 1-min time intervals; concentrations below 0.1% of maximum model concentrations on the landfill surface were associated with numerical error and discarded. The remaining data in each scatter plot of VF2 versus CF1 measurements were linearly regressed and the slope of the best-fit line used to estimate $C_{CH_4}/C_{C_2H_2}$ in equation (2.1) to calculate CH_4 emissions during each 1-min interval.

To examine the relationship between CH₄ emissions and wind speed on the landfill surface, the average wind speed over the region of CH₄ emissions was first determined for each 1-min time interval: $\bar{V}(t) = \int_{t-0.5 \text{ min}}^{t+0.5 \text{ min}} V_m(t') dt' / 1 \text{ min}$, where V_m is the wind speed at the wind monitor location interpolated from the model grid. This wind speed was propagated to the downwind measurement location by adding the travel time $\bar{V}(t + T(t))$. Wind speed data were linearly interpolated to provide the wind speed that corresponded to the midpoint of each 1-min emissions measurement. CH₄ emissions were then normalized with the average emission over the 2-h simulation time and plotted in Figure 2.7 for each 1-min time increment versus wind speed, also normalized with the average wind speed over 2 h. Data at 2.5 and 85 m AGL were correlated with wind speed ($R^2 = 0.39$ and $R^2 = 0.31$), but the correlation was not strong and emissions did not vary with a slope close to 1.0 for 85 m data, as would be expected from equation (2.7).

Because the 1:1 relationship between CH₄ emissions and wind speed was specified in simulation VF2 (see equation (2.7)) but was not reproduced with the TDM for data at 85 m, data filtering techniques were explored. Foster-Wittig et al (2015) and Monster et al. (2014) examined data analysis procedures for TDM-measured CH₄ emissions. Using downwind transects of landfill gas plumes, Foster-Wittig et al. (2015) developed three method quality indicators to determine if measurements were acceptable: signal to noise ratio > 10 , $R^2 > 0.80$ for correlation between C_{CH_4} and $C_{C_2H_2}$ during the transect, and normalized difference in emissions measurement between regression of scatter plot data versus integration of the gas plumes < 0.20 . While a formal data quality analysis procedure

was not developed by Mønster et al. (2014), they recommended the plume integration method over three alternative analysis procedures, with measurement uncertainty determined by replicate sampling of the gas plumes.

In this work measurements were made at a fixed spatial location, so the data filtering steps developed by Foster-Wittig et al. (2015) are not directly applicable. Nevertheless, the goodness of fit criterion used by Foster-Wittig et al. (2015) was applied: data were only used if $R^2 > 0.80$ for 1-min linear regressions of C_{CH_4} versus $C_{C_2H_2}$. During periods of rapid wind speed variation, linearly interpolated wind speed assigned to each 1-min emissions measurement might result in a poor estimate of actual wind speed. Linear interpolation is reasonable only if wind speed varies smoothly with time, which was assessed by examining the second derivative of wind speed with respect to time. Linearly interpolated wind speed data were excluded if $|(\bar{V}(t_2) - 2\bar{V}(t_1) + \bar{V}(t_0))/(2\bar{V})| > 0.175$, where this finite difference expression approximates the second derivative of the wind speed at time t_1 using data at times t_0 , t_1 , and t_2 , multiplied by the time increment $(\Delta t)^2$, and normalized by the mean wind speed over the 2-h measurement period. The 0.175 criterion was selected based on a visual assessment of the data.

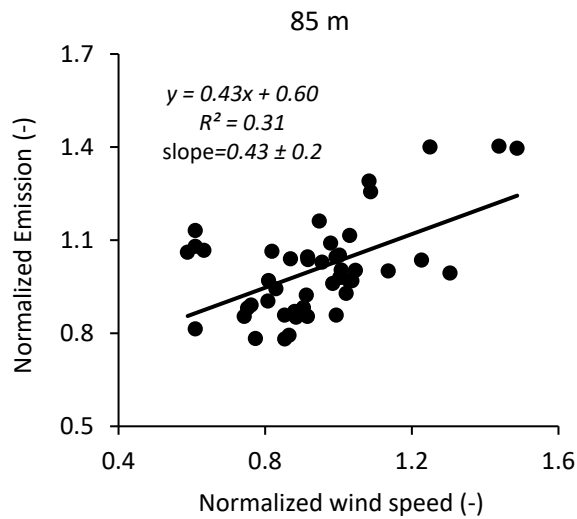
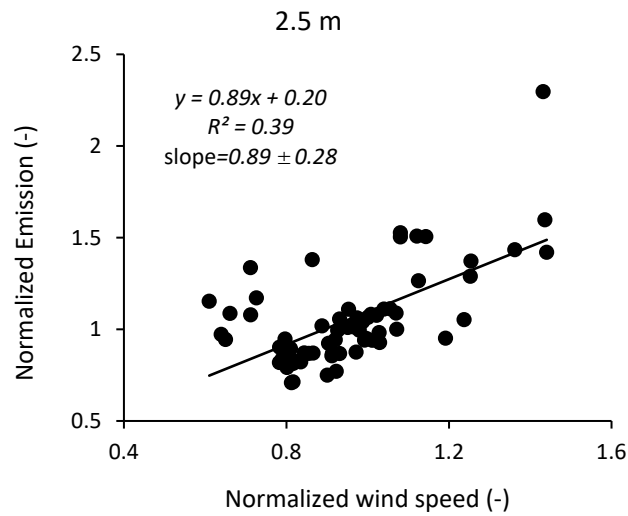


Figure 2.7 Normalized emissions calculated with TDM using 1-min data from simulation pair VF2/CF1 at 2.5 and 85 m AGL at measurement location in Figure 1. Emissions plotted versus normalized wind speed on landfill surface with no data filtering. 95% confidence intervals on individual data points are so small as not to be visible.

Applying these filtering criteria to the simulation pair VF2/CF1 (raw data in Figure 2.7) resulted in the 1-min emissions versus wind speed data in Figure 2.8. Filtering had a

minor effect on measurements at 2.5 m AGL: R^2 decreased slightly from 0.39 to 0.35, while there was a small change in slope from 0.89 ± 0.28 to 0.85 ± 0.38 . Filtering improved the results at 85 m AGL: R^2 increased from 0.31 to 0.56 and the slope increased from 0.43 ± 0.20 to 0.67 ± 0.24 . Filtering criteria had a more noticeable effect on airborne than ground data because gas concentrations were smaller at 85 m, and smaller gas concentrations rendered emissions estimation more susceptible to error. While the TDM measurements at both heights do not reproduce the 1:1 relationship between emissions and wind speed that was specified in the model, CH_4 emissions clearly increase with wind speed. Thus, hypothesis #1 cannot be disproved: if local CH_4 emissions vary with wind speed causing wind-induced variations of whole landfill emissions, TDM emissions measurements may also be correlated with wind speed.

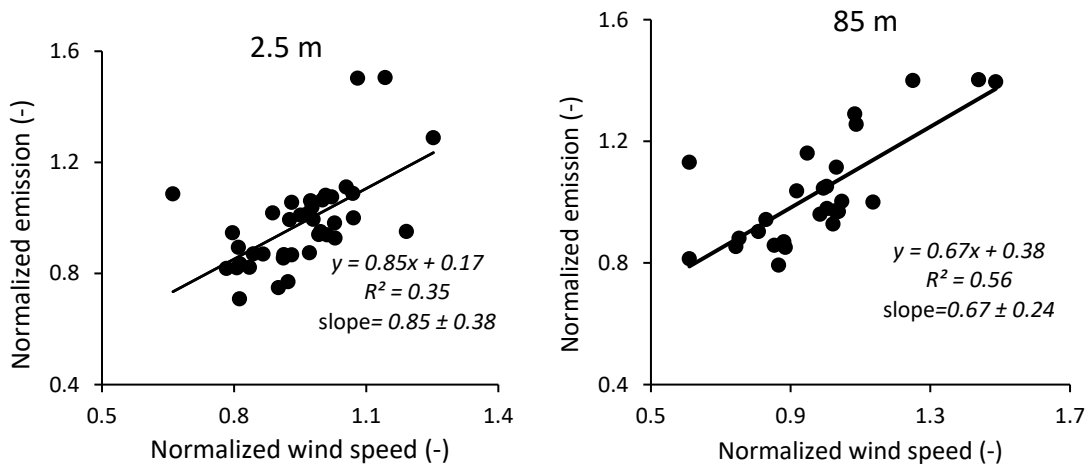


Figure 2.8 Same as Figure 2.7 except using data filtering: R2 and second derivative of wind velocity criteria.

The failure to reproduce the 1:1 relationship between emissions and wind speed is associated, we believe, with mixing of high and low emissions plumes between successive sampling times. This effect is illustrated with the 2 s data in Figure 2.6: high actual emissions are slightly underpredicted with VF2/CF1 downwind measurements, while low actual emissions are overpredicted. This effect can be described mathematically

$$C_{CH_4}^{low} < C_{CH_4}^{downwind} = \frac{C_{CH_4}^{high} \times P^{high} + C_{CH_4}^{low} \times P^{low}}{P^{high} + P^{low}} < C_{CH_4}^{high} \quad (2.8)$$

where $C_{CH_4}^{high}$ and $C_{CH_4}^{low}$ are mean CH₄ concentrations in downwind plumes during high and low emissions, respectively, and P^{high} and P^{low} are plume volumes correspond to $C_{CH_4}^{high}$ and $C_{CH_4}^{low}$ emissions periods. Gas plumes from the landfill move at different speeds because of wind speed variations. If portions of these plumes mix by the time they reach the downwind measurement location, observed $C_{CH_4}^{downwind}$ will be a weighted average concentration of the two plumes and fall between $C_{CH_4}^{high}$ and $C_{CH_4}^{low}$. Thus, high CH₄ emissions will be slightly underestimated and low CH₄ emissions slightly overestimated because of plume mixing, and the observed sensitivity of emissions with wind speed using downwind data will be less than at the landfill surface. This is the reason that the 1:1 relationship between emissions and wind speed imposed in the VF2/CF1 simulation may be less than 1:1 (slope less than 1) for downwind measurements at 2.5 and 85 m AGL.

2.3.5 Testing Hypothesis 2: Heterogeneous but Steady Emissions

It is possible that TDM-measured CH₄ emissions might exhibit a correlation with wind speed on the landfill surface if *local* CH₄ emissions vary with wind speed even if whole landfill emissions are constant. The simulation pair VF1/CF1 was used to test this

hypothesis, where VF1 represents spatially-varying CH₄ emissions due to local variations in wind speed (equation (2.6)) and CF1 represents a constant tracer emission perfectly aligned with CH₄ emission (equation (2.3)).

Data from the VF1/CF1 simulation pair were filtered as described above and results are plotted in Figure 2.9. For measurements at 2.5 and 85 m AGL, emissions were not correlated with wind speed: $R^2 = 0.02$ and 0.11 for 2.5 and 85 m AGL, respectively. These results are relatively insensitive to filtering, with $R^2 \leq 0.14$ for all conditions examined (see Table 2.1). Thus, hypothesis #2 is disproved: if local CH₄ emissions vary with wind speed but whole landfill emissions are constant, TDM emissions measurements will not be correlated with wind speed.

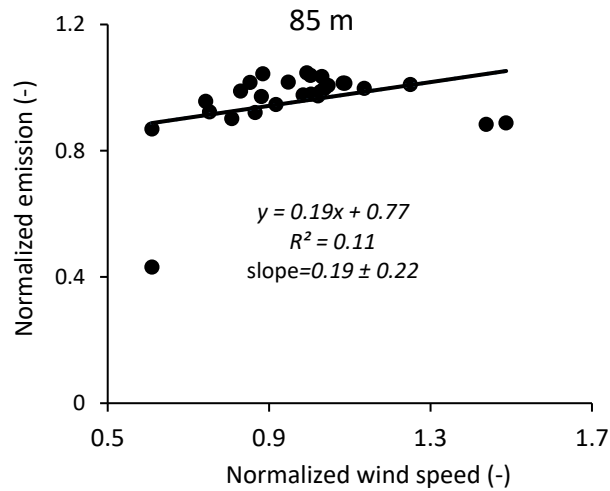
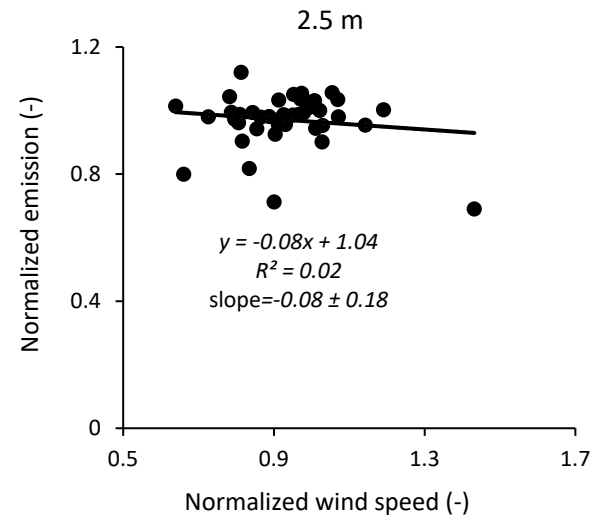


Figure 2.9 Normalized emissions calculated with TDM using 1-min data from simulation pair VF1/CF1 at 2.5 and 85 m AGL at measurement location in Figure 2.1. Emissions plotted versus normalized wind speed on landfill surface with data filtering: R^2 and second derivative of wind velocity criteria. 95% confidence intervals on individual data points are so small as not to be visible.

2.3.6 Testing Hypothesis 3: Steady Emissions and Misalignment of Tracer

For steady CH₄ emissions, misalignment of tracer and CH₄ emission locations may cause TDM-measured emissions to exhibit a correlation with wind speed. The simulation pairs CF1/3Pts and CF2/3Pts were used to test this hypothesis, where for these simulation pairs alone CF1 and CF2 represented spatially uniform and temporally constant CH₄ emissions (equations (2.3) and (2.4)), and 3Pts represented constant tracer emissions from three locations corresponding to field tracer release points (equation (2.2)). Misalignment of CF1 and 3Pts is primarily parallel to the mean wind direction, while CF2 and 3Pts are misaligned perpendicular to the mean wind direction. The centers of CF1 and 3Pts, or CF2 and 3Pts emission sources were 250 m or 175 m apart, respectively.

Data from the CF1/3Pts simulation pair were filtered following the procedures described above and results are shown in Figure 2.10. For measurements at 2.5 and 85 m AGL, emissions were not correlated with wind speed: $R^2 = 0.001$ and 0.05 for 2.5 and 85 m AGL, respectively. These results are insensitive to filtering, with $R^2 \leq 0.06$ for all conditions examined (see Table 2.1). Tracer misalignment parallel (CF1/3Pts) or perpendicular (CF2/3Pts) to the mean wind direction did not result in a statistical meaningful relationship between wind speed and CH₄ emissions. Thus, hypothesis #3 is disproved: if local CH₄ emissions are constant but significantly misaligned with tracer emission locations, TDM emissions measurements will not be correlated with wind speed.

Table 2.1 Linear regression of normalized methane emission versus normalized wind speed for three simulation pairs with and without data filtering.

Simulations	Data type							
	Unfiltered				Filtered			
	Ground height (2.5m)		Airborne height (85 m)		Ground height (2.5m)		Airborne height (85 m)	
	Slope \pm 95%CI	R^2	Slope \pm 95%CI	R^2	Slope \pm 95%CI	R^2	Slope \pm 95%CI	R^2
VF1/CF1	-0.05 \pm 0.13	0.01	0.13 \pm 0.15	0.06	-0.08 \pm 0.18	0.02	0.19 \pm 0.22	0.11
CF1/3Pts	-0.20 \pm 0.56	0.008	-0.36 \pm 0.47	0.03	-0.14 \pm 1.32	0.001	-0.58 \pm 0.83	0.05
CF2/3Pts	-0.81 \pm 2.22	0.006	1.51 \pm 6.85	0.003	-0.96 \pm 3.78	0.01	-2.00 \pm 4.34	0.11
VF2/CF1	0.89 \pm 0.28	0.39	0.43 \pm .20	0.31	0.85 \pm 0.38	0.35	0.67 \pm 0.24	0.56

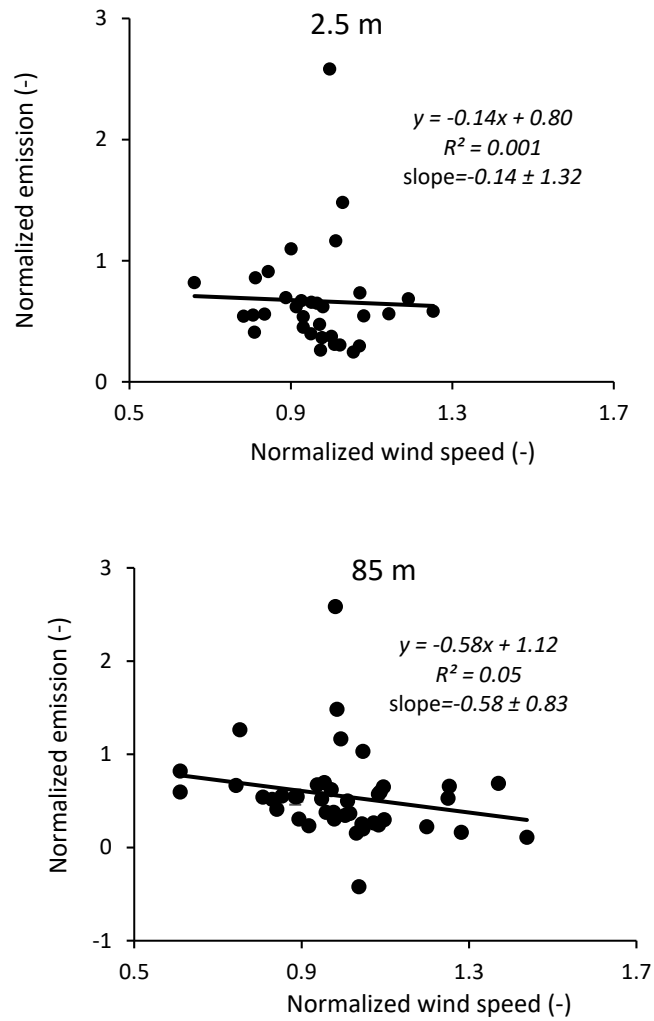


Figure 2.10 Normalized emissions calculated with TDM using 1-min data from simulation pair CF1/3Pts at 2.5 and 85 m AGL at measurement location in Figure 2.1. Emissions plotted versus normalized wind speed on landfill surface with data filtering: R^2 and second derivative of wind velocity criteria. 95% confidence intervals on individual data points are so small as not to be visible.

2.3.7 Field Emission Correlation with Wind

Atmospheric dispersion model simulations indicate that for the conditions at Sandtown Landfill on March 6, 2010, if CH₄ emissions vary with wind speed at the landfill surface a correlation between emissions and wind speed might be detected with TDM. TDM data from the field test at Sandtown Landfill were analyzed to assess if CH₄ emissions were correlated with wind speed. Here, the same data filtering techniques developed for the model simulations were applied. A sensitivity analysis of the results to the filtering criteria is discussed in Appendix A. The travel times from landfill surface to measurement location were determined using simulation 3Pts, since tracer emissions were not dependent on wind speed and located in close proximity to actual field tracer release points, therefore accurately tracking the wind path. $\bar{V}(t)$ at the landfill surface was taken from wind monitor data.

The results from this analysis are shown in Figure 2.11. As with the simulations, data are normalized with mean CH₄ emissions (emissions data) or mean wind speed (wind data) to facilitate comparison with simulation results. There are fewer data points from the field compared to simulations for two reasons. First, field data were only collected for 18 and 31 1-min measurement windows at 2.5 and 85 m AGL, respectively, while simulation data were available for 120 1-min measurement windows at both heights. Second, there was more scatter in gas concentrations in the field data than in the simulations, likely because of greater small-scale mixing in the field that was not captured with the model. This resulted in visible error bars for field data in Figure 2.11 and more data that violated the $R^2 > 0.80$ criterion.

At 2.5 and 85 m AGL field data were positively correlated with wind speed: $R^2 = 0.51$ and $R^2 = 0.55$, respectively. However, the data are sparse at 2.5 m and it is difficult to draw conclusions about the wind dependency of emissions at this height. While linear regressions were used to evaluate the relationship between wind speed and emissions, the actual relationship may be nonlinear. The variations of emissions with wind speed can be compared with previous measurements over a portion of a landfill (McBain et al., 2005). McBain et al. (2005) found emissions linearly correlated with wind speed between ≈ 1.3 to 5.8 m/sec ($R^2 = 0.48$) with the slope of normalized mission versus normalized wind speed approximately 0.67. The correlation with wind speed in this field study was similar to that of (McBain et al., 2005), although the sensitivity of emissions to wind speed was greater here with the slope of the regressed line 2.00 ± 5.94 and 2.20 ± 1.63 at 2.5 and 85 m AGL, respectively.

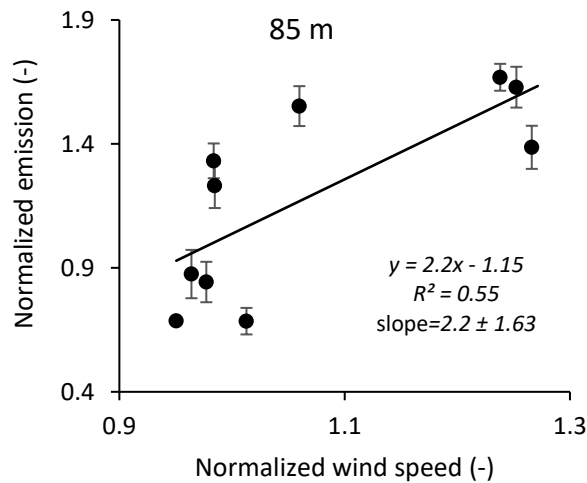
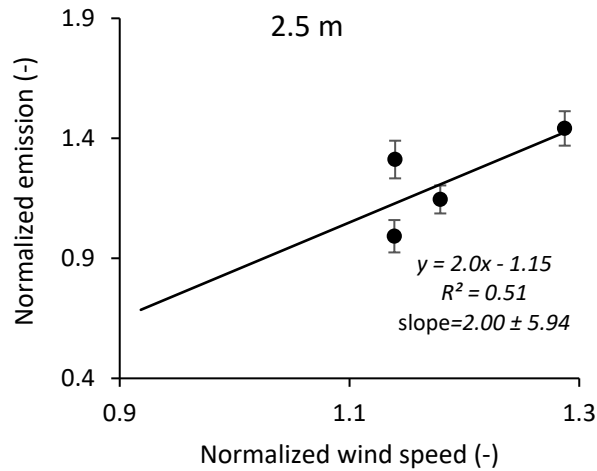


Figure 2.11 Normalized emissions calculated with TDM using 1-min field data at 2.5 and 85 m AGL at measurement location in Figure 2.1. Emissions plotted versus normalized wind speed on landfill surface with data filtering: R^2 and second derivative of wind velocity criteria.

The greater sensitivity of CH₄ emissions to wind speed at Sandtown Landfill versus that determined by McBain et al. (2005) may have been due to wet landfill conditions at Sandtown. Although the landfill cover soil moisture was not quantified during the

Sandtown Landfill field test, the landfill and landfill cover were wet with some near-surface gas collection wells clogged with leachate (Munyan, 2010). Conversely, McBain et al. (2005) reported that their landfill cover soil was dry. Gas pressure fluctuations at the landfill surface caused by wind turbulence and their impact on landfill gas emissions were simulated by Poulsen and Moldrup (2006). In a sensitivity analysis, Poulsen and Moldrup (2006) showed that wind-induced landfill gas fluxes were more significant for wet conditions when air-filled porosities were small. Although total gas fluxes are likely smaller in wet landfill covers because of the reduction in gas permeability and gas diffusion through the soil, Poulsen and Moldrup (2006) found that the relative importance of wind on emissions is more significant for such conditions. Thus, the greater sensitivity of TDM-measured emissions to wind speed in this study than that found by McBain et al. (2005) for eddy covariance measurements may have been due to a wetter cover soil at Sandtown Landfill.

Because McBain et al. (2005) showed wind-induced landfill gas emissions could be important for wind speeds greater than or equal to 1.3 m/sec and since the tracer dilution method typically requires wind speeds greater than 1 m/sec (Jakober et al., 2015), landfill emissions measured using TDM may be affected by wind. Therefore, TDM emissions measurements may be systematically higher than CH₄ emissions averaged over periods of high and low wind speed conditions at some landfills.

2.4 Conclusions

The objectives of this work were to determine if short-term variations in whole-landfill CH₄ emissions measured with TDM might be due to variation of wind speed, and to evaluate the utility of atmospheric dispersion modeling for understanding the influence of atmospheric conditions on emissions measurements. A field experiment was conducted at the Sandtown Landfill, Delaware, and an atmospheric model developed for the site that described atmospheric conditions and gas plume transport. This is the first application of an atmospheric dispersion model to a landfill for understanding gas transport patterns that we are aware of. The atmospheric model provided a reasonable match to measured wind speed and direction on the landfill surface and downwind tracer concentration at the measurement location.

The atmospheric model was then used to generate synthetic data and examine the correlation between TDM-measured CH₄ emissions and wind speed on the landfill surface at Sandtown Landfill. Three hypotheses were tested: TDM emissions measurements will be correlated with wind speed if (1) local CH₄ emissions vary with wind speed causing wind-induced variations of whole landfill emissions, (2) if the spatial distribution of CH₄ emissions varies with wind speed but whole landfill emissions are constant, and (3) if local CH₄ emissions are constant but significantly misaligned with tracer emissions locations. Using computer simulations the only hypothesis not disproved at Sandtown Landfill was hypothesis (1), indicating that wind-induced variations of whole landfill emissions could result in similar variations in TDM emissions measurements. Using the travel times between the landfill and the downwind measurement location from the atmospheric

dispersion model, field data were analyzed and showed a correlation between emissions and wind speed on the landfill surface, with emissions increasing by a factor of 2 as wind speed increased by approximately 30% (85 m AGL data). Higher gas concentrations and a larger signal to noise ratio were observed for data collected at 85 m than 2.5 m AGL. Thus, for some landfills and atmospheric conditions, measurements significantly above ground level may result in more accurate emissions estimates.

This study examined CH₄ emissions for a 2-h measurement period from a single landfill. While the results indicate that short-term variations in emissions determined from TDM were likely due to wind speed variations on the landfill surface, the significance of this effect for whole-landfill emissions at other landfills is unknown. Future study at other landfills is needed before generalizing this result. Based on the work of Poulsen and Moldrup (2006), wind-induced emissions will be more important for wet landfill covers with small air-filled porosity and for high wind speeds, where wind-induced turbulence is greater.

If indeed CH₄ emissions from landfills are wind dependent for some landfill cover conditions, landfill gas management might be altered to improve gas collection under such conditions. For example, under windy conditions for a wet landfill cover when emissions are expected to be more sensitive to wind speed, landfill gas extraction might be increased to decrease CH₄ concentrations in cover soils that would result in a reduction in emissions. This might be feasible without causing undesired air ingress into the landfill, since soil gas permeability decreases significantly as cover soils become wet (Poulsen and Moldrup, 2006). In addition, if CH₄ emissions from landfills are wind dependent, care should be

exercised in extrapolating whole-landfill emission measurements made under particular wind conditions to emissions under different atmospheric conditions.

Chapter 3

DIURNAL LANDFILL METHANE FLUX PATTERNS ACROSS DIFFERENT SEASONS AT A LANDFILL IN SOUTHEASTERN US

This chapter is a version of the paper entitled “Diurnal landfill methane flux patterns across different seasons at a landfill in Southeastern US”, submission planned to the *Waste Management* Journal. Because of no limitation in number of figures and tables the dissertation compared to the *Waste Management* Journal, some figures from supporting information were moved to the main body of this chapter. These figures and table are: Fig. 3.1, Fig. 3.2, Fig. 3.3, Fig. 3.4, Fig. 3.6, and Table 3.1.

3.1 Introduction

Landfills are estimated to contribute approximately 16% of the anthropogenic methane emissions in the United States (US EPA, 2019). To develop or evaluate measures to control emissions or to estimate emissions for greenhouse gas inventories, it is necessary to quantify methane emissions from individual landfills. Most emission-quantifying methods (e.g., tracer dispersion method (TDM) and flux chambers) are conducted over a few hours (Mønster et al., 2019). It is common to calculate the average of these short-term emission measurements during a single day as the measured emission rate for that day (Mønster et al., 2015; De la Cruz et al., 2016); however, methane emissions vary with

atmospheric parameters including wind speed (Delkash et al., 2016), air temperature (Teclé et al., 2009), atmospheric pressure (Xu et al., 2014), and solar radiation (Xin et al., 2016). Because of diurnal variations of these atmospheric parameters, methane fluxes from landfills, particularly those without final covers, vary diurnally as well. Thus, short-term emission-quantifying methods may inaccurately estimate average diurnal emissions.

As one solution, models could be used to predict emissions during unmeasured periods. However, most inventory models including IPCC (IPCC, 2006) and LANDGEM (Thorneloe et al., 1999) only consider the amount of organic waste landfilled to estimate annual methane emissions and ignore emission fluctuations caused by atmospheric and soil conditions. Among models that account for methane transport processes, the California Landfill Methane Inventory Model (CALMIM) (Spokas et al., 2011) assumes molecular diffusion describes methane mass transfer through cover soils and landfill emissions, and the Weather Research and Forecasting Model (WRF) with the Noah land surface model has been used to estimate gas emissions as a function of atmospheric and soil conditions (Taylor et al., 2018). The advancement of models that account for processes affecting diurnal emission fluctuations would allow better estimates of daily and annual emissions from field measurements typically limited to daylight hours. Alternatively, it may be possible to determine optimal measurement times during the day where short-term measurements provide reasonable estimates of diurnal emission rates.

To investigate these issues, an eddy covariance (EC) dataset collected between June 2012 and February 2013 at a Southeastern US landfill is considered. Because this landfill had mostly an intermediate cover ($\geq 90\%$) and lacked a gas collection system, atmospheric

parameters may have been more important in controlling emissions than at other sites with gas collection. Data were collected during three periods with different soil moisture and temperature conditions: dry and warm (June 2012); wet and cold, after a rainfall event (December 2012); and wet and cool (February 2013). Analysis of these data provide insight into diurnal methane flux patterns at this landfill and may be indicative of diurnal variations at other landfills too. This study investigates the correlations between methane flux and atmospheric parameters and is also intended to evaluate if the significant diurnal changes in methane emissions predicted from model simulations at two landfills, the Sandtown Landfill in Delaware US (Taylor et al., 2018) and this Southeastern US landfill (Taylor, 2017), are consistent with field data.

3.2 Theory

Methane moving up from buried solid waste encounters resistances until it reaches the atmosphere. For a daily or intermediate landfill cover, methane first passes through the soil cover. The resistance in soil depends on soil moisture (Poulsen and Møldrup, 2006), wind speed that may produce short-term pressure pumping (Poulsen and Møldrup, 2006) and may be modeled as increased molecular diffusion (Pourbakhtiar et al., 2017), and temperature that affects molecular diffusion (Massman, 1998). Molecular diffusion is often assumed to be the dominant transport process in cover soils (Spokas et al., 2011); however, advective gas flux may be important if significant cracks form (Weisbrod and Dragila, 2006). Thicker final covers slow vertical gas transport and provide sufficient time for

methane oxidation. As methane nears the ground surface, methane transport may be affected by vegetation and topsoil (Bian et al., 2018; Abichou et al., 2015).

After moving through the vegetation and/or topsoil, methane is transported through a quasi-laminar boundary layer by molecular diffusion (Wyngaard, 2010). This resistance is a stagnant air film on the ground surface and its thickness ranges from a few millimeter (typical conditions) to several meters (low wind conditions), depending on gas type and shear velocity (u^*) (see Appendix B) (Pleim and Ran, 2011; Wesley and Hicks, 1977). Shear velocity is a measure of the near-surface shear stress and it is not a real wind speed (De Visscher, 2013). Because wind speed increases as elevation from the ground increases, shear stress forms near the surface, which can induce turbulence. Atmospheric turbulence can be described by the velocity fluctuations in the horizontal and vertical directions, u' and w' , respectively, where $u = \bar{u} + u'$ and \bar{u} = mean wind speed (m s^{-1}) (De Visscher, 2013). Shear velocity can be defined in terms of the covariance between these velocity fluctuations, u' and w' :

$$u^* = \sqrt{\overline{w'u'}} \quad (3.1)$$

As the average product of the perturbations in horizontal and vertical wind increase, u^* increases. Because u' varies with mean horizontal wind speed (Calif et al., 2008; Stull, 1988; Wyngaard, 2010), u^* also increases with wind speed.

Above the quasi-laminar boundary layer, methane flux occurs through the aerodynamic layer. While the thickness of the quasi-laminar boundary layer and thus this layer's resistance is affected by u^* , turbulence and the upward flux of methane in the

aerodynamic layer is affected by u^* . An additional process affecting transport in the aerodynamic layer is atmospheric buoyancy, which is related to vertical variations of air temperature and results in different atmospheric stability conditions: stable (lighter air over heavier), neutral (minimal stratification in air density), and unstable (heavier air over lighter). (See Appendix B for further discussion and classification of atmospheric stability.) Finally, atmospheric pressure variations may cause vertical pressure gradients in the landfill cover soil and induce upward (or downward) gas flow, which affects methane flux in some situations.

Flux of methane from landfill waste into the atmosphere will be controlled by transport through the most resistive layer, which is commonly thought to be the cover soil (Bogner et al., 1997; De Visscher and Van Cleemput, 2003; Spokas et al., 2011). However, as shown by multiple experimental (e.g., Rees-White et al., 2019; Xu et al., 2014; Gebert et al., 2011) and modeling studies (Jung et al., 2009; Poulsen and Møldrup, 2006), atmospheric conditions can affect transport through cover soil. For example, Bahlmann et al. (2020) utilized experiments and numerical modeling to demonstrate that wind enhances multidimensional gas transport even in low permeability soils, and that this effect is enhanced for low density gases, like methane. They found that wind enhances subsurface gas transport and increases vertical concentration gradients, causing enhanced diffusion in soil. Thus, while methane flux can be described by transport through a series of layers, transport in these layers may not be independent from processes in the atmosphere affecting transport through the soil and vegetation/topsoil layers. Atmospheric conditions and their

influence on methane flux through the landfill cover soil, vegetation/topsoil, quasi-laminar boundary layer, and aerodynamic layer are discussed in more detail in Appendix B.

Wind speed, atmospheric buoyancy associated with vertical variations of air temperature, and atmospheric pressure fluctuations affect gas flux through the four resistance layers listed above. While there is no universally accepted model describing these effects on landfill gas emissions, a first-order mass transfer equation for methane flux was recently used to describe these effects using the WRF model (Taylor et al., 2018)

$$Q = C_d u^* (c_{topsoil} - c_{atmosphere}) \quad (3.2)$$

where C_d is the bulk transfer coefficient that is a function of atmospheric stability and air density ($-$), and $c_{topsoil}$ and $c_{atmosphere}$ are methane concentrations at 5 cm depth in the topsoil and about 7.5 m above ground in the atmosphere ($\frac{g}{m^3}$), respectively. This equation explicitly includes wind impacts on emissions through u^* , while C_d represents the influence of atmospheric stability. The atmospheric stability is a function of heat and momentum fluxes, which are related to variations in buoyancy (air temperature gradients) and pressure. The field measurements in this paper are used to evaluate the importance of atmospheric parameters on methane emissions at one landfill site, and to assess if their variability supports the diurnal changes in methane emissions predicted from application of Eq. 3.2 to two landfills (Taylor, 2017; Taylor et al., 2018).

3.3 Material and Methods

3.3.1 Site Description

The Southeastern US landfill selected for this study has been operated since 2010 with an annual waste placement rate of 264-330 thousand tons that increased to 1.16 million metric tons in 2013 (De la Cruz et al., 2016). There was no active gas collection system during the methane flux measurements reported in this study. During this period, the landfill was covered primarily by an intermediate cover with a small area of daily cover (<5%). The cover soil is a clay loam (USDA classification) with ~ 35% clay and ~ 47% sand. The intermediate cover ranged between 0.3 and 0.9 m in thickness and was approximately 0.6 m thick across most of the landfill. Topographic maps of the landfill from approximately the time of the field measurements for this study are shown in Figure 3.1.

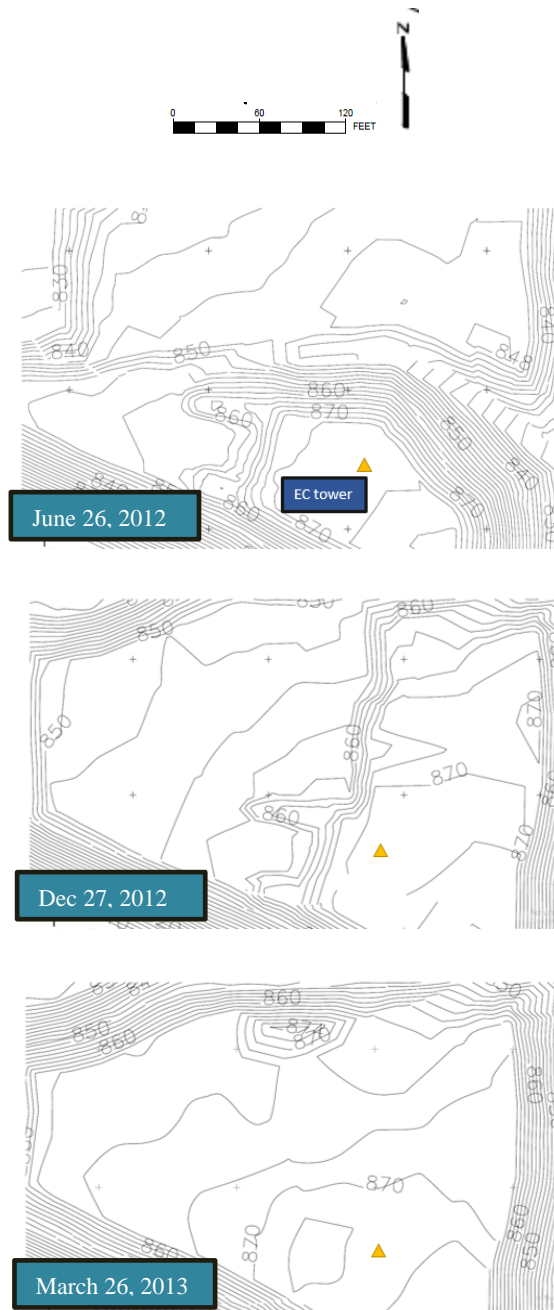


Figure 3.1 Topography of the landfill at the nearest date to each test period. The date of surveying is shown bottom left of each map. The EC tower location is displayed by yellow triangle.

3.3.2 Methane Flux Measurements

An EC tower (LI-7500A Open Path CO₂/H₂O Analyzer) was placed at a fixed spot on the landfill summit between April 2012 and May 2013 to measure high frequency methane concentrations and meteorological parameters including wind data at 2.25 m above ground level. The EC method applies statistical analysis to estimate vertical gas flux averaged for a certain time range, typically 30 min (Lohila et al., 2007; Mc Bain et al., 2005; Laurila et al., 2005; Xu et al., 2014). The 30-min averaged vertical methane flux was estimated using $c_{CH_4}^{air}$

$$Q_{CH_4} = \frac{1}{t_2 - t_1} \int_{t_1}^{t_2} (c_{CH_4}^{air}(t) - \overline{c_{CH_4}^{air}})(w(t) - \overline{w}) dt \quad (3.3)$$

where Q_{CH_4} is the estimated flux ($\frac{kg}{s m^2}$), $c_{CH_4}^{air}$ is methane concentration in the air, overbars are 30-min averaged quantities, and t_1 and t_2 initial and final times over which Q_{CH_4} is measured (Burba, 2013; Xu et al., 2014).

In addition to EC methane flux measurements, 495 independent tracer dilution method (TDM) measurements were conducted periodically over 34 days between 2011 and 2013 (Foster-Wittig et al., 2015). At most sites including the Southeastern US landfill, the TDM is usually deployed during daytime when the atmosphere has some instability (Foster-Witting et al., 2015; Mønster et al., 2015). To help determine whether any meteorological parameter is correlated with methane emissions in a 24-hour period under a particular atmospheric stability condition, the TDM dataset was used to confirm the results found by the EC data. The TDM data represents the whole-landfill methane emissions (landfill area 10,000~ m² in this study), while the EC method quantifies

emissions over a portion of the landfill surface. Because TDM measures mass emissions, e.g., kg/min, the emissions were divided by the landfill area (192,451 m²) to convert to flux for comparison with the EC data (Li et al., 2015).

3.3.3 Time Periods of Investigation

Because methane emissions may depend on soil and atmospheric conditions that vary diurnally and seasonally, three 7- to 8-day periods were considered between June 2012 and February 2013 that encompassed a range of conditions. Air temperature data were measured 2.25 m above ground with the EC tower, while soil volumetric water content was estimated from measurements at 10 cm depth at the three nearest weather stations that encircled the landfill within a radius of 47 km. Daily measurements of the air temperature and soil volumetric water contents are reported in Figures 3.2 – 3.4 for June 2012 through February 2013.

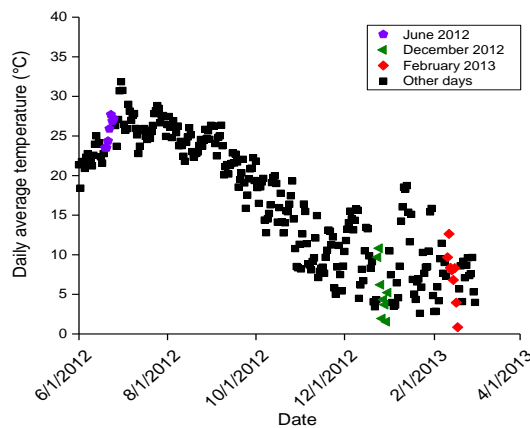


Figure 3.2 Temporal variations of daily-averaged T obtained from EC tower.

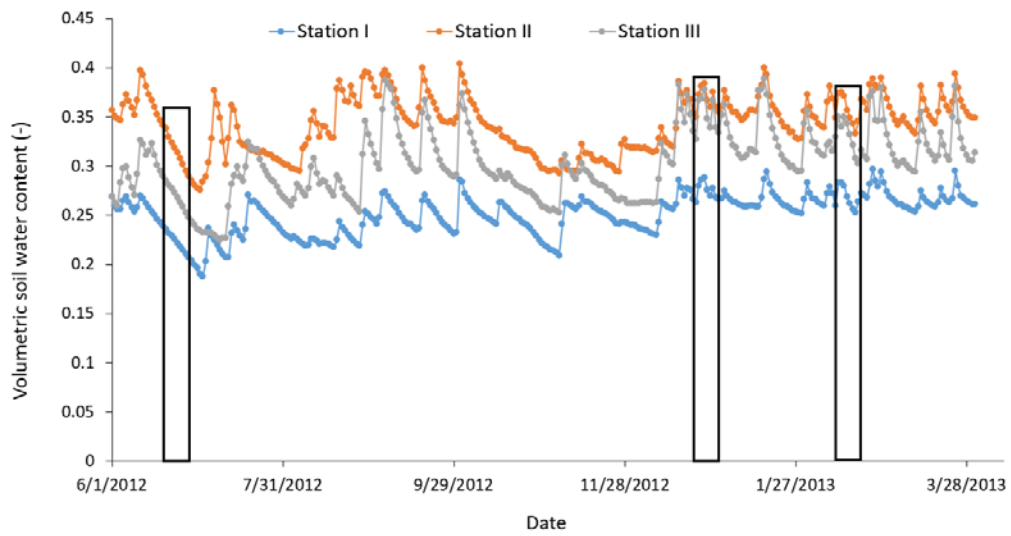


Figure 3.3 Temporal variations of daily-averaged volumetric soil moisture (at 10 cm depth) between June 2012 and February 2013 measured at three nearest weather stations (each about 47 km distance from the landfill). The black boxes indicate the three studied periods.

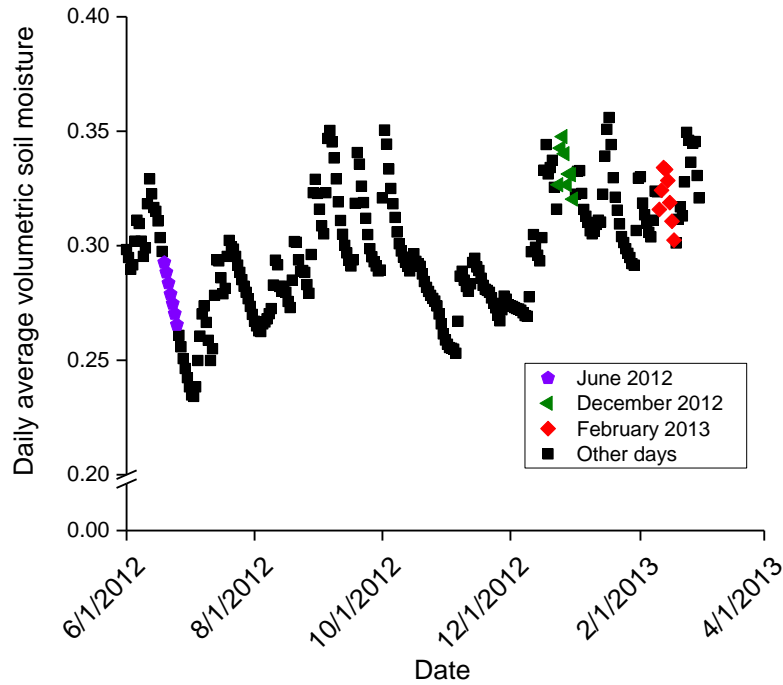


Figure 3.4 Daily average volumetric water content at 10 cm depth between June 2012 and February 2013 measured at three nearest weather stations (each about 47 km distance from the landfill).

During the first period (between June 19 and 25, 2012), the landfill cover soil was dry (volumetric water content, $\theta_w = 0.28 \pm 0.03$ SE, SE = one estimated standard error of the mean) and the air warm (26.9 ± 0.5 SE °C); for the second period (between December 24 and 31, 2012) the soil was wet ($\theta_w = 0.33 \pm 0.03$ SE) and the air cold (6.5 ± 1.4 SE °C); and for the third period (between February 10 and 17, 2013) the soil was wet ($\theta_w = 0.32 \pm 0.03$ SE) and the air slightly warmer (9.2 ± 1.6 SE °C). We hypothesize that the number and total volume of connected gas-filled soil pores was reduced in December 2012 and February 2013, and soil resistance played a more important role in methane emissions

than June 2012. Field measurements indicate that the fraction of the generated methane that was oxidized in June (OX=0.4 measured on 6/28/2012) was greater than in winter (OX= 0.14 measured on 12/5/2012 and OX=0.03 measured on 3/7/2013) (De la Cruz et al., 2016). Thus, biological processes were expected to be less relevant for methane flux in December and February.

3.3.4 EC Data Filtering

Although the EC method provides a long-term dataset of methane concentrations and meteorological parameters, not all recorded data are useful. First, since one purpose of this study is to investigate correlations between meteorological parameters and diurnal methane flux, the range of diurnal wind direction variation was limited to 90° for each 24 h (midnight to midnight) to keep the contributing area relatively “fixed”. Thus, for EC data collected during any 24 h period, measurements were only used in this analysis when wind direction was within a specified 90° quadrant as shown in Figure 3.5. This quadrant might shift between days due to wind direction variations but was fixed for any one day.

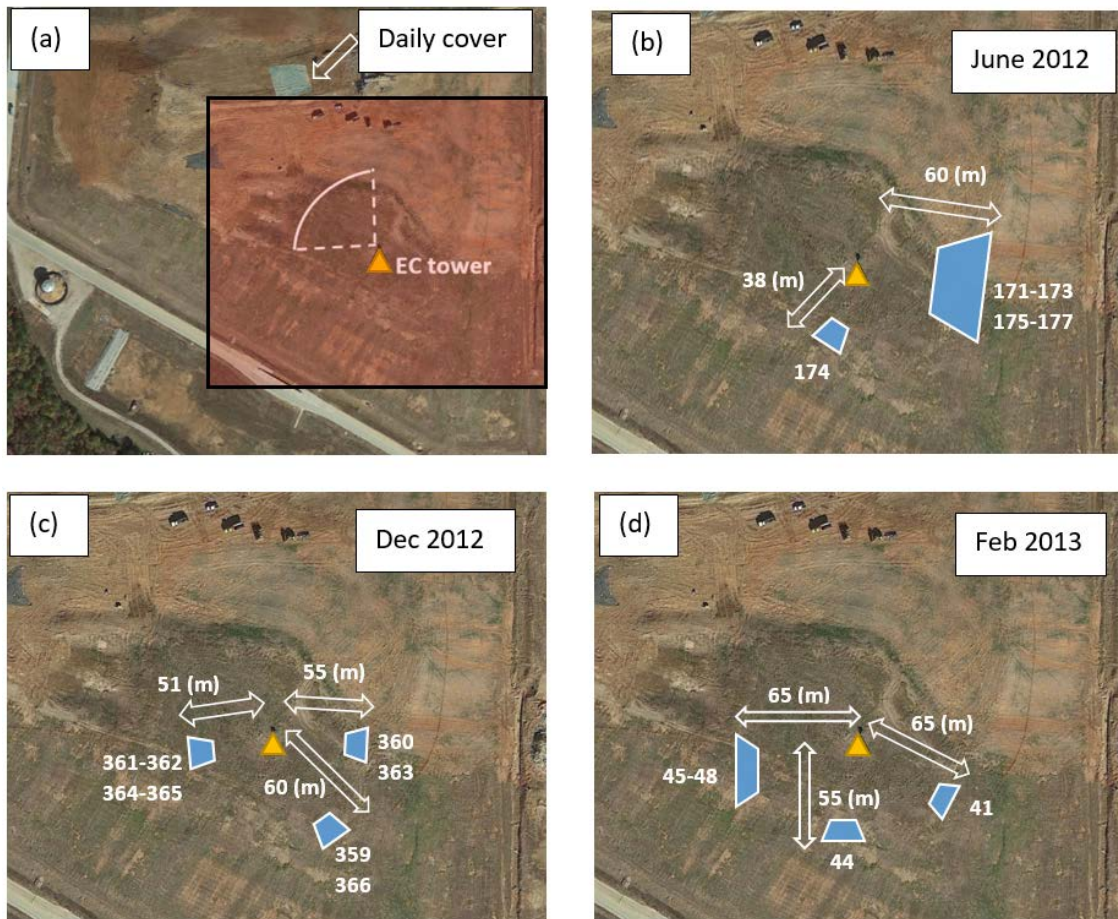


Figure 3.5 Scheme of field measurements. The EC tower is shown with a yellow triangle. (a) Illustration of the 90° filter for wind direction. The transparent rectangle shows the area of focus in the other figures. Locations of x_{50} are within blue shaded regions for (b) June 2012; (c) December 2012; and (d) February 2013. The blue arrows indicate the distance between the EC tower location and x_{50} locations, while white numbers are Julian days associated with the EC measurements that occur in each blue region. The error tolerance of these illustrations is less than 10 m.

Second, data with $u^* < 0.1 \text{ m s}^{-1}$ were discarded to ensure that there was sufficient turbulence for mixing the near-surface gas and to diminish the influence of spatial heterogeneity in emissions on measurements of the average flux using the EC tower (Lohila

et al., 2007; Xu et al., 2014). Xu et al. (2014) concluded that this criterion ensures good mixing in the atmosphere and results in sufficiently accurate emission measurements even when point sources such as vents are present on the landfill surface.

Third, data with a large fetch (> 200 m) were neglected to keep the emissive areas inside the landfill (Li et al., 2015; Xu et al., 2014). The locations of x_{50} , the distance from the EC tower to the location where 50% of the total contributed plume is measured from, are shown in the blue shaded areas of Figure 3.5 for each of the test periods. Text in white are Julian days and are indicated for each blue region. All x_{50} locations were within the intermediate cover region. Interestingly, x_{50} was less variable in December and February than June, which we postulate is due to a greater proportion of neutrally stable conditions in December and February.

3.3.5 Correlations Between Methane Flux and Meteorological Parameters

Two hypotheses have been postulated in the literature for the influence of P_{atm} on methane flux: either instantaneous P_{atm} (Czepiel et al., 2003; Gebert and Groengroeft, 2006) or $\frac{dP_{atm}}{dt}$ (Xu et al., 2014) are negatively correlated with methane flux (detailed discussion in Appendix B). These hypotheses were examined to determine if they can explain variations in methane flux from the landfill. Thirty-minute average P_{atm} was used in our analyses: For example, P_{atm} averaged between 14 and 14:30 was ascribed to methane measurements for the same time period. For the second hypothesis, the backward

pressure differences between two consecutive 30-min average measurements were used to estimate temporal pressure variations

$$\frac{dP_{atm}}{dt} \approx \frac{P_{atm,2} - P_{atm,1}}{t_2 - t_1} \quad (3.4)$$

where $P_{atm,1}$ and $P_{atm,2}$ are the measured P_{atm} at consecutive times t_1 and t_2 , respectively. In this hypothesis, for example, the difference in average P_{atm} between 13:30 and 14:00 ($P_{atm,1}$) and the average P_{atm} between 14:00 and 14:30 ($P_{atm,2}$) were examined for their correlation with average methane flux between 14:00 and 14:30 of a certain day.

Incoming solar radiation can warm the ground and near-surface atmosphere causing buoyancy and unstable atmospheric conditions. Although Xin et al. (2016) found that solar radiation correlated better with methane flux than atmospheric temperature (T) for a landfill covered with vegetation, T was selected as the independent variable rather than solar radiation in our study for three reasons. First, T correlated better with methane flux than solar radiation during daytime at this site, which may be due to less vegetation on the landfill cover compared to the site that Xin et al. (2016) investigated. Second, T affects other factors discussed above, e.g., methane diffusion and oxidation. Third, when net solar radiation was negative (mostly during nighttime) no meaningful statistical relationship between solar radiation and methane flux was found. Aghdam et al. (2019) also found T to be more strongly correlated than solar radiation with the methane extracted from gas collection systems in two landfills with poor vegetation in Denmark. Therefore, T may sufficiently represent the impact of the solar radiation on flux for some situations.

While most previous research investigating the influence of wind on emissions focused on u (Delkash et al., 2016; McBain et al., 2005), the surface flux is formulated with u^* (Eq. 3.2). Therefore, u^* was selected for correlation analysis here. Since u^* and u are related to each other by a site-specific coefficient, which for this study was $u^* \approx 0.1u$ (see Appendix B), the results for the impact of u^* on methane flux should be similar to that for u .

In summary, four parameters were selected to evaluate their correlation with methane flux: P_{atm} , $\frac{dP_{atm}}{dt}$, T , and u^* . Correlations were examined for each day in the three measurement periods described earlier and for unstable and neutral atmospheric conditions. All EC data collected under stable conditions were filtered out because all had $u^* < 0.1 \text{ m/s}$. The methodology for determining atmospheric stability conditions at the site is described in Appendix B.

During a typical day, unstable atmospheric stability conditions usually occurred during daytime, while neutral atmospheric stability conditions were most frequent in the early morning and evening. Correlations were only examined among data for each stability condition. Only days with at least six independent measurements for each stability condition were included to have a meaningful statistical analysis. Although all the days had sufficient number of neutral data to be involved in the analysis, only six, one, and two measurement days had sufficient unstable data for June 2012, December 2012, and February 2013, respectively.

3.3.6 Statistical Tests for Significance of Correlations

Two criteria were used to rank significance of the correlations between each meteorological parameter and methane flux: the Pearson correlation coefficient (R), and the absolute ratio of the 95% confidence interval (CI) on the best-fit slope to the fitted slope from linear regression $\left| \frac{95\% \text{ CI}}{\text{slope}} \right|$. A dataset exhibits a moderate to strong correlation if $R > 0.5$ (Mukaka, 2012). Here, we selected 0.5 as the minimum R for which meaningful correlations were concluded to exist between the methane flux and meteorological parameter. The fraction of days in each measurement period where $R > 0.5$ is also reported, which is a measure of how persistent the correlation was during each measurement period.

The 95% CI of the slope is a measure of the uncertainty in the slope, and the dimensionless $\left| \frac{95\% \text{ CI}}{\text{slope}} \right|$ is a relative measure of the confidence in the best-fit slope. The meteorological parameter with the smallest $\left| \frac{95\% \text{ CI}}{\text{slope}} \right|$ for a linear regression between the meteorological parameter and methane flux is the parameter with the best correlation with flux.

3.4 Results

3.4.1 Meteorological Parameter Dependency

The primary parameters that affect landfill gas emissions over diurnal periods have been suggested to be P_{atm} , $\frac{dP_{atm}}{dt}$, T , and u^* (or u) (Xu et al., 2014; Park and Shin, 2001; Delkash et al., 2016). The correlations between these four parameters are shown in Table

3.1 and Figure 3.6. In general, at this landfill T is positively correlated with u^* : when air temperatures rise so generally does wind shear velocity. On the other hand, P_{atm} and $\frac{dP_{atm}}{dt}$ show a general negative correlation with both u^* and T .

Table 3.1 Correlation coefficients between the meteorological parameters (P = atmospheric pressure; T = air temperature; u = shear velocity; dP/dt = temporal variations of atmospheric pressure) for different measurement periods. The standard errors of the daily-average correlation coefficients are shown with \pm values.

Date	Length (day)	Correlation coefficient					
		T vs. P	P vs. u_*	T vs. u_*	T vs. $\frac{dP}{dt}$	P vs. $\frac{dP}{dt}$	$\frac{dP}{dt}$ vs. u_*
June	1	-0.27±0.15	-0.05±0.12	0.79±0.02	-0.47±0.07	0.05±0.05	-0.49±0.06
	7	-0.31	-0.21	0.73	-0.42	0.12	-0.51
December	1	-0.43±0.60	-0.08±0.18	0.15±0.18	0.09±0.07	-0.15±0.08	0.10±0.03
	7	-0.34	0.47	0.19	0.06	0.06	0.04
February	1	-0.40±0.44	-0.23±0.15	0.57±0.08	-0.38±0.09	0.27±0.09	-0.33±0.15
	7	-0.23	-0.18	0.38	-0.45	-0.02	-0.30
Year 2012	365	-0.35	-0.18	0.38	-0.21	0.36	-0.29

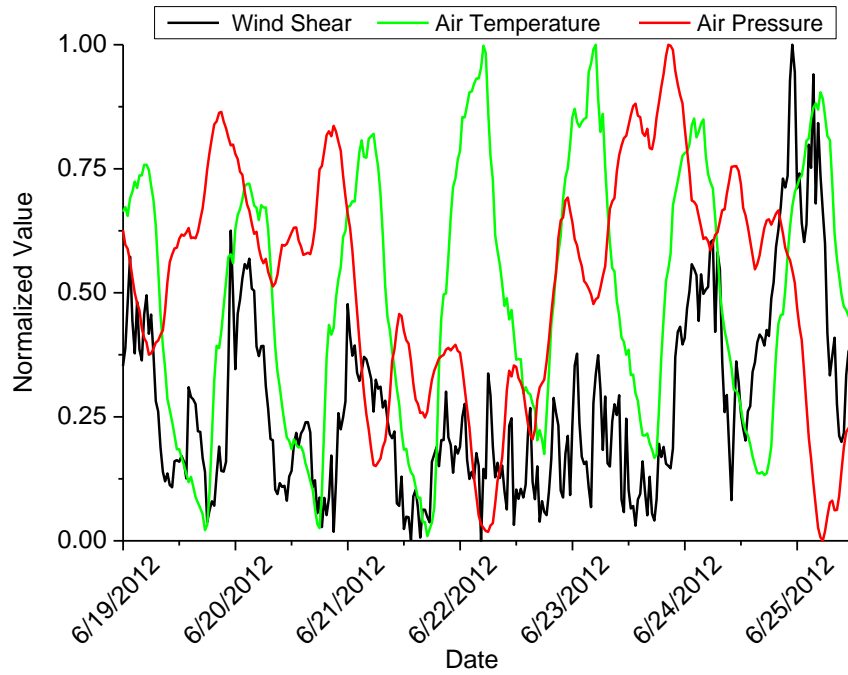


Figure 3.6 Temporal variations of the normalized 30-min averaged meteorological parameter $\left(\frac{X_i - X_{min}}{X_{max} - X_{min}}\right)$ between June 19 and 25, 2012. Air pressure is detrended.

Previous investigations have shown that landfill methane emissions are higher under windy conditions (Delkash et al., 2016), higher T (Park and Shin, 2001) and lower P_{atm} (Xu et al., 2014). Because high u^* , high T , and low P_{atm} and $\frac{dP_{atm}}{dt}$ often coincide (Table 3.1 and Figure 3.6), it may be difficult to ascribe changes in methane emissions to a single meteorological parameter. Instead, we suggest considering “emission-increasing atmospheric conditions” when air temperature and wind speed are high and air pressures low, and “emission-decreasing atmospheric conditions” when air temperature and wind

speed are low and air pressures are high. Occurrence of these emission-driving atmospheric conditions depend on climatic patterns at the geographic location of each landfill.

3.4.2 Pressure-Induced Flux

The results of correlations between each meteorological parameter and methane flux are compiled in Table 3.2. Data are grouped for each measurement period (June, December, and February) and for either unstable or neutral atmospheric conditions. The instantaneous P_{atm} is always negatively correlated with flux, and it has the weakest correlation among the meteorological parameters: in June, 50% and 14% of the days with an unstable or neutral atmosphere have $R > 0.5$, respectively.

Table 3.2 Correlation coefficient of each meteorological parameter with methane flux under different atmospheric conditions and time periods. The N is the number of days during each period that have either unstable or neutral atmospheric conditions. Fraction is the fraction of measurement days in the 7 or 8 day period where $R > 0.5$. Note that R is only calculated if at least six data points are available.

Month	Parameter	Unstable			Neutral		
		<i>N</i>	Fraction $R > 0.5$	Average [95% CI/slope]	<i>N</i>	Fraction $R > 0.5$	Average [95% CI/slope]
June	P_{atm}		0.5	-2.46		0.14	-3.06
	$\frac{dP_{atm}}{dt}$	6	0.83	-1.19	6	0.67	-1.64
	u^*		0.67	2.08		0.33	0.90
	T		1	0.85		0.33	1.30
Dec	P_{atm}		1	-1.67		0.25	-2.37
	$\frac{dP_{atm}}{dt}$	1	0	-12.50	8	0.75	-0.68
	u^*		0	4.78		0.25	1.37
	T		1	0.03		0.25	1.43
Feb	P_{atm}		0.5	-9.85		0.43	-3.56
	$\frac{dP_{atm}}{dt}$	2	1	-5.57	7	0.71	-0.45
	u^*		1	1.57		0.86	0.45
	T		0.5	0.35		0.71	0.70

Just as in June, P_{atm} had the poorest correlation with methane flux in December and February: the fraction of days with $R > 0.5$ was smallest (or equal to the smallest) of

all meteorological parameters for both unstable and neutral atmosphere, and mean $\left| \frac{95\% \text{ CI}}{\text{slope}} \right|$ was the largest. The only exception was for single day in December where unstable atmospheric conditions existed, where $\frac{dP_{atm}}{dt}$ and u^* were more poorly correlated with flux.

In the second approach, correlations were examined between $\frac{dP_{atm}}{dt}$ and methane flux. Similar to instantaneous P_{atm} , $\frac{dP_{atm}}{dt}$ was always negatively correlated with flux. During unstable atmospheric conditions in June, 83% of days (five out of six days) had $R > 0.5$ and average $\left| \frac{95\% \text{ CI}}{\text{slope}} \right| = 1.19$. Thus, the fraction of $R > 0.5$ was larger and $\left| \frac{95\% \text{ CI}}{\text{slope}} \right|$ smaller than analyses with P_{atm} , indicating better correlation. Similar results are reported for correlations under neutral conditions in June: $\frac{dP_{atm}}{dt}$ was better correlated with flux than P_{atm} , where four of six days had $R > 0.5$ and average $\left| \frac{95\% \text{ CI}}{\text{slope}} \right| = 1.64$.

Unstable atmospheric conditions occurred for one and two days in December and February testing periods, respectively. Correlations with methane flux for unstable conditions improved using $\frac{dP_{atm}}{dt}$ rather than P_{atm} in February: fraction of days with $R > 0.5$ increased from 0.5 to 1, and $\left| \frac{95\% \text{ CI}}{\text{slope}} \right|$ decreased from 9.85 to 5.57. Similarly, for neutral stability conditions, $\frac{dP_{atm}}{dt}$ correlated better with methane flux than P_{atm} in both December and February: analyses using $\frac{dP_{atm}}{dt}$ had a larger fraction of days with $R > 0.5$ and smaller

$\left| \frac{95\% \text{ CI}}{\text{slope}} \right|$. Overall, results at this landfill for all measurement periods indicate that $\frac{dP_{atm}}{dt}$ correlates better with methane flux than P_{atm} .

The importance of $\frac{dP_{atm}}{dt}$ on methane flux may be influenced by the gas permeability of the landfill cover soil and the peak-to-peak amplitudes of P_{atm} . In December and February when $\frac{dP_{atm}}{dt}$ was more strongly correlated with methane flux than in June, soils were wetter which increased resistance to diffusive relative to advective gas transport in soil. In addition, peak-to-peak amplitudes of P_{atm} for June, December, and February were 2 kPa, 6 kPa, and 5 kPa, respectively. The increased importance of gas advection and the greater peak-to-peak amplitudes of P_{atm} in winter months were contributing factors to the improved correlation between $\frac{dP_{atm}}{dt}$ with methane flux. These factors are discussed in more detail in Appendix B.

3.4.3 Wind-Induced Flux

Table 3.2 shows that u_* is strongly correlated with methane flux under a neutral atmosphere. In June and February, u_* has the smallest average $\left| \frac{95\% \text{ CI}}{\text{slope}} \right|$ under neutral atmospheric conditions with values of 0.90 and 0.45, respectively. It is worth reiterating that u^* and u are related to each other by a site-specific coefficient that is a function of the domain geometry (see Appendix B).

When the soil is wettest in December, though, the correlation between u^* and flux is weaker. In the June 2012 and February 2013 time periods, the air can intrude farther into the soil (drier soil) that results in a more noticeable impact of u^* on the flux. Maier et al. (2012) found that wind-induced pressure pumping was more important for higher permeability soils. Figure 3.7 displays the relationship between methane flux and u^* for February 2013. At this site, u^* is the dominant meteorological parameter affecting flux when the atmospheric stability condition is neutral.

The correlation between u^* and flux under neutral conditions is stronger during February 2013 than June 2012 (Table 3.2). We postulate that a higher methane oxidation rate in June 2012 than February 2013 contributed to this result. High u^* can cause greater air intrusion into a dry cover soil (Pourbakhtiar et al., 2017). Therefore, increasing u^* would enhance oxygen intrusion and methane oxidation more in June 2012 than February 2013. Measurements of methane oxidation rate reported by De la Cruz et al. (2016) are consistent with this argument. De la Cruz et al. (2016) reported the fraction of methane oxidized decreased from OX=0.4 in June 2012 to OX=0.14 in December 2012 and OX=0.03 in March 2013 for this landfill. Therefore, while u^* increases the methane flux from the cover soil, it also enhances oxygen intrusion and the oxidation of methane to carbon dioxide. These opposite effects might explain the weaker correlation between u^* and methane flux in June 2012 than February 2013.

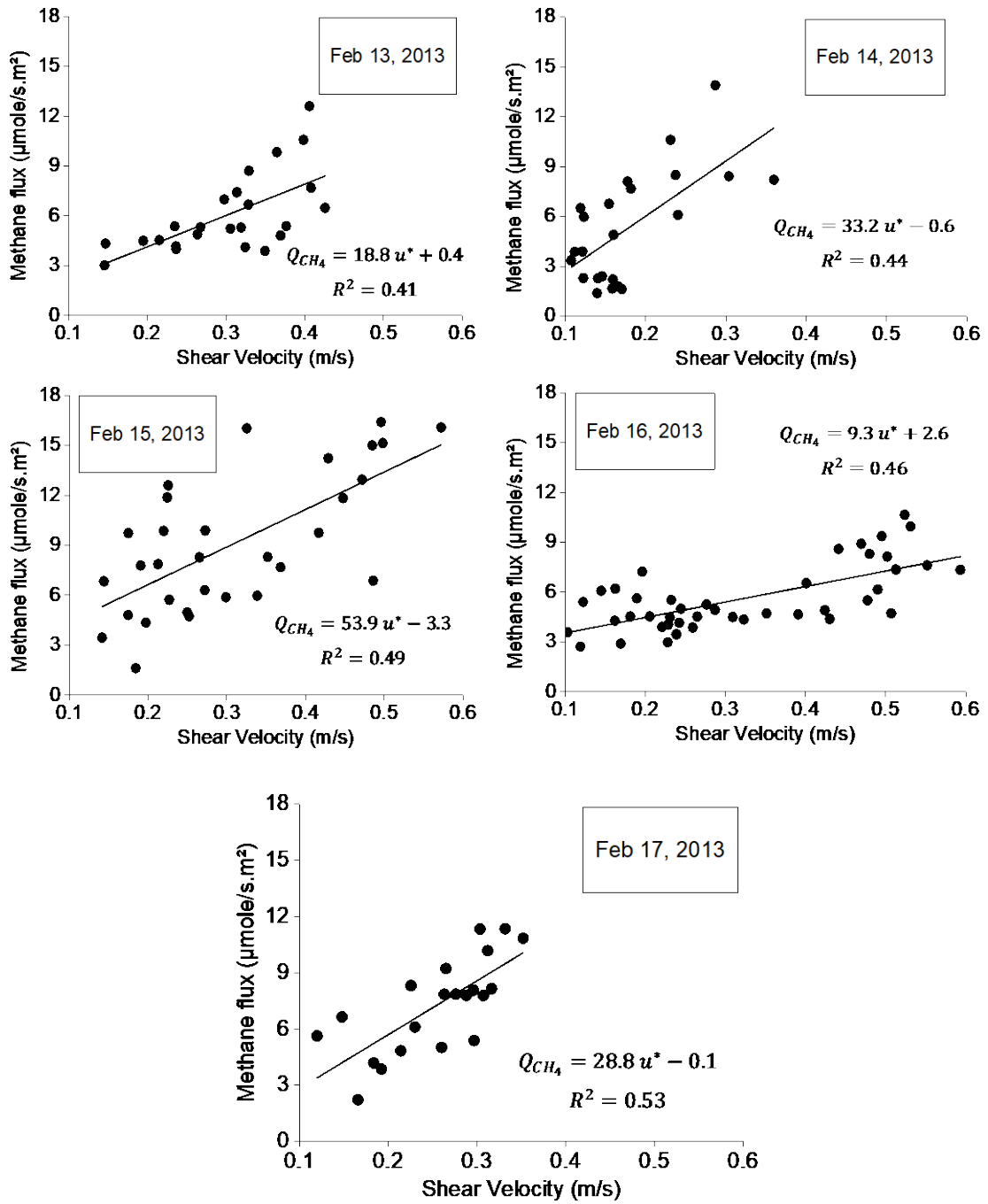


Figure 3.7 Temporal variations of methane flux measured by the EC tower versus u^* under neutral atmosphere for February 2013.

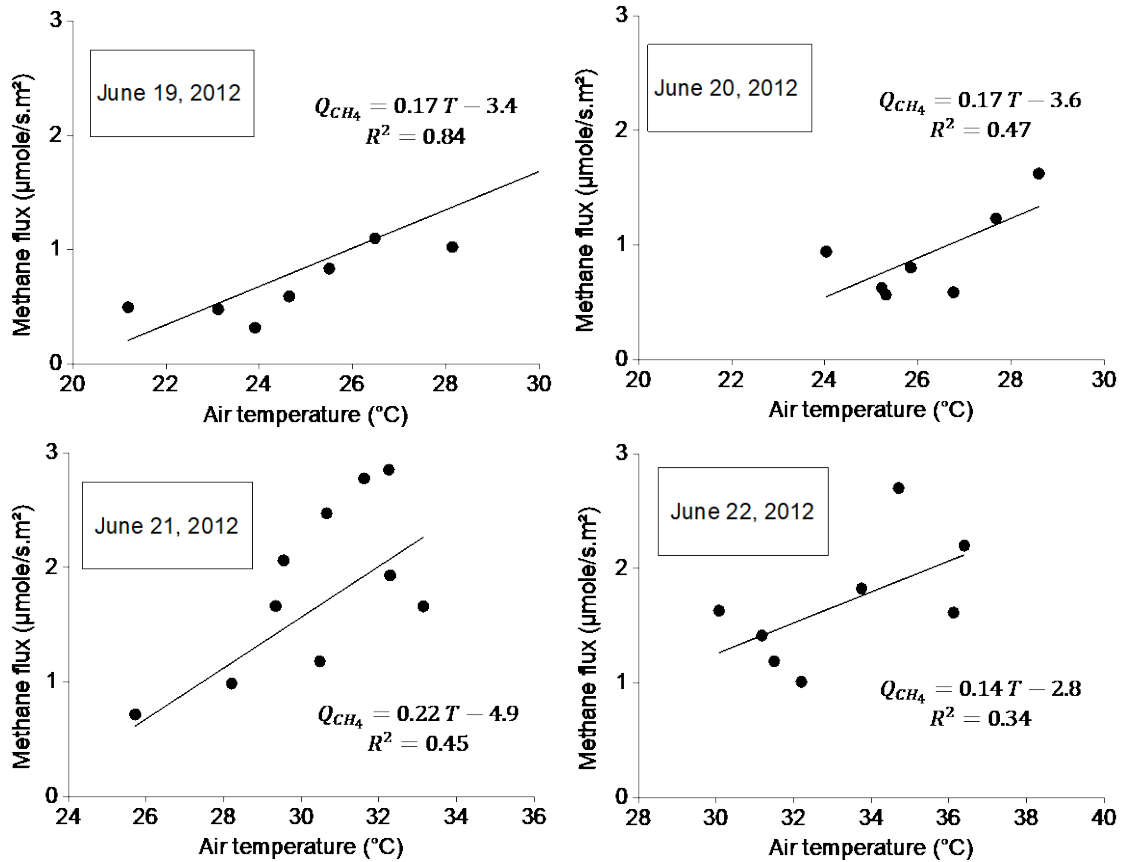
Because detailed wind field data are not available, the correlation between shear velocity and methane emissions using TDM is not investigated in this paper. As Delkash et al., (2016) discussed, wind impact investigations on methane emissions using TDM require extensive wind field observations and atmospheric modeling for every single measurement to determine the travel time (the time methane travels from the landfill to the downwind measurement area). Because the wind shear velocity (i.e. wind speed) changes in seconds, this travel time is required to subtract from measurement times to determine the emission time.

The analyses for unstable atmospheric conditions indicate a weaker correlation between u^* and methane flux compared to neutral atmospheric conditions, where the correlation is strongest. For example in June, four days had $R > 0.5$ with an average $\left| \frac{95\% \text{ CI}}{\text{slope}} \right| = 2.08$ among the six days in this period with unstable atmospheric conditions.

3.4.4 Buoyancy-induced flux

As noted, u^* was strongly correlated with methane flux under neutral conditions. On the other hand, T exhibited the strongest correlation with flux for unstable conditions: all six unstable days in June had $R > 0.5$ and average $\left| \frac{95\% \text{ CI}}{\text{slope}} \right| = 0.85$. Buoyancy plays an important role in turbulence formation for unstable atmospheric conditions and is more intense as near-surface air temperature increases. Thus, T may be the best predictor of emissions among the investigated meteorological parameters for unstable conditions at this site. Figure 3.8 depicts the relationship between T and flux for June 2012. On all days, T is

positively correlated with methane flux, which is consistent with the literature. McBain et al. (2005), Tecele et al. (2009), and Xin et al. (2016) found positive correlations between methane flux and T . Therefore, although increases in temperature generally enhance methane oxidation, at this site and in some other studies this effect is less significant than the enhanced mixing from near-surface turbulence that occurs at elevated T , since methane flux generally increase as T increases.



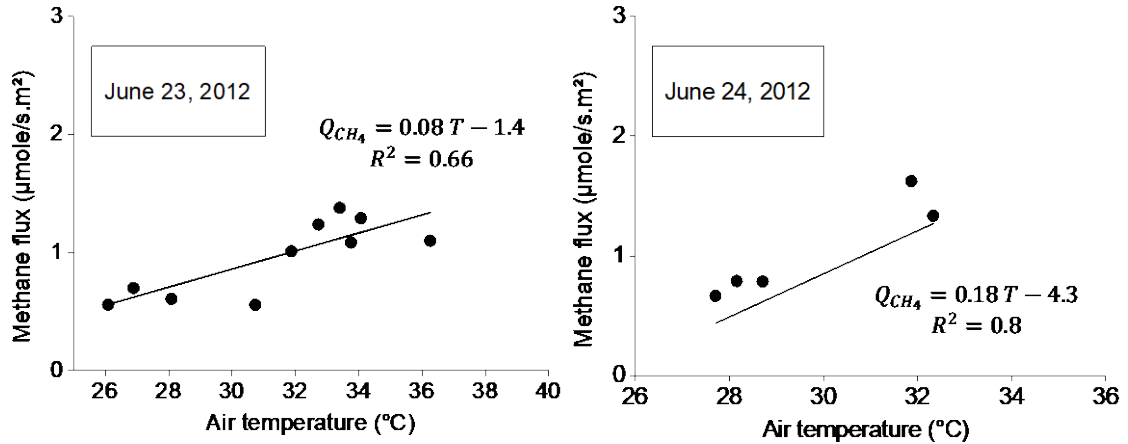


Figure 3.8 Variations of methane flux measured by the EC tower with T under unstable atmosphere for June 2012.

While the number of unstable days in December and February are insufficient to draw robust conclusions about the effect of meteorological parameters on methane flux for these conditions, the available data suggest that T correlates better than the other meteorological parameters for unstable conditions on these days too. As indicated in Table 3.1, average $\left| \frac{95\% \text{ CI}}{\text{slope}} \right|$ values for the correlation between T and flux are 0.03 and 0.35 for days with unstable atmospheric conditions in December and February, respectively.

Although Table 3.2 indicates that T has noticeable correlations with flux under a neutral atmosphere, this correlation is weaker than for unstable atmospheric conditions. Only two days in June with a neutral atmosphere have $R > 0.5$ with $\left| \frac{95\% \text{ CI}}{\text{slope}} \right| = 1.3$. Similar to June, the performance of T as a flux predictor in December and February may be better for unstable than neutral atmosphere.

Based on the EC data, TDM emissions were expected to be positively correlated with T under both unstable and neutral atmospheric conditions. Field measurements were selected for days where TDM measurements covered a sufficient portion of the day such that air temperatures varied at least 4°C. The correlation between methane flux measured by the TDM and T for March 8, 2013 when the atmosphere was unstable is shown in Figure 3.9. The results of TDM data for other days with neutral atmospheric conditions between April 2012 and May 2013 are shown in this Figure as well. A positive correlation ($0.6 < R < 0.81$) is found between methane flux and T , which is consistent with the results obtained with EC data (Figure 3.8). The regression slope between whole-landfill emissions and T is stronger than that for EC emissions: slopes range between 0.17 and 1.04 for TDM measurements (Figure 3.9), but only between 0.08 and 0.22 for EC data (Figure 3.8). This may be because whole-landfill emissions capture methane emitted from regions of daily and intermediate cover while EC measurements were only from the intermediate cover regions. Daily cover emissions are expected to be more sensitive to atmospheric turbulence than intermediate cover regions, since the daily cover soil is thinner.

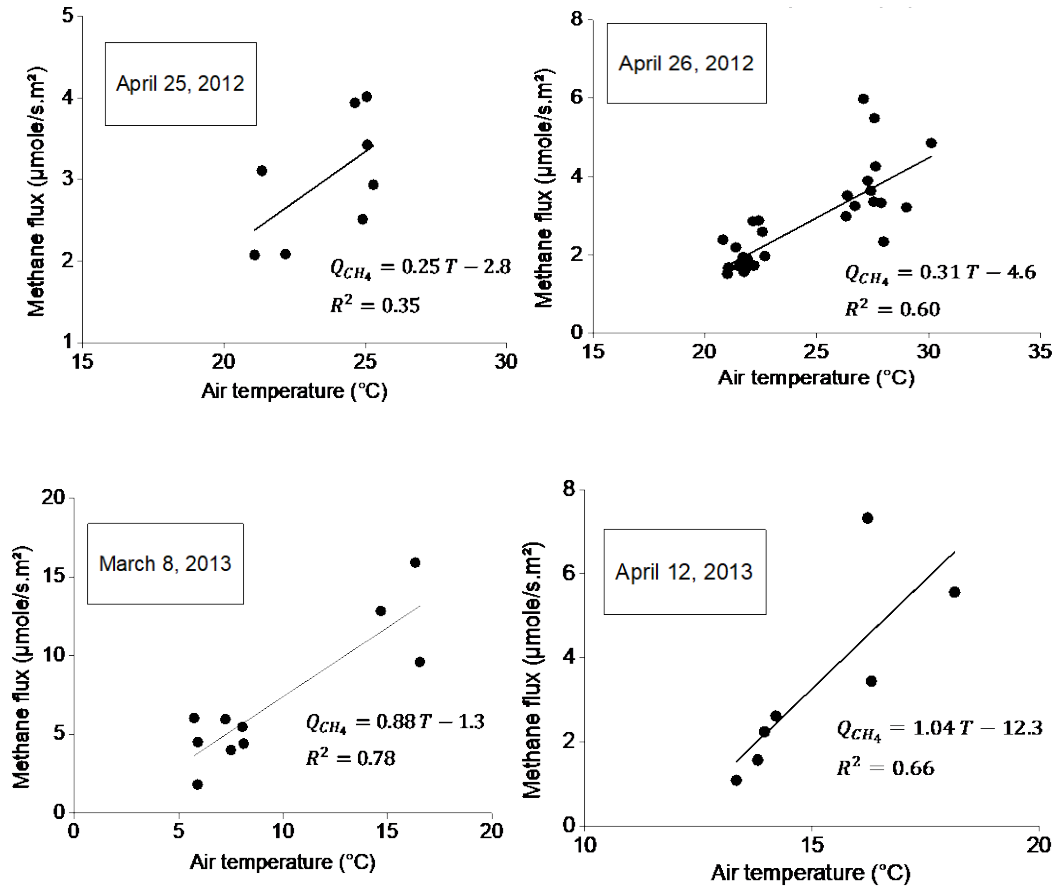


Figure 3.9 Temporal variations of TDM flux versus T for March 8, 2013.

3.5 Implications

3.5.1 Validity of WRF Methane Flux Equation

Models for methane emissions from landfills that only include soil resistance may be biased if atmospheric processes significantly affect transport through the soil, which likely occurred at this site. As an effort to incorporate Eq. 3.2 into modeling of methane

emission from landfills, Taylor et al. (2018) employed Eq. 3.2 in the WRF atmospheric model to describe methane flux between shallow soil and the atmosphere. This equation explicitly indicates that u^* affects gas flux, which is consistent with observations in this study and the literature (Delkash et al., 2016; Frey et al., 2013).

Although our statistical results show a positive correlation between T and methane flux especially under unstable atmospheric conditions, T is not explicitly shown in Eq. 3.2. It is well known that for an unstable or neutral atmosphere warmer air near the surface implies greater instability (de Visscher, 2013) and larger eddy diffusivity (K_z) in the atmospheric boundary layer (Eq. B8). Larger K_z leads to a larger aerodynamic conductance ($C_D u^*$) in Eq. 3.2 (Seigneur, 2019). Thus, the positive correlation between methane flux and T for unstable and neutral atmospheric conditions is consistent with Eq. 3.2.

Methane fluxes at this landfill are negatively correlated with $\frac{dP_{atm}}{dt}$, which has been reported in several other studies for emissions from landfills (Xu et al., 2014; Gebert and Gröngröft, 2006). While Eq. 3.2 does not explicitly include the effect of atmospheric pressure on emissions, we reiterate that u^* , T , and $\frac{dP_{atm}}{dt}$ do not behave independently. In this study, u^* and $\frac{dP_{atm}}{dt}$ are negatively correlated for December and February ($R = -0.49 \pm 0.06SE$ and $-0.33 \pm 0.15SE$, respectively, Table 3.1), and very weakly correlated in June ($R = 0.10 \pm 0.03SE$). Thus, when barometric pressure decreased at this site, wind shear velocity and methane flux usually increased. Based on this observation, Eq. 3.2 indirectly accounts for some of the effects of barometric pressure change on methane flux.

3.5.2 Diurnal Variations of Methane Flux

Our analysis of the EC data reveals that diurnal variations of methane flux correlate positively and most strongly with T under an unstable atmospheric condition and with u^* under neutral conditions. For this landfill, these meteorological parameters change diurnally, with both T and u^* generally higher during daytime. This implies that methane fluxes may have diurnal patterns at other landfills where meteorological parameters vary diurnally. However, the amplitude of the variations depends on landfill gas generation rate, presence of gas collection system, cover properties (type and thickness), and the range of variation in meteorological parameters. Table 3.3 presents the time of maximum and minimum EC fluxes on each measurement day after applying the filtering criteria described in Section 3.3.4. For this landfill, the highest methane flux usually occurred in the afternoon between 12:30 and 15:00, whereas the lowest flux happened in the early morning between 4:00 and 10:00 or at night after 20:00. The ratio of maximum to minimum flux on any one day varies between 1.81 and 23.20 for the investigated days. The coefficient of variation of the fluxes measured for each day ranges between 0.22 and 0.67.

Table 3.3 Diurnal variations of methane flux in the studied periods: June 2012, December 2012, and February 2013.

Day	Number of filtered data	Time of max flux (h)	Time of min flux (h)	max/min flux ratio [-]	COV flux [-]
171	25	13	4	7.53	0.48
172	29	14	7.5	4.68	0.38
173	20	14.5	8	5.78	0.43
174	16	22	19	3.99	0.49
175	20	12.5	9.5	3.77	0.37
176	25	13	7.5	4.58	0.38
177	36	16	20.5	9.21	0.38
359	10	2	16.5	3.86	0.27
360	10	13	10	7.29	0.57
361	27	8	17.5	2.77	0.26
362	16	16.5	10	3.77	0.31
363	16	14.5	4.5	3.26	0.4
364	34	11.5	10	5.5	0.53
365	27	13	9.5	23.2	0.67
366	19	12.5	9.5	4.91	0.29
41	31	13	8	10.09	0.45
42	-	NA	NA	NA	NA
43	5	8	10	1.81	0.22
44	24	13.5	20.5	4.17	0.39
45	27	14	6.5	10.07	0.59
46	24	14	22.5	7.87	0.51
47	43	13	2	3.91	0.35
48	21	14.5	8	5.1	0.35

To further verify the significant diurnal flux variations found from EC data, the temporal flux variations measured by TDM are shown in Figure 3.10 for the days in 2011-2013 when measurements spanned at least five hours. On all days, methane flux was smallest in the morning, with flux increasing during the afternoon and decreasing in the late evening. TDM fluxes varied significantly during each day, with fluxes generally

highest between 14:00-16:00, consistent with the EC measurements. While the TDM data in the winter (November 2011 and December 2012) show a descending trend in the late evening, descending trends are not seen in the summer data (April 2012, April 2013, and June 2013). Because of the later time of sunset in the summer (~ 21:00) than the winter (~18:00), the transition from an unstable to a stable atmosphere occurs later in day in the summer. Therefore, later TDM measurements may be required in summer to capture descending emission trends.

The TDM plots in Figure 3.10 are consistent with the EC data, and similar diurnal landfill methane fluxes have been reported from flux chamber measurements (Teclé et al., 2009; Xin et al., 2016; Gebert et al., 2011). For instance, Teclé et al. (2009) found higher methane fluxes measured by a flux chamber during daytime and lower fluxes during nighttime for an inactive landfill with 90-cm thick final clay cover. Diurnal gas flux variations were reported from agricultural soils as well: Shurpali et al. (2016) measured nitrous oxide flux from soils in Finland and found a clear diurnal trend with maximum during daytime and minimum during nighttime.

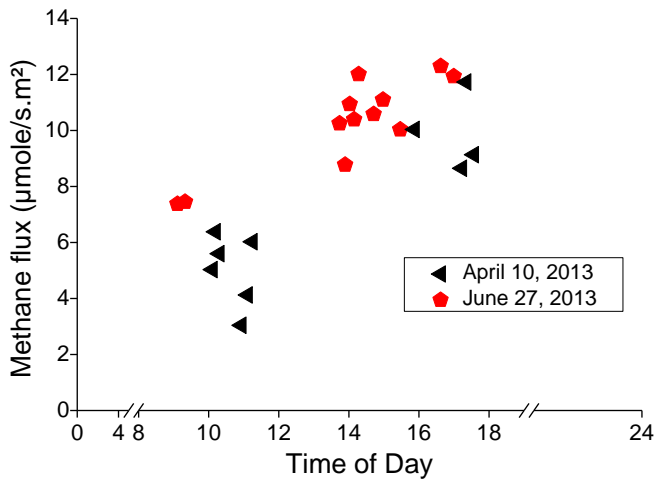
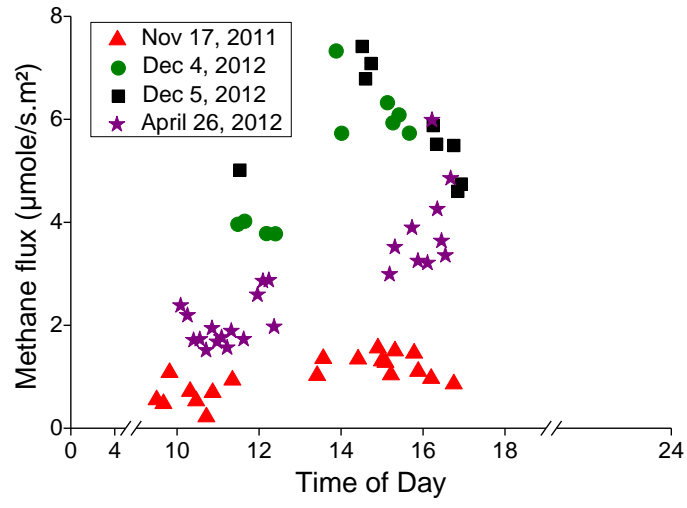


Figure 3.10 Examples of diurnal flux variations measured by the TDM at the Southeastern US landfill. The dataset is filtered with $R^2 > 0.8$ between methane and tracer concentrations. The days are categorized into two plots to clearly display diurnal variations. The data with lower emissions in 2012 are depicted in the left plot and the higher emission data during 2013 are shown in the right plot.

The diurnal variations of air temperature and wind speed in midlatitude regions, like this Southeastern US landfill, depend on vertical radiative and turbulent fluxes (He et

al., 2012). The typical diurnal pattern of wind speed in inlands (70 km or more away from large waterbodies (Lapworth, 2005) is maximum in the afternoon and minimum in the late night (Dai and Deser, 1999; Peterson and Parton, 1983). However, land surface wind speeds may be greater at night than during the day if winds blow from offshore regions to inlands (Barthelmie et al., 1996). Under such conditions, the emission-increasing atmospheric conditions may occur at night. Therefore, the implications discussed in this section about time of maximum and minimum fluxes are only expected at landfills with similar wind and air temperature diurnal patterns.

The limited TDM data at this site support the WRF modeling predictions for diurnal methane fluxes for two 24 h periods at a Delaware US landfill (Taylor et al., 2018) and one 24 h period at this same Southeastern US landfill (Taylor, 2017). At the Delaware landfill, simulations indicated diurnal flux varied by a factor of 2 (max/min), while for the Southeastern US landfill flux varied by a factor of 12 (November 2011), consistent with the EC data reported for this site. WRF simulations were also completed for 6-h periods from 11:00 to 17:00 on four days at the Southeastern US landfill (November 2011, June 2012, December 2012, and April 2013). Here, methane fluxes varied between 1.7 to 4.3 (max/min) for each simulation day (Taylor, 2017), which is consistent with the 1.6 to 7.0 variation reported for TDM measurements for similar measurement periods (Figure 3.10). However, in most cases TDM data will fail to capture the full 24-h diurnal variations because of the limited time over which TDM measurements are conducted. For example, of the TDM data conducted between 2011 and 2013 at the Southeastern US landfill, 64% of the 495 measurements were collected between 12:00 and 18:00. Failing to capture

diurnal variability in methane flux may make TDM measurements susceptible to biases in estimates of diurnal-average fluxes.

3.5.3 Preferred Times of Day for Measurement

The EC and TDM data indicate diurnal variations in methane flux from this inland landfill. Many emission measurement methods and to the best of our knowledge all whole-landfill methodologies including the TDM are deployed during daytime. Therefore, it is instructive to assess the best time of day for measuring the “diurnal average” flux. Obtaining the diurnal average flux is the first step for developing accurate annual emission inventories. To achieve this for each of the three test periods, the flux data at each time interval, Q_i , (averaged at 30-min intervals) for each day were normalized ($\frac{Q_i - Q_{daily\ min}}{Q_{daily\ max} - Q_{daily\ min}}$). Then, the fluxes measured at each 30-minute time interval for each 7 or 8-day measurement period (e.g., flux measured at 4 am on December 24 through 31, 2012, for December) were averaged and are shown in Figure 3.11, where error bars represent the standard errors of the means. Finally, the diurnal average fluxes of each 7 or 8-day period were calculated and are shown in this figure. The intersection of this average line with the 30-minute average data indicates the most representative times for short-term flux measurements.

The normalized average EC flux in June 2012 was ~ 0.38 and the most representative time of day for measuring the diurnal average flux was either 11:00 or 19:00. As mentioned before, the majority of the TDM data were collected between 12:00 and

18:00 at this landfill. The average of the normalized EC methane flux between 12:00 and 18:00 in June 2012 was ~ 0.60 , which is 58% greater than the diurnal average flux measured by the EC tower. Thus, the TDM measurements likely overestimated daily-average methane emissions during this period by approximately 60%.

In December 2012, the times of day when TDM measurements provided the most representative estimates of diurnal average flux were 10:00 and 18:00. The normalized flux average between 12:00 and 18:00 during this period in December is ~ 0.62 , which is 55% greater than the normalized EC flux of ~ 0.40 in this week. In February 2013, the average EC flux intersects the flux variations at approximately 11:00 and 17:00. The normalized flux average between 12:00 and 18:00 during this period in February is ~ 0.62 , which is 73% greater than the normalized EC flux for this week. Thus, for this measurement period, a typical TDM measurement at this landfill likely overestimated diurnal average fluxes by up to 73%.

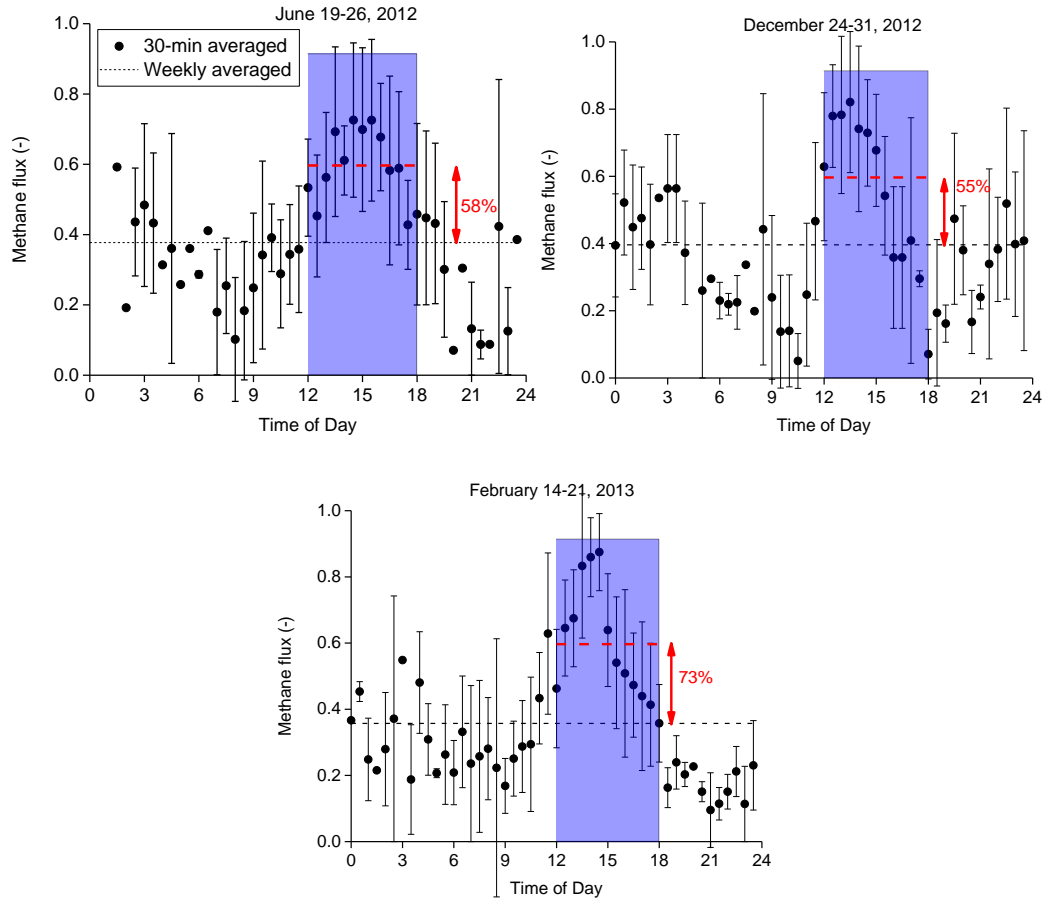


Figure 3.11 Normalized variations of the weekly-averaged flux measured by the EC tower during the three measurement periods. Black dashed line shows the average of normalized flux measured by the EC tower during each period. Blue shading displays the measurement window typical for TDM measurements at this landfill. Dashed red lines are the average of all data within each blue area, and the average percent errors of diurnal methane flux estimates using TDM measurements only during the blue shading periods are indicated in red.

At this landfill, short-term flux measurements that are most representative of diurnal average flux may be obtained at two times: between 10:00 and 11:00, and between 17:00 and 19:00. These times depend on the atmospheric conditions during the day, which vary with season and geographical location of the site. It is important to reiterate that this

time of day for measurement is applicable for landfills with similar diurnal wind and air temperature patterns. For landfills near large waterbodies, we anticipate that inverse wind patterns would cause an emission underestimation using daytime TDM measurements.

3.6 Conclusions

A careful assessment of EC flux data from a Southeastern US landfill indicates that methane flux was positively correlated with T and u^* , and negatively correlated with P_{atm} and $\frac{dP_{atm}}{dt}$. Flux was most strongly correlated with T when the atmosphere was unstable, while flux correlated most strongly with u^* under neutral conditions. The correlation was stronger for $\frac{dP_{atm}}{dt}$ than P_{atm} alone. Although similar results are reported in previous studies, this is the first investigation we are aware of where effects of these meteorological parameters were examined at a single site simultaneously. Together, these observations support the atmospheric modeling in Taylor et al. (2018) where a mass transfer flux model that accounts for effects of wind and solar radiation was used to simulate landfill methane emissions.

Using average 30-min fluxes, the EC data showed that the diurnal methane flux variation (max/min) ranged from 1.8 to 23 over the 23 days tested in June 2012, December 2012, and February 2013. If only limited TDM measurements are possible, it is recommended that measurements be conducted either in the late morning or late afternoon/early evening at this landfill, when measured emissions are closest to diurnal average emissions.

Chapter 4

DEPENDENCY OF THE TRACER DISPERSION METHOD ACCURACY ON ENVIRONMENTAL PARAMETERS FOR LANDFILL GAS EMISSION ESTIMATION

This chapter is a paper entitled “Dependency of the Tracer Dispersion Method Accuracy on Environmental Parameters for Landfill Gas Emission Estimation”, to be submitted in *Atmospheric Environment*.

4.1 Introduction

Several methods have been developed over the past three decades to quantify methane emissions from landfills. These methods include flux chambers (Metcalf and Farquhar, 1987), the tracer dispersion method (Czepiel et al., 1996), inverse plume modeling (Flesch et al., 2004), and micrometeorological eddy-covariance (Laurila et al., 2005). Among these methods, the tracer dispersion method (TDM) is perhaps the most promising method for quantifying whole-landfill methane emissions because of development of high-performance and inexpensive technologies measuring methane and gas tracers (Foster-Wittig et al., 2015). The United States Environmental Protection Agency (US EPA) has included this method in Category C as “other test method” (OTM) 33B as a reliable approach to estimate gas emissions from large sources (Foster-Wittig et al., 2015).

In the TDM methodology, methane emission is estimated by releasing a tracer gas located on the landfill and measuring both methane and the tracer gas far enough downwind (obtaining fully-mixed conditions), when they both can be considered point sources (Mønster et al., 2014; Foster-Witting et al., 2015; Taylor et al., 2016, Mønster et al., 2019). Methane emissions with the TDM are calculated using

$$Q_M = Q_T \left(\frac{C_M}{C_T} \right) \quad \text{or} \quad \overline{Q_M} = Q_T \overline{\left(\frac{C_M}{C_T} \right)} \quad (4.1)$$

where Q_M and Q_T are the methane and tracer mass emission rates $\left(\frac{g}{s} \right)$, and C_M and C_T are the downwind concentrations of methane and the tracer gas after subtraction of background concentrations $\left(\frac{g}{m^3} \right)$. To obtain $\overline{\left(\frac{C_M}{C_T} \right)}$, $\left(\frac{C_M}{C_T} \right)$ in Eq. 4.1 are frequently integrated in time or space, depending on whether stationary or mobile measurements methods are used.

Because the tracer gas is released at a constant rate, the average methane emission estimation using the TDM strongly depends on the consistency of the $\frac{C_M}{C_T}$ in a field measurement dataset. Consistency means that this ratio should keep constant value throughout a field measurement to yield reliable emission estimations. Atmospheric simulations and field tests using controlled releases of methane and tracer have reported errors up to 42% using TDM (Foster-Wittig et al., 2015; Delkash et al., 2016; Mønster et al., 2019; Scheutz and Kjeldsen, 2019). Thus, TDM data with significant errors may not be useful to estimate methane emissions in all cases: reliable data must be segregated from inaccurate data. Foster-Wittig et al. (2015) presented a large TDM dataset (1876

measurements) collected during 131 field deployment days for 15 landfills between 2009 and 2013. They applied three filtering criteria to remove the unreliable data and reported that 76% of the data failed their filtering criteria. Similarly, Delkash et al. (2016) used filtering criteria and discarded 22% of the TDM data. Thus, a significant portion of collected TDM data may be poor.

As mentioned above, the reliability of the TDM data depends on the consistency of $\frac{C_M}{C_T}$. Previous research has shown that downwind measured $\frac{C_M}{C_T}$ depends on landfill topography, properties of downwind measurements (e.g., distance to downwind roads and alignment compared to landfill) (Mønster et al., 2014; Taylor et al., 2016; Maticchiera et al., 2019; Monster et al., 2019; Scheutz and Kjeldsen, 2019), gas tracer setups (number of tracer bottles and their locations compared to high methane emission spots) (Mønster et al., 2014; Taylor et al., 2016; Maticchiera et al., 2019; Monster et al., 2019; Scheutz and Kjeldsen, 2019), and meteorological conditions (wind direction, wind speed, and atmospheric stability) (Mønster et al., 2014; Foster-Witting et al., 2015; Taylor et al., 2016). Thus, understanding the impacts of these variables on $\frac{C_M}{C_T}$ and TDM data reliability is essential for reducing the collection of poor TDM measurements.

To assess the impact of landfill topography on TDM accuracy, Taylor et al. (2016) used atmospheric simulations for two different wind directions: one with a one-hour average wind direction 47° and a standard deviation 7.6° , and the other with the same conditions but a 90° change in the wind direction. The measurement error in methane emissions using eq. 4.1 for each downwind transect varied between 10% and 42% for the

original simulation and between -10% and 10% when the simulated wind direction changed by 90°. This difference in measurement error was associated with the interaction between landfill topography and wind direction, which affected plume transport including downwind dispersion.

The importance of the locations(s), typically discrete point(s), of gas tracer release on TDM accuracy was investigated using field measurements (Mønster et al., 2014) and atmospheric simulations (Taylor et al., 2016; Matacchiera et al., 2019). These studies concluded that any misalignment of the tracer gas and methane sources along or perpendicular to the transport vector can negatively affect TDM accuracy. Matacchiera et al. (2019) showed that increasing the number of tracer release points from one to two would decrease the error in landfill emission estimation up to 50%. This finding was associated with the observation that placing more tracer gas bottles on top of the methane emission region improved the alignment of tracer gas and methane plume. Taylor et al. (2016) showed that a misalignment between five tracer gas bottles and methane hotspots of a landfill by placement the tracer gas bottles on the upwind edge of the methane hotspot region might cause as much as 40% error in emission estimation. Taylor et al. (2016) also compared their results with other studies and concluded that the dependency of TDM accuracy on the landfill topography, wind direction, and tracer gas setup is site-specific, which implies additional investigation of this dependency is needed at other landfills before general guidelines can be developed for optimal TDM measurements.

Research regarding the influence of meteorological parameters on TDM accuracy has focused on the impact of wind speed on the distance away from the emission source

for optimal TDM measurements (Matacchiera et al., 2019), and qualitative visual assessments of field measurements regarding the influence of wind speed and atmospheric stability (Foster-Wittig et al., 2015; Scheutz and Kjeldsen, 2019). Foster-Wittig et al. (2015) qualitatively reported that uncertainty in TDM emission estimates was high for unstable atmospheric conditions and low wind speed. However, no study has used field data to quantify the correlations between meteorological parameters and data filtering criteria that increase TDM data reliability. Such information would allow one to determine the best seasons and time of day for accurate field measurements. If a TDM dataset passes the filtering criteria, the estimated emissions would be reliable. However, determining the optimal conditions for conducting TDM measurements obtains the most reliable methane emissions data. Fredenslund et al. (2019) conducted two field-controlled campaigns and reported that 96% and 70% of the data were discarded when they applied one filtering criterion ($R^2 > 0.80$). They showed that if the average of estimated emissions of the transects is used for total emission estimations, a decrease in number of transects because of applying filtering criteria might increase the variability of emission estimations. They concluded that applying filtering criteria removes a significant number of collected data that another source of error in emission estimations is created – an inadequate number of measurements to determine mean emission rate. This conclusion emphasizes the importance of conducting the TDM field measurements under favorable atmospheric conditions to optimize the number of useful data for a more certain emission estimation. An increase in number of reliable TDM dataset would enhance certainty in emission estimations.

This study uses data collected at a landfill with the largest dataset of TDM measurements reported in the literature (Foster-Wittig et al., 2015). This landfill has been operated in the Southeastern US since 2010, and TDM methane emission measurements were conducted between June 2011 and November 2013. During this period, the landfill was covered primarily by an intermediate cover with a small area of daily cover (<5%) and without a gas collection system. Statistical analysis was used to examine correlations between the meteorological conditions and TDM filtering criteria. A knowledge about these correlations will help to determine optimal measurement conditions for TDM measurements at any site in the world.

4.2 Method

4.2.1 Tracer Dispersion Method

In the TDM, tracer gas is released at a measured emission rate from tracer releasing point(s) (usually between 2 to 5 points) located on the landfill surface (Scheutz and Kjeldsen, 2019). To achieve fully mixed gas plumes, the methane and tracer concentrations are measured far enough downwind, e.g., four times the landfill width in Mønster et al. (2014), where both the methane and tracer releases can be considered point sources. Generally, two different approaches have been implemented to collect downwind gas concentrations: stationary and mobile. During a stationary measurement, temporal methane and the tracer gas concentrations are collected at a single point or perhaps several points (Czepiel et al., 1996; Galle et al., 2001; Delkash et al., 2016). If the measurement locations are not selected appropriately, landfill gas plumes might be only sampled intermittently

because of variations in wind direction (Mønster et al., 2019). In the mobile approach, data are collected from transects of the downwind plumes, typically from vehicle-mounted measurement instruments that ideally operate perpendicular to the mean wind direction with speed 20-30 km/hr (Mønster et al., 2015).

4.2.2 TDM Field Deployments

The Southeastern US landfill studied here has been operated since 2010 with an annual waste placing rate of 264 to 330 thousand metric tons in 2010 that increased to 1.16 million metric tons in 2013 (De la Cruz et al., 2016). Emission estimates were obtained from 515 TDM data sets, including 452 mobile and 63 stationary measurements carried out within 10 primary campaigns over 34 days between June 2011 and November 2013. Each primary campaign included field measurements during 2 to 4 consecutive days. This data collection effort resulted in the highest density of TDM data that we are aware of. Before each campaign, the dominant wind direction, the locations of the landfill with highest methane emissions, and nearby roads suitable for conducting the mobile measurements were identified. On most measurement days, two compressed gas cylinders of acetylene tracer gas separated by a maximum distance of about 270 m were placed on top of the landfill in the most emissive regions and each released 21.3 g/min. Actual locations of the tracer gas cylinders were determined based upon wind direction and selection of the downwind road for TDM transects. If the downwind measurements are too far from the landfill, depending on the measurement instrument detection limit and background methane and acetylene concentrations, the gas plumes cannot be distinguished

from background gases. At this site, downwind measurements were made between 0.6 and 5.4 km from the center of the tracer bottle geometry, with an average distance of 1.8 km.

The concentration measurement instrument was a Picarro Model G1203 CRDS (Picarro Inc. Santa Clara, CA, USA). This instrument measures methane and acetylene with precisions of 0.463 ppb for methane and 0.088 ppb for acetylene at frequency of 0.5 Hz and has been extensively employed to collect gas concentrations (Mønster et al., 2014; Mønster et al., 2015; Delkash et al., 2016). The instrument was mounted 2 m above the ground on a vehicle to deploy mobile measurements. Figure 4.1 shows the three primary roads that were used to carry out the mobile measurements.

4.2.3 Meteorological Parameters

An R.M. Young model 81000 3-D sonic anemometer was installed 2.25 m atop the landfill to record the meteorological parameters, including wind speed and direction, during all three-year measurements. The four investigated meteorological parameters are wind speed, wind direction standard deviation (*WDS*), turbulence intensity (*TI*), and atmospheric stability index (*ASI*) that are described below.

Wind direction is a circular measurement; that is, there is no difference between 0° and 360°. Circular standard deviations (Appendix C) were employed here to accommodate circular data (Berens, 2009).

Separating the measured wind speed ($u = \bar{u} + u'$) into mean wind speeds (\bar{u}) and turbulent velocity (u'), *TI* is defined by

$$TI = \frac{u'}{\bar{u}} \quad (4.2)$$

The atmospheric stability describes the mixing of air vertically. Under an unstable atmosphere, turbulence causes significant mixing and vertical gas transport compared to stable and neutral atmosphere. Further description about the atmospheric stability conditions can be found in Chapter 3. The *ASI* ranges from 1 to 7 and is a quantitative way of characterizing atmospheric stability. The *ASI* is determined based upon the values of *TI* and *WDS* using *TI* increments of 0.025 and *WDS* increments of 0.1. For example, *ASI* = 1 is defined for conditions $TI > 0.205$ and $WDS > 0.7$, which occurs under unstable atmospheric conditions, and *ASI* = 7 corresponds to $TI < 0.08$ and $WDS < 0.2$ that represents stable atmospheric conditions. Table C.1 in the Appendix C defines the conditions for all seven *ASI*. The seven *ASI* classifications correspond roughly to the Pasquill Stability classes A through D (De Visscher, 2013).

4.2.4 Methane Emission Quantification

Two methods are commonly used to quantify emissions using the TDM (eq. 4.1). The regression slope method considers the linear equation obtained by regressing C_M versus C_T (Czepiel et al., 1996; Galle et al., 2001; Mønster et al., 2014; Delkash et al., 2016)

$$C_M = m \times C_T + b \quad (4.3)$$

where m and b are the slope and intercept of the linear regression, respectively. If the intercept b is negligible compared to the first term on the right hand side of this equation, the slope is $\left(\frac{C_M}{C_T}\right)_r$, the average concentration ratio obtained by regression. All data points in the regression slope method play an equal role in quantifying the average (Mønster et al., 2014). However, methane and tracer gas plumes may have different widths, and for this reason the ratio of concentrations can vary significantly at the margins of the plumes for mobile measurements, which undermines the accuracy of this approach. The regression slope method also assumes that all data are equally accurate, which can cause substantial measurement error (Mønster et al., 2014).

The second method is the weighted average method which assigns greater weight to higher gas concentration data and lower weight to data from the margins of gas plumes (Mønster et al., 2014). Thus, this method reduces inaccuracies from the plume margins by focusing on higher concentration data. This approach has been applied in several investigations (Mønster et al., 2014; Taylor et al., 2016). Mønster et al. (2014) examined the TDM under different tracer gas and methane source configurations and determined that the weighted average method provided more accurate measurements in most cases.

The equation to compute $\left(\frac{C_M}{C_T}\right)_w$ is

$$\left(\frac{C_M}{C_T}\right)_w = \frac{\int_0^l \left(\frac{C_M}{C_T}\right) * (C_T) dx}{\int_0^l (C_T) dx} = \frac{\int_0^l (C_M) dx}{\int_0^l (C_T) dx} \quad (4.4)$$

where l is the plume width. The integration from $x = 0$ to l captures the concentrations higher than background levels across the plume width.

4.2.5 Method Quality Indicators

Although the TDM has become a well-established method to quantify landfill methane emissions, not all TDM data are useful. Foster-Wittig et al. (2015) developed several filtering criteria to eliminate TDM data of poor reliability. These criteria are used in this study as TDM data quality indicators.

4.2.5.1 Correlation of plumes

The square of the Pearson correlation coefficient (R^2) for equation (4.3) is used as a quality indicator to determine the level of mixing for gas plumes. This parameter describes the linear relationship between tracer gas and methane concentrations, and a linear relationship between these concentrations is the basis of the TDM. Thus, the higher R^2 the greater linearity between the gas concentrations and thus the higher certainty in emission estimates. It is generally agreed that if $R^2 > 0.80$, then TDM measurements are reasonably accurate (Mønster et al., 2014; Delkash et al., 2016; Taylor et al., 2016).

4.2.5.2 Distinguishing signal from noise

High background concentrations of the tracer or methane gas, or significant variability in the background concentrations, may result in low signal-to-noise ratios that adversely affect the quality of TDM data (Foster-Wittig et al., 2015). Two criteria are defined to assess this effect on data quality. The first criterion employs the standard deviation of the background concentration (beyond the edges of the plume) of each gas species - methane (σ_M) or acetylene gas (σ_A), which assesses the variability of the background concentrations. The reason for this background concentration fluctuations might be wind direction variations. During a mobile measurement transect, the vehicle

begins measurements outside the margins of the plume, then crosses the plume and collects data until the vehicle is out of the plume again, to assure a complete transect of the plume is covered. Therefore, background concentrations (outside of the plume area) are recorded in the mobile approach. This criterion considers standard deviations of these background concentrations. A higher background concentrations might lead to a more uncertain emission estimation.

The second criterion involves the signal-to-noise ratio of methane (SN_M) and acetylene (SN_A). Downwind gas concentrations must be sufficiently high to discern the landfill signal, whether it be methane or the tracer, from the background noise. The signal to noise parameter is described by

$$SN = \frac{2H}{h} \quad (4.5)$$

where H is the signal height of the peak concentration of the gas, and h is the signal height of the maximum peak background concentration of the same gas. Foster-Wittig et al. (2015) set 10 as the minimum SN for a reliable TDM dataset. Further information about this criterion is provided by Foster-Wittig et al. (2015).

4.2.5.3 Emission Rate Difference

For a linear relationship between methane and the tracer concentrations (eq. 4.3), m can be used as a surrogate for $\left(\frac{C_M}{C_T}\right)$ whenever $b \ll m \times C_T$. This produces another filtering parameter – the emission rate difference (ERD) (Foster-Wittig et al., 2015)

$$ERD(\%) = 100 \times \frac{|Q_{M,w} - Q_{M,r}|}{0.5|Q_{M,w} + Q_{M,r}|} \quad (4.6)$$

The ERD criterion is $ERD < 20$, which ensures that the emission estimations of the quantification methods – regression slope ($Q_{M,r}$) and weighted average ($Q_{M,w}$) – are similar (Foster-Wittig et al., 2015).

A significant difference between $Q_{M,w}$ and $Q_{M,r}$ can indicate a mismatch of the gas plume boundaries. The $Q_{M,r}$ assigns the same weight to the margins and peak of the plume; however, the $Q_{M,w}$ specifies higher weights to the plume peaks. The presence of another methane or tracer gas source near the landfill might affect the gas plume shapes especially at the plume margins. The marginal areas of the plumes are more sensitive to the presence of other sources because of lower concentrations in these regions. Therefore, the presence of other methane or tracer gas sources might affect $Q_{M,r}$ more significantly than $Q_{M,w}$.

4.2.6 Correlation Analysis

This study examines the relationships between each meteorological parameter (wind speed, WDS , ASI , and TI) and each TDM filtering criterion. To achieve this goal, the influence of other variables on the TDM criteria were controlled. These other variables include stationary or mobile TDM approach, landfill topography, tracer setup, downwind transect location, and methane emission rate.

Although the abovementioned variables vary throughout the dataset, their variations should be controlled during investigations of correlations between one meteorological parameter and one filtering criterion. Therefore, some actions were required to control these variations. For example, data collected from the mobile approach

(88% of data) and stationary approach were separately analyzed. Landfill topography and the pathway from the landfill to the downwind roads where gas concentration measurements also affect the plume meandering and TDM accuracy (Taylor et al., 2016). Therefore, the TDM data collected with the mobile approach were separated into three categories based upon the downwind road used for data collection, shown in Fig. 4.1. For examining the relationships between each meteorological parameter and each TDM filtering criterion, the variations of the other meteorological parameters should be controlled as well. For this purpose, the statistical analysis was conducted when the other meteorological parameters were limited to above or below their average values.

Quantity of methane emissions can affect signal to noise ratio criterion (Delkash et al., 2016). Because methane emissions may vary over short time periods, e.g., an hour (Delkash et al., 2016), it is not possible to keep it invariant for our statistical analysis. To resolve this issue, statistical analysis between the TDM filtering criteria and the meteorological parameters were investigated over different measurement periods and different seasons. If consistent patterns were found between TDM filtering criteria and meteorological parameter across different measurements periods and seasons, this implies that methane emission variations did not significantly affect the correlations between the TDM filtering criteria and the meteorological parameters for this landfill.

As mentioned earlier, a controlled dataset helps relate the variations of one filtering criterion to the investigated meteorological parameter. Thus, the data collected using the mobile approach were categorized according to the downwind road that the data were collected. As shown in Fig. 3.1, the topography of the landfill quickly changed

because of the activities between 2011 and 2013 in the landfill. Therefore, we expect the landfill had the least variations in its topography during a few consecutive days. The highest number of data point during a few consecutive days was 61 mobile transects collected on the downwind road III (Fig. 4.1) between June 25 and 27, 2013. This dataset is called Case study I and because of the minimum variations of the mentioned variables, we expected to see less interference of other variables. The methane emission during this period varied between 1231 g/min and 5924 g/min and the average emission was 2150 ± 888 SD g/min.

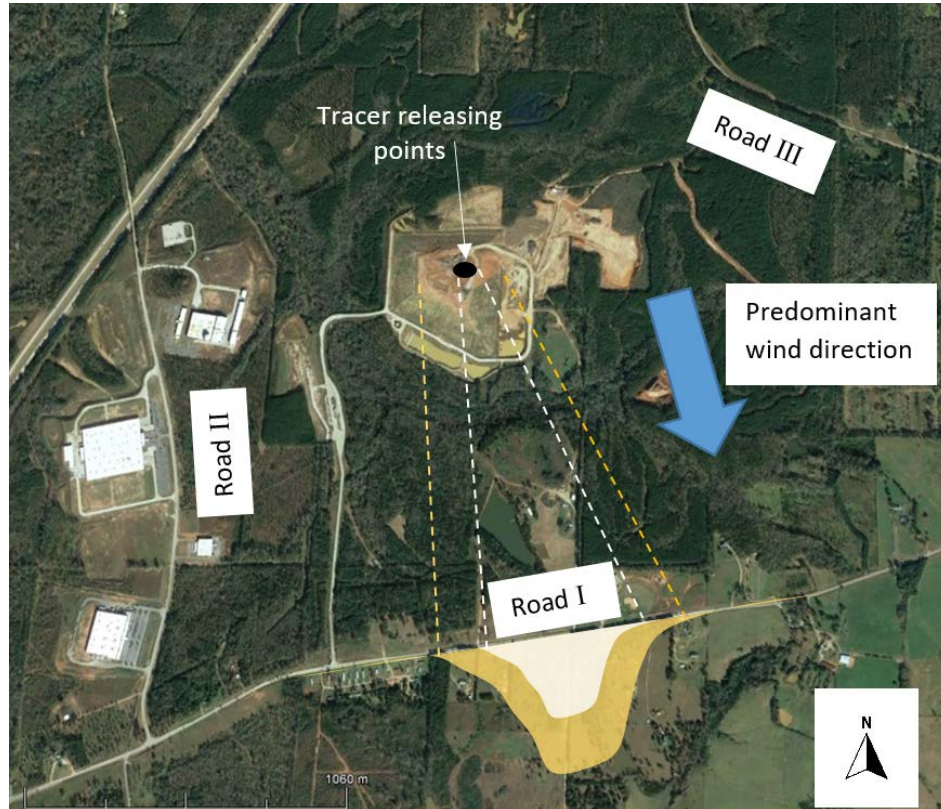


Figure 4.1 Google Earth image of the landfill with the three roads used for mobile deployments. The white and yellow areas indicate tracer gas and methane plumes, respectively. The yellow and white dashed lines represent the margins of the methane and tracer gas plumes. The black area on the landfill indicates the approximate locations of tracer gas releases. The blue arrow indicates predominant wind direction.

Anchoring to Case study I, the extension of the data in Case study I would assess the randomness of the results obtained in Case study I. If the results of the correlation analysis in the extended Case study I (called Case study II) are consistent with Case study I, the hypothesis of the randomness of the results is disapproved. For this purpose, the field data measured on Road III in May 2013 (29 data points) were combined with data measured in June 2013 (Case study I). Methane emissions varied between 984 and 5924

g/min for the period between May 2013 and June 2013, with mean emissions of 2050 g/min and standard deviation of 850 g/min.

To evaluate if the results found in Case study I would occur in a different season, Case study III was considered. This case study includes 53 mobile transects that were collected on Road III between November 5 and 8, 2013. The methane emission during this period varied between 1577 g/min and 4652 g/min and the average emission was 2523 ± 677 SD g/min. The weather conditions and landfill topography differed between this case study and Case study I.

Case study IV includes all 452 transects (from June 2011 through November 2013) from the 10 measurement campaigns. The methane emission during this period varied between 21 g/min and 5924 g/min and the average emission was 1176 ± 943 SD g/min. All parameters including meteorological parameters, emissions, topography, and the downwind road vary in Case study IV. A weaker correlation in Case study IV compared to the other three would indicate that these other variables significantly influence the relationships between TDM filtering criteria and meteorological parameters. A summary of the case configurations is presented in Table 4.1.

Table 4.1 Case studies: Measurement locations and emissions data

Case Study	N ¹ Road I	N Road II	N Road III	Emission range (g/min)	Emission average \pm SD ² (g/min)
1	-	-	61	(1231, 5924)	2200 \pm 900

2	-	-	90	(984, 5924)	2100 ± 900
3	-	-	53	(1577, 4652)	2500 ± 700
4	99	254	143	(21, 5924)	1200 ± 900
Stationary	8	37	18	(1030, 2742)	2000 ± 500

¹ N indicates number of data point.

²standard deviation

Table 4.2 lists the four Pearson correlation coefficients used to investigate the impacts of the meteorological parameters on the TDM filtering parameters. The first coefficient (R_1) is the Pearson correlation coefficient between individual values of the meteorological parameter and the TDM filtering parameter. The other three correlation coefficients are related to statistical measures of the TDM filtering parameter and how they vary with meteorological parameter. In the analyses for each case study, the data were grouped based on meteorological parameter into different bins.

The coefficients R_2 , R_3 , and R_4 are the Pearson correlation coefficients between the mean of the meteorological parameter for each group of binned data and the median (R_2), the standard error (R_3), and the skewness (R_4) of the investigated TDM filtering parameter for the binned data, respectively. Descriptions of each of these statistical measures can be found in the literature (Warpole, 1974). R_1 and R_2 indicate how the meteorological parameter affects the TDM filtering parameter: if R_1 and R_2 are large and positive (> 0.3), for example, then the TDM filtering parameter increases with the meteorological parameter. The R_3 coefficient is the correlation coefficient between the standard error of TDM filtering parameter for each group of binned data and the meteorological parameter. Positive R_3 indicates that variation in the TDM filtering

parameter increases with the meteorological parameter, which indicates greater uncertainty in emission estimation.

Finally, R_4 is the correlation coefficient between the skewness of the TDM filtering parameter for each binned data set and the meteorological parameter. The skewness describes the relative position of the mode, median, and mean in the TDM parameter sample distribution. Positive skewness means that the tail lies to the right (i.e., mode < median < mean) while negative skewness implies the tail lies to the left (i.e., mean < median < mode) (Von Hippel, 2005). The conclusion drawn about R_4 depends on the sign of the skewness and R_4 . For instance, when data are positively skewed, a positive R_4 indicates that the probability of extremely high values of the TDM filtering parameter increases as the meteorological parameter increases. This increase is favorable for the TDM filtering parameters R^2 , SN_A , and SN_M where high values are desirable, but unfavorable for TDM filtering parameters σ_M , σ_A , and ERD where small values are better.

Table 4.2 Description of the Pearson correlation coefficients between TDM filtering parameters and meteorological parameters.

Statistical measure	Property of TDM Filtering Parameter	Property of Meteorological Parameter
R_1	Individual parameter values	Individual parameter values
R_2	Median of binned data	Midpoint of binned data range
R_3	Standard error binned data ¹	Midpoint of binned data range

R_4	Skewness of binned data ²	Midpoint of binned data range
-------	--------------------------------------	-------------------------------

$$^1(\text{std. dev}) / \sqrt{\#data}$$

$$^2 [\text{mean} - \text{median}] / (\text{std. dev})$$

Considering R_2 , R_3 , and R_4 that deal with bins in boxplots, the meteorological parameters need to be categorized in sufficient number of bins to calculate the correlations. Only boxplots with at least six bins for each pair of the meteorological parameter and filtering criterion were included to compute Pearson correlation coefficients. On the other hand, at least five data points are recommended for each bin of a box plot (Krzywinski and Altman, 2014). Therefore, the width of the data bins for wind speeds, WDS , and TI were selected to be 0.5 m/s, 0.05, and 0.02, respectively, to satisfy these conditions.

4.3 Results and discussion

4.3.1 TDM Mobile Approach

As explained in Table C.2, the ASI was neglected for statistical analysis because it was significantly correlated with the other meteorological parameters. Correlation analysis was conducted between the three meteorological parameters (wind speed, WDS , and TI) and six TDM filtering parameters (R^2 , σ_M , σ_A , SN_M , SN_A , and ERD) which resulted in 18 different paired analyses for each of the four case studies. Because variables including landfill topography, tracer setup, downwind transect location, methane emission rate, and meteorological parameters change the least in Case study I, this case study can reveal the correlations more clearly compared to the other case studies. Therefore, Case

study I was analyzed as a basis to determine the pairs that have sufficient data to study impacts of the meteorological parameters on the TDM data reliability. Using the data in Case study I, 12 meteorological classes were obtained after categorizing the three meteorological parameters into one primary parameter and two secondary parameters, where the secondary parameters were categorized into “above the average” and “below the average.”

The number of bins and total data points for these 12 meteorological classes are shown in Table C.3 in the Appendix C. As seen in Table C.3, two classes have at least six bins: 1) when wind speed is the primary investigated parameter and both *WDS* and *TI* are below the average, and 2) when *WDS* is the primary parameter and wind speed is above the average and *TI* is below the average. These results are consistent with Table C.2, where higher wind speed coincides with lower *TI* and *WDS*. According to Table C.2, occurrence of high wind speed, low *TI* and low *WDS* is common, and these two classes were expected to have a higher number of data points.

After choosing these meteorological classes with the highest number of data points and bins, the filtering criteria with the most sensitivity to meteorological parameters were determined for Case study I. A minimum Pearson correlation coefficient 0.30 is required for a pair to have a (weak) correlation (Mukaka, 2012). Table C.4 shows the Pearson correlation coefficients between each filtering parameter and the two meteorological parameter classes. Table C.4 indicates that only three filtering criterion/meteorological pairs exceed the minimum Pearson correlation coefficient of 0.30: R^2 /wind speed,

SN_A /wind speed, and R^2 / WDS . Correlations between the other TDM filtering parameters and meteorological pairs are weak and reported in Appendix C.

If emissions between Case study I and Case study II differed, the impacts of methane emissions on TDM filtering criteria could be examined as well; however, the t-test of means indicates that the emissions of these two case studies are not statistically different ($p=0.65$). Therefore, it is not possible to comment on impacts of methane emissions on the TDM filtering criteria. However, because methane emissions mostly affect the signal to noise ratio (Delkash et al., 2016), the required methane and tracer emission rates to satisfy this filtering criterion are discussed in Appendix C.

4.3.1.1 Wind speed

Figure 4.2 shows the impact of wind speed on the R^2 filtering parameter when WDS and TI are below their means for each Case study (e.g., $WDS < 0.24$, $TI < 0.11$ for Case study I). Wind speed data were binned in 0.5 m/s increments, with the wind speed associated with the center of each bin selected to represent data in that bin. In the all four case studies, there is a positive correlation between individual wind speed measurements and corresponding individual filtering parameter R^2 (R_1) as well as wind speed at center of each binned data set and median R^2 for the binned data (R_2). Thus, an increase in wind speed causes an increase in R^2 .

Interestingly, for individual data points in Case study III, most R^2 are greater than 0.80, which suggests that data in this case study are more reliable than Case studies I and II (Fig. 4.2). A plausible explanation is that this is due to much higher wind speeds during

November 2013 than in Case studies I and II. Seasonal variations of the TDM filtering parameters will be presented later.

In Case study IV, although significant variability in R^2 was observed (large interquartile range, IQR) for wind speeds between 1.5 and 3.5 m/s, the IQR decreases as wind speed increases. Thus, R_3 is large and negative (-0.84), indicating that variations of the R^2 filtering parameter decrease as wind speed increases. Thus, the probability of a lower R^2 decreases as wind speed increases, which increases the confidence in methane emission estimation from TDM at high wind speed.

Since the mean R^2 filtering parameter is smaller than the median in most of the case studies (see Fig. 4.2), the distribution of the R^2 filtering parameter is negatively skewed for most data and particularly for Case study IV. This negative skewness decreases with wind speed for Case studies III and IV, since R_4 is negative. Thus, the probability of higher R^2 increases with increasing wind speed, which is favorable.

Several researchers have suggested a $R^2 > 0.80$ as an acceptable R^2 filtering criterion (Delkash et al., 2016; Foster-Wittig et al., 2015). However, the required wind speed to meet this criterion has not been reported. For Case study IV which includes all field data from the landfill, the mean R^2 are above 0.80 for all wind speeds, which indicates that the mobile approach has an acceptable performance for wind speeds > 1.25 m/s, although clearly measurements are better (smaller IQR and higher mean R^2) at higher wind speeds.

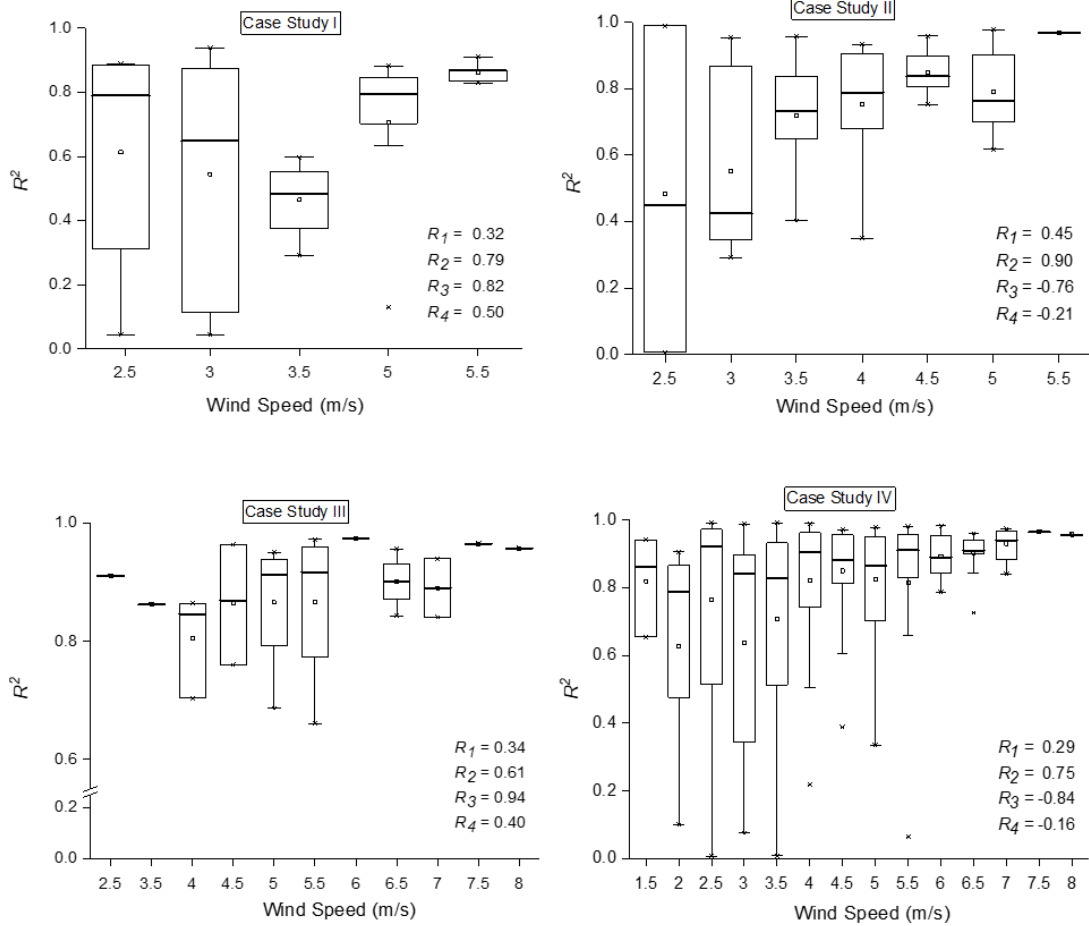


Figure 4.2 Variations of the R^2 TDM filtering parameter versus wind speed when WDS and TI are low ($<$ mean) for the four defined case studies.

The variation of SN_A versus wind speed when WDS and TI are small ($<$ mean), is displayed in Fig. 4.3. The correlations between SN_A and wind speed (R_1) and median SN_A and wind speed (R_2) are positive in Case studies I and II, which indicates more accurate TDM measurements at higher wind speed. Similar to the R^2 parameter, SN_A are greater in Case study III than Case studies I and II, which indicates the sensitivity of TDM accuracy

to season. For Case study IV, which includes all field data, R_1 and R_2 are approximately zero indicating little variability of SN_A with wind speed. However, because $R_3 = -0.48$ for Case study IV, the standard error of SN_A decreases with increasing wind speed, which indicates fewer data points with small SN_A and thus more accurate TDM measurements.

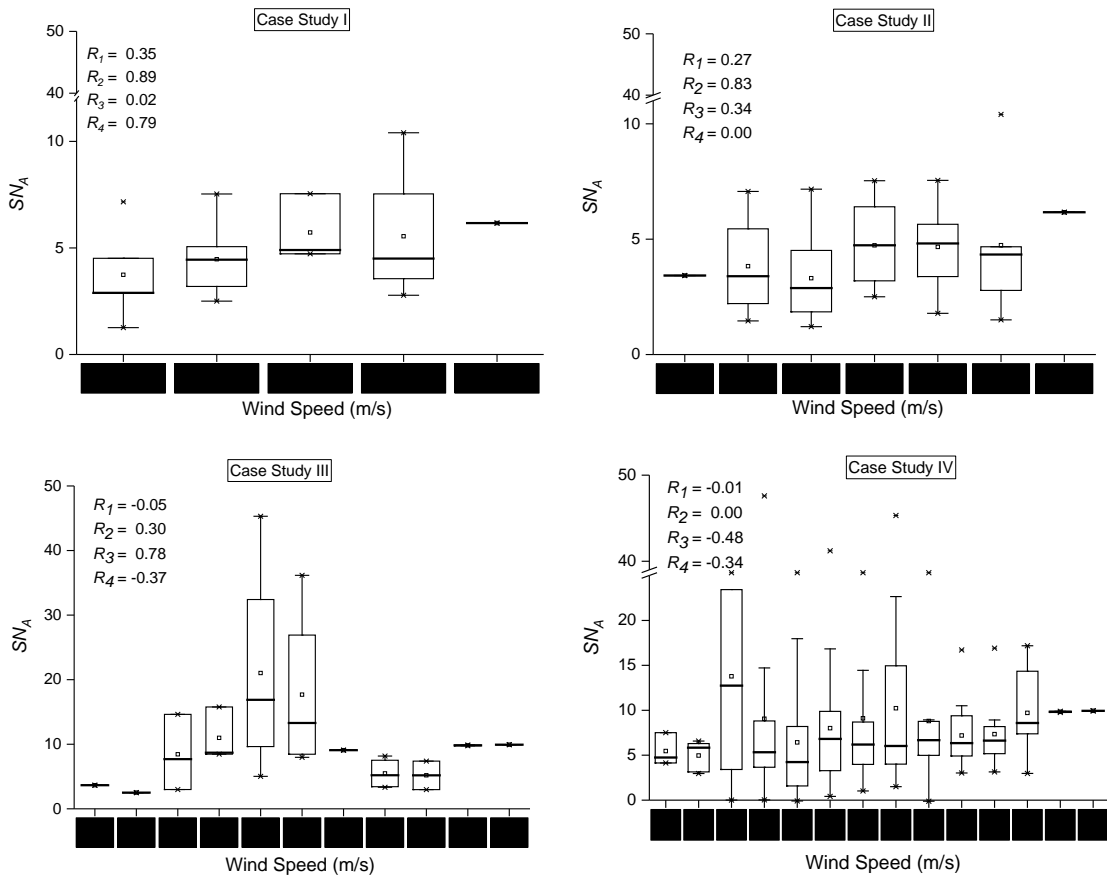


Figure 4.3 Variations of the acetylene (the tracer gas) signal to noise ratio (SN_A) versus wind speed when WDS and TI are small ($<$ mean) for the defined case studies.

The positive impacts of wind speed on the reliability of TDM data are consistent with meteorological conditions recommended by Scheutz and Kjeldsen (2019). Scheutz and Kjeldsen (2019) suggest avoiding TDM measurements when wind speed is low ($<$ 2 m/s) and the atmosphere is stable. As discussed earlier, a higher ASI indicates more stable

atmospheric conditions. Table 4.3 shows that wind speeds have a positive correlation ($R = 0.58$) with ASI . Therefore, a lower wind speed generally coincides with more stable atmospheric conditions.

4.3.1.2 Wind direction standard deviation

Figure 4.4 presents the variations of the R^2 filtering parameter with WDS , when wind speeds are above the average and TI values are below the average for each case study (e.g., wind speed > 3.4 m/s and $TI < 0.11$). In principle, one expects greater WDS to result in lower R^2 between methane and the tracer. Large WDS should increase the meandering of the methane and acetylene gas plumes from the landfill, making it more difficult to differentiate between landfill-emitted methane and acetylene and background concentrations of these gases. As shown in Fig. 4.4, WDS is generally negatively correlated with R^2 (R_1). The correlation coefficients between the median of R^2 and WDS (R_2) are -0.43, -0.42, -0.88, and -0.56 in Cases I, II, III, and IV, respectively. Thus, as WDS increases, the filtering parameter R^2 decreases and TDM data are less reliable, just as expected.

Regarding the correlation between standard error of R^2 and WDS (R_3), an increase in WDS is expected to increase the range of R^2 variations with a larger number of small R^2 between methane and the tracer. For Cases I, II, and IV, R_3 are 0.64, 0.58, and 0.49, respectively, which indicates that the standard error of R^2 increases with WDS , as expected. Because a $R^2 > 0.80$ is usually required for methane emission estimation

(Foster-Wittig et al., 2015; Delkash et al., 2016), a high *WDS* increases TDM measurement uncertainty.

Since the mean is less than the median for most data, the data are negatively skewed. For these negatively skewed data, positive R_4 in Case studies III and IV indicate a decrease in the occurrence of high R^2 , as *WDS* increases, which is not favorable.

As explained before, R^2 are higher for the TDM campaign in November 2013 (Case III in Fig. 4.5). If data are only used for methane emissions estimation when $R^2 > 0.80$, Case studies IV (Fig. 4.4d) indicates $WDS < 0.50$ for reliable TDM deployment. Although there are some observations with $R^2 < 0.80$ when $WDS < 0.50$, the median R^2 of each binned data group is still above 0.80.

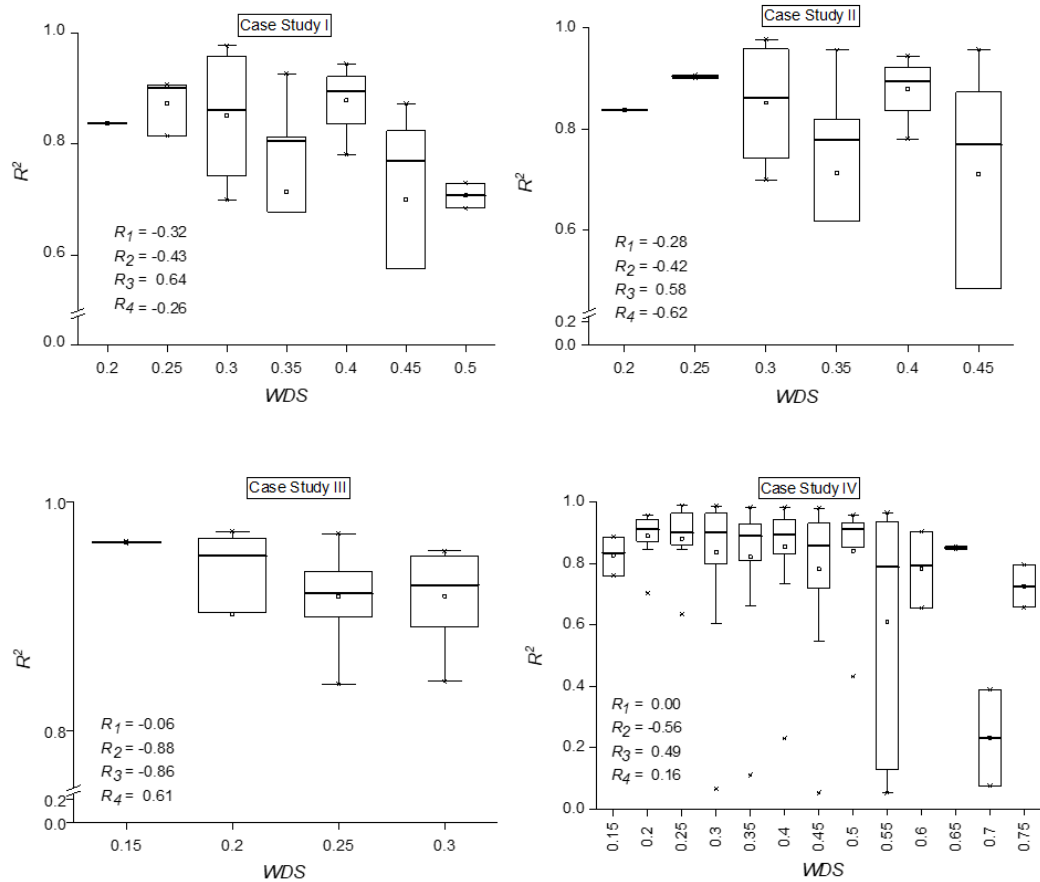


Figure 4.4 Variations of the R^2 filtering parameter versus circular wind direction variations standard deviation (WDS) for high wind speed ($>$ mean) and low TI ($<$ mean) for the four defined case studies.

4.3.1.3 Diurnal variations of the filtering parameters

After investigating impacts of each variable on the TDM filtering criteria, temporal variations of the TDM filtering criteria are discussed here. One important question in TDM measurements concerns the preferred time of the day to conduct measurements to maximize the collection of accurate data. Diurnal variations of the R^2 TDM filtering parameter for the Case study IV (452 mobile campaigns) show that R^2

between methane and the tracer is highest between 9 am and 5 pm local time and lower in early morning (~8 am) and late evening (~6 pm) (Fig. 4.5a). In addition to the R^2 filtering parameter, *ERD* is also higher during early morning and late evening (Fig. 4.5b), both of which indicate poor measurement accuracy in these periods. Poorer TDM measurement accuracy during these periods may be due to methane sources/sinks during TDM deployment, perhaps methane pooling over the landfill during calm weather in those periods (Foster-Wittig et al, 2015). This section analyzes the points stated by Foster-Wittig et al. (2015) about these two filtering criteria.

To show impacts of methane pooling over the landfill due to low wind speed at night and in the early morning, a 24-hr wind dataset is required. For this landfill, 24-hr wind data were available between Feb 10 and 16, 2013, as shown in Fig. 4.5c and Fig. 4.5d. The diurnal wind patterns in these days are similar to other days at this inland landfill. Further explanation about diurnal wind inland patterns can be found in Chapter 3.

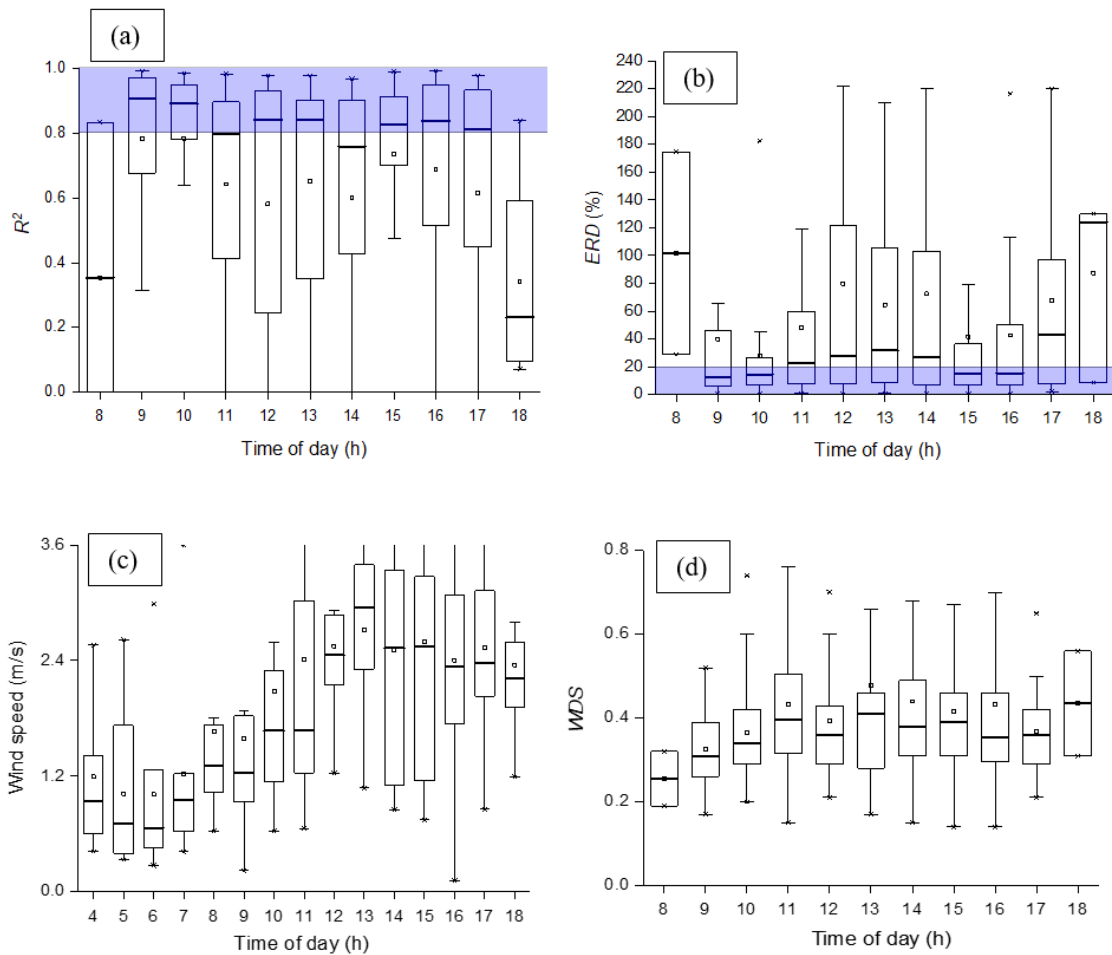


Figure 4.5 Hourly averaged TDM filtering or meteorological parameters for Case study IV data: a) R^2 , b) ERD , c) wind speed, and d) WDS . The blue highlight areas in plots (a) and (b) indicate the conditions when the TDM has reliable data. The wind speed and WDS variations during seven days between February 10th and 16th 2013 are available and shown in this figure.

The diurnal variations of wind speed and WDS between Feb 10 and 16, 2013, are shown in Fig. 4.5. As explained earlier, the complete diurnal wind data was available for this week, and it was shown in Chapter 3 that diurnal wind patterns for this inland landfill are similar to this week. Therefore, wind data during this week would approximately

represent the typical diurnal wind conditions at this landfill. During late night in many geographical locations, there is less vertical air movement, which creates a thick (~ 100m) near-surface stable layer associated with low wind speed (De Visscher, 2013). After sunrise in such regions, the vertical temperature profile is altered and results in greater turbulence that increases near-surface wind speed. For such conditions, wind speed is higher during the afternoon and evening compared to early morning and late night (De Visscher, 2013; Stull, 1988), which is consistent with the data in Fig. 4.5c. Higher wind speed results in larger R^2 , smaller ERD , and more accurate TDM measurements, which is reported in Fig. 4.5a and 4.5b.

4.3.1.4 Seasonal variations of the TDM filtering parameters

Along with diurnal variations of meteorological parameters, their seasonal variation can affect the collection of accurate TDM data. The R^2 filtering criterion is by far the most used filtering criterion in the literature (Delkash et al., 2016; Taylor et al., 2016; Mønster et al., 2014; Mønster et al., 2015) and is usually the most difficult to satisfy. For example, Fredenslund et al. (2019) applied this criterion to two dataset and 70% and 96% of the total data were discarded. Therefore, R^2 is the focus of the rest of the analysis.

For the measurement period conducted between June 2011 and November 2013, Fig. 4.6 indicates that the R^2 filtering parameter is larger with less variability, i.e., smaller IQR, for measurements carried out in November 2011, April 2012, December 2012, and November 2013. On the other hand, R^2 was smaller in June 2012, and between March 2013 and June 2013. A portion of the seasonal differences in R^2 might be associated with

1) microbial activities and emissions from other sources/sinks during warmer seasons that might oxidize/generate methane under warmer conditions (Bogner et al., 1997) and 2) differences in atmospheric physics. A plausible explanation for high R^2 during the abovementioned months is the occurrence of either high wind speeds or low WDS . High wind speeds in November 2011 coincided with high R^2 with low WDS (see Fig. 4.6). The higher temperature difference between the polar and mid-altitude regions (location of this landfill) during winter compared to summer causes stronger winds during winter (Hall et al., 2015). Fig. 4.6 indicates that TI does not change significantly within months and this parameter might not have a clear impact on R^2 . In addition, fewer unstable atmospheric conditions were recorded at the site during these colder months. It is important to reiterate that Scheutz and Kjeldsen (2019) recommend avoiding TDM campaigns when the atmosphere is unstable. During wintertime at this landfill, sustained winds tend to be greater and vertical atmospheric dispersion smaller (discussed in Chapter 3 that unstable atmospheric conditions occur less often in winter times). The collected data indicates that the average wind speed in November 2013 was (4.9 ± 0.2) m/s, while it was (3.7 ± 0.1) m/s in June 2013. This sustained wind in winter provided better conditions for accurate TDM measurements.

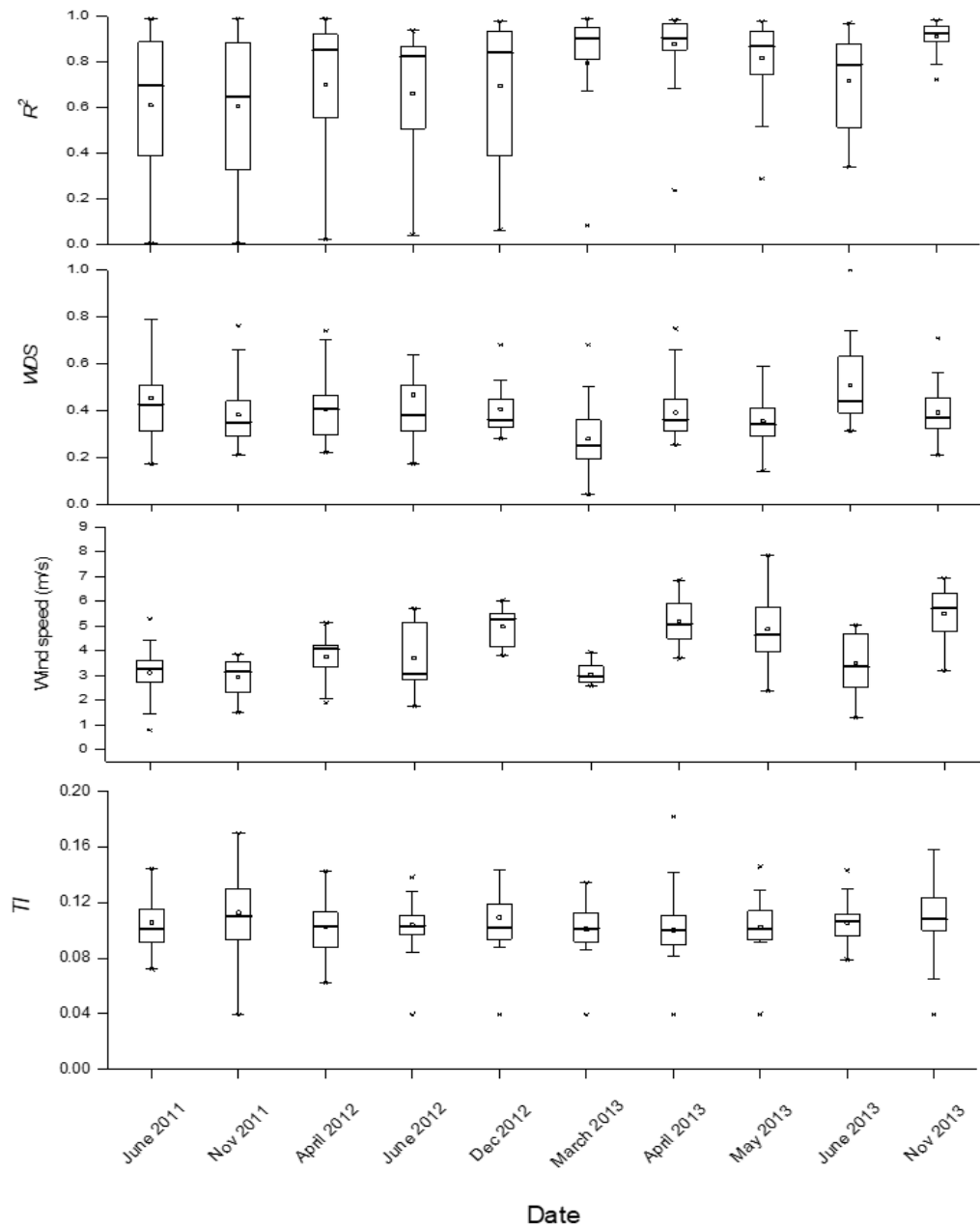


Figure 4.6 Seasonal variations of the R^2 filtering parameter obtained using mobile TDM data and seasonal variations of WDS, wind speed and TI .

4.3.2 TDM Stationary Approach

For the 63 stationary deployments, the variation of the R^2 filtering parameter with wind speed and WDS is shown in Fig. 4.7. Due to the limited number of stationary measurements, all data are analyzed together. The data point correlation (R_1) between wind speed and the R^2 filtering parameter is 0.38 and between the median of the groups (R_2) and wind speeds is 0.59, which suggests that an increase in wind speeds leads to a higher R^2 between C_M and C_T . The correlation between the skewness of the R^2 and wind speed is -0.64 . This indicates that the occurrence of a greater mode is more probable for higher wind speeds. Referring to Foster-Wittig et al. (2015) and Delkash et al. (2016) who applied $R^2 > 0.80$ as a filtering criterion for the TDM, the data obtained by the stationary approach is reliable only when wind speeds are greater than 5 m/s – an event that occurs infrequently. Acknowledging that $R^2 > 0.80$ is the criterion for reliable TDM data, 77% of the stationary data were not acceptable.

R^2 is negatively correlated with WDS: $R_1 = -0.17$ (Fig. 4.7b), which indicates that WDS has a weak negative impact on TDM accuracy. Similarly, the correlation between the medians of the binned data and WDS is $R_2 = -0.34$. Since $R_3 = 0.77$, an increase in WDS leads to an increase in standard error of R^2 , which is less desirable. Since the mean values are less than the median, the distributions of R^2 for binned data are negatively skewed. Because $R_4 = -0.51$, an increase in WDS leads to a decrease in modal value of R^2 , which is not favorable. These results are consistent those for mobile

deployments, although it should be noted that the criterion $R^2 > 0.80$, which filters out poor data, sometimes occurs for stationary data when $WDS < 0.4$.

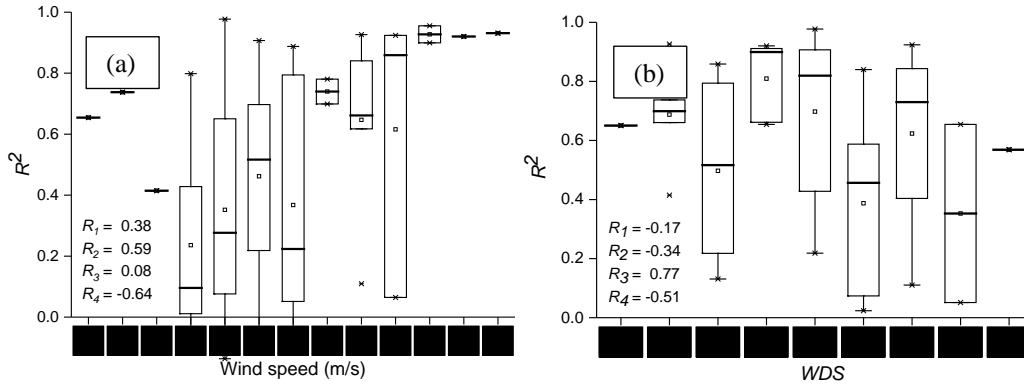


Figure 4.7 Dependency of the R^2 filtering parameter on a) wind speed and b) WDS for TDM data collected with the stationary approach.

4.3.3 Comparison between the mobile and stationary approaches

The average wind speed during stationary approach was 4.6 ± 0.15 m/s and only 23% of the total stationary data points had $R^2 > 0.80$. However, the average wind speed during the mobile approach was 4.0 ± 0.06 m/s and about 40% (180 transects of 452 transects) of the mobile dataset had $R^2 > 0.80$. This finding indicates that at this landfill the mobile TDM approach is clearly superior over the stationary approach.

Figure 4.8 shows variations of R^2 for six days where stationary and mobile approaches were conducted. Except for May 8, 2013, the mobile approach showed superior performance to the stationary approach. While all field measurements using either approach had $R^2 > 0.80$ on November 7, 2013, this is due to the high wind speed during this day (Fig. 4.8).

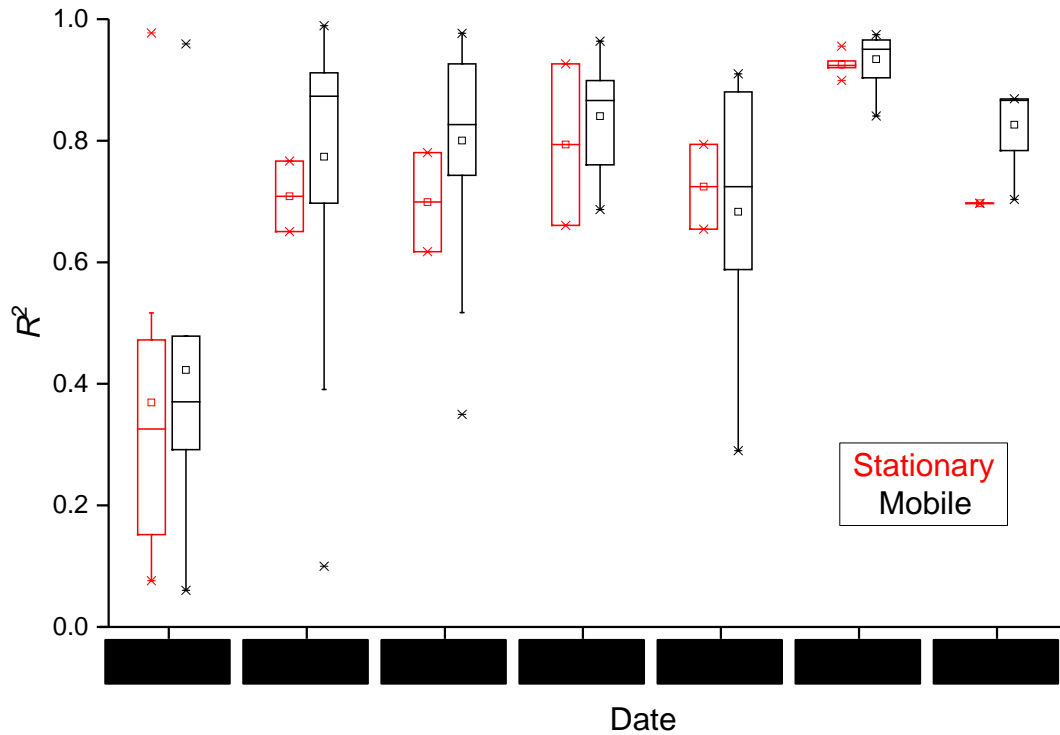


Figure 4.8 Comparison of the R^2 filtering parameter for stationary and mobile approaches on dates when both TDM methods were applied.

The percentage of data with $R^2 > 0.80$ in the mobile approach (39%) is higher than the stationary approach (23%). While the stationary approach has an acceptable performance under high wind speeds ($> 5\text{m/s}$), acceptable results from the mobile approach can be found at even lower wind speeds. The mobile approach had a better performance when $WDS < 0.5$. However, only 10% of the stationary data had $R^2 > 0.80$ when $WDS < 0.4$.

4.4 Implications and Conclusions

From a monetary perspective, TDM campaigns require 1) travel and accommodation costs of the technicians; 2) payment to these laborers; 3) equipment rental fees and supplies including the gas analyzer, vehicle, and tracer gas; and 4) insurance and liability costs. As an example, a 5-day deployment in California with four technicians is estimated to cost approximately \$15K (Imhoff, personal communication, 2021). Efficient deployment of the TDM is necessary to save time and money. With this analogy, the cost of these three-year field measurements reported in Foster-Wittig et al. (2015) should be about \$150K (10 campaigns).

Foster-Wittig et al. (2015) reported that among 1876 transect campaigns at 15 landfills, only 456 (24%) passed all the three criteria ($R^2 > 0.80$; $ERD < 20\%$; and SN_A & $SN_M > 10$), while 40% of the total data had $R^2 > 0.80$, 40% had $ERD < 20\%$, and 50% of the total data had both SN_A and $SN_M > 10$. This indicates that while filtering the TDM data is essential to provide reliable estimates of emissions, this process wastes a significant amount of time and money. For instance, ignoring 800 deployments to maintain one filtering criterion (e.g., SN) means squandering tens of thousands of dollars. Therefore, a better understanding about factors affecting the accuracy of the TDM method would help landfill operators schedule their campaigns during times when wind speeds are high and wind direction variations are low. Although applying filtering criteria enables data from either mobile or stationary approaches to be used, we found that fewer data were discarded using the mobile approach. The reliability

of the stationary approach ($R^2 > 0.8$) improved when wind speed was greater than 5 m/s and $WDS < 0.4$.

In addition, the TDM filtering criteria exhibit diurnal and seasonal variations. The TDM has the least accuracy during early morning and late evening hours due to the low wind speeds. Moreover, since wind speeds are usually high and WDS are usually low when campaigns were carried out during cold seasons as compared to summer campaigns, TDM measurements during the winter were more accurate at this landfill.

Moreover, we suggest weather forecast considerations be used during field planning to increase the fraction of accurate TDM data (e.g., high R^2). To illustrate this point, the mobile TDM data collected in all 10 primary campaigns (data collected in each primary campaign within a 3-4 day period) are considered. The relationship between average wind speeds and average R^2 in each campaign would reveal the importance of desktop tasks prior to field measurements. Figure 4.9 depicts the relationship between R^2 filtering parameter and the average wind speeds for each group, where error bars represent one standard deviation. The correlation coefficient between the R^2 filtering parameter and wind speed is 0.65. This means that if high wind speed is forecast for several days, conducting TDM measurements during that period is promising for reliable TDM data. Consistent with this point, Scheutz and Kjeldsen (2019) recommend TDM campaigns if wind speed is at least 2 m/s and the wind direction is favorable, i.e., in a direction that coincides with favorable locations of downwind roadways for mobile measurements.

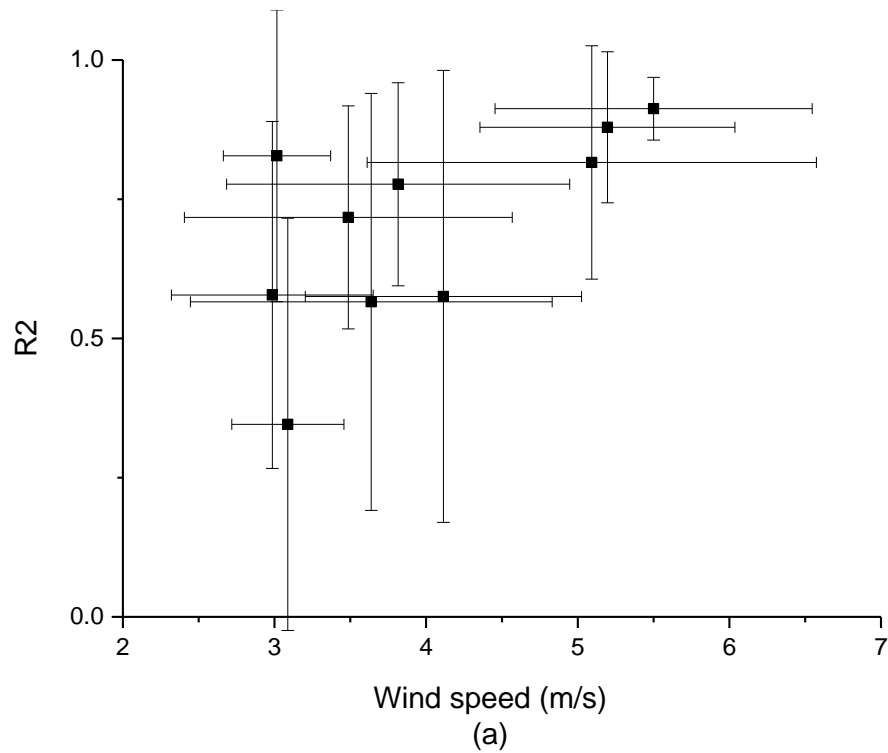


Figure 4.9 Variation of the R^2 filtering parameter versus wind speed for TDM data grouped into 3-4 day periods. Data of group is averaged and shown as a single data point. The bars indicate one standard deviation.

We reiterate that if a TDM dataset passes the filtering criteria developed by Foster-Wittig et al. (2015), the estimated emission should be reliable. This study discussed the rates of passing filtering criteria under different atmospheric conditions and TDM approaches. In addition to the concern about high ratio of TDM data passing the filtering criteria, Scheutz and Kjeldsen (2019) noted the importance of emission measurements representing “normal site conditions”. Acknowledging that meteorological parameters affect diurnal methane emissions (Chapter 3), Scheutz and Kjeldsen (2019) recommend conducting measurements during the periods when barometric pressure is within ± 3 mbar of the normal barometric pressure at the site. In our previous work for the Southeastern

US landfill, we showed that diurnal average emissions occur before noon (~ 11 am) and afternoon (~ 4 pm) (Delkash et al., in review). Considering that finding and the results of this paper indicates that the preferred times of TDM measurement at this landfill are before noon (~ 11 am) and afternoon (~ 4 pm) to have a high rate of data passing filtering criteria and represent diurnal average emissions.

Chapter 5

FUTURE WORK

To improve our understanding of short-term methane emission variations at landfills, additional research is needed. Recommended future work can be grouped into three categories: (I) Understanding the effect of meteorological parameters on annual methane emission estimations at different time spans (weekly, monthly, and seasonally) to ultimately estimate annual emissions, (II) Assessing the current landfill methane emission regulations together with the findings in this dissertation to validate their robustness, and (III) Collecting data from field-scale systems to investigate how diurnal meteorological parameters affect the methane mass balance in landfills. These diurnal patterns of emissions infer a diurnal pattern for gas collection system as well. A better understanding of diurnal patterns of gas collection systems would help more efficiently collect gas.

(I) Annual emission estimation

An accurate annual landfill methane emission estimation requires continuous measurements. However, such measurements are costly and for most measurement technologies difficult to implement. Therefore, understanding temporal emission variations would help researchers interpolate emissions for unmeasured periods. Under constant gas generation and with no gas collection, short-term temporal variations of emissions were

found here to be associated with temporal fluctuations of some atmospheric parameters. Atmospheric conditions can promote or suppress gas emissions during different time frames, from a few minutes (Delkash et al., 2016) to seasonal time frames (Gebert et al., 2011). Understanding the mechanisms that affect variations in methane emission from landfills will result in more accurate estimates of emission during unmeasured days. For instance, methane emissions have a positive correlation with wind speed for short term measurements (Delkash et al., 2016) and a negative correlation with barometric pressure for a period of several days (Xu et al., 2014). Thus, measuring these atmospheric parameters could indicate the magnitude of methane emissions from landfills during unmeasured days. In this dissertation, it was found that diurnal methane emissions vary with air temperature and wind speed, depending upon atmospheric stability conditions. Using these observations, I postulate that diurnal-average methane emissions can be obtained using limited short measurements. Xu et al. (2014) found that temporal variations of air pressure are responsible for methane emissions for a period of 1 to 10 days. Thus, average emission estimation for this period of time might be obtained by combining insights from this dissertation and Xu et al. (2014). Further investigations are required for longer time periods to finally estimate annual emissions using limited field measurements.

In addition to using meteorological parameters to predict methane emissions during unmeasured days, the remote sensing science can be used to estimate methane emissions as well. With the extent of different satellites and improving their resolutions and periods, the remote sensing technique can produce high resolution images of methane concentrations within short periods. These obtained concentrations by remote sensing

technique should be trained using field emission measurements to estimate emissions at unmeasured days using the trained model and high resolution images of methane concentrations within short periods.

- (II) Assessing current landfill methane emission regulations against the findings in this dissertation to validate their robustness

Findings in this dissertation challenge current methane emission regulations. For example, the State of California requires surface scanning using flame ionisation detector (FID) (10 cm above the ground) for methane concentrations when average wind speed $< 2.2 \text{ m.s}^{-1}$. There is currently no approved field measurement when average wind speed is higher than 2.2 m.s^{-1} . Any surface concentration above 500 ppm indicates landfill conditions that are in need of remediation. One issue with this approach is that the relationship between surface concentration and methane flux depends on surface roughness, wind speed, and atmospheric stability, which are ignored in the current regulation. Therefore, there is no universal relationship between concentrations at 10 cm above the ground and methane emissions. Moreover, while it is well-known that higher wind speed leads to higher surface fluxes, higher wind speeds also decrease surface concentrations because it expunges methane near the ground surface. Therefore, the surface scanning approach mistakenly finds that wind speeds decrease surface fluxes. These regulations should be revisited using the findings from this dissertation.

(III) Improving gas collection system efficiency

Although diurnal variations of methane emissions from landfills were investigated in this dissertation, diurnal variations in gas collection systems have not been examined. Most of gas collection systems are operated under a constant methane flow. Under emission-decreasing conditions, air intrudes into landfills and methane contents in landfill gas decrease. Therefore, a higher vacuum needs to be applied to collect more landfill gas to meet that constant methane flow. This higher vacuum pulls more air into the gas collection systems. However, during emission-increasing conditions, methane content in landfill gas is higher and a smaller vacuum is needed. Thus, less air content is expected in the collected landfill gas. Collected landfill gas has some impurities including oxygen and nitrogen (results of air intrusion into landfills during emission-decreasing conditions) that need to be treated under costly processes. As one solution for gas collection efficiency improvement, a more than system capacity landfill gas can be collected and stored during emission-increasing conditions (higher methane content). Appropriately, a less than system capacity landfill gas can be collected during emission-decreasing conditions (lower methane content). The stored methane can be injected into the system during emission-decreasing conditions (lower methane content) to compensate methane flow. This action causes exemption of some gas treatment steps, which are costly. Moreover, methane emission is decreased by collecting more gas during emission-decreasing conditions.

REFERENCES

- Abichou, T., Kormi, T., Yuan, L., Johnson, T., Francisco, E., 2015. Modeling the effects of vegetation on methane oxidation and emissions through soil landfill final covers across different climates. *Waste Manage.* 36, 230-240.
- Aghdam, E.F., Scheutz, C., Kjeldsen, P., 2019. Impact of meteorological parameters on extracted landfill gas composition and flow. *Waste Manage.* 87, 905-914.
- Allen, M.R., Braithwaite, A., Hills, C.C., 1997. Trace organic compounds in landfill gas at seven UK waste disposal sites. *Environ. Sci. Technol.* 31, 1054–1061.
- Barthelmie, R.J., Grisogono, B., Pryor, S.C., 1996. Observations and simulations of diurnal cycles of near-surface wind speeds over land and sea. *Journal of Geophysical Research: Atmospheres* 101, 21327-21337.
- Bear, J., Verruijt, A., 1987. *Theory and Applications of Transport in Porous Media.* Springer.
- Berens, P., 2009. CircStat: a MATLAB toolbox for circular statistics. *J Stat Softw* 31, 1-21.
- Bian, R., Xin, D., Chai, X., 2019. Methane emissions from landfill: influence of vegetation and weather conditions. *Environ. Technol.* 40, 2173-2181.
- Binning, P.J., Postma, D., Russell, T.F., Wesselingh, J.A., Boulin, P.F., 2007. Advective and diffusive contributions to reactive gas transport during pyrite oxidation in the unsaturated zone. *Water Resour. Res.* 43.
- Bogner, J., Meadows, M., Czepiel, P., 1997. Fluxes of methane between landfills and the atmosphere: natural and engineered controls. *Soil Use Manage.* 13, 268-277.
- Bogner, J.E., Spokas, K.A., Burton, E.A., 1997. Kinetics of methane oxidation in a landfill cover soil: temporal variations, a whole-landfill oxidation experiment, and modeling of net CH₄ emissions. *Environ. Sci. Technol.* 31, 2504-2514.
- Börjesson, G., Samuelsson, J., Chanton, J., Adolfsson, R., Galle, B., Svensson, B.H.,

- Burba, G., 2013. Eddy Covariance Method for Scientific, Industrial, Agricultural and Regulatory Applications: A Field Book on Measuring Ecosystem Gas Exchange and Areal Emission Rates. LI-Cor Biosciences.
- Calif, R., Emilion, R., Soubdhan, T., Blonbou, R., 2008. Wind speed classification using dirichlet mixtures. arXiv preprint arXiv:0810.4422
- Chanton, J., Liptay, K., 2000. Seasonal variation in methane oxidation in a landfill cover soil as determined by an in situ stable isotope technique. *Global Biogeochem. Cycles* 14, 51–60.
- Choi, J., Tillman, F.D., Smith, J.A., 2002. Relative importance of gas-phase diffusive and advective trichloroethene (TCE) fluxes in the unsaturated zone under natural conditions. *Environ. Sci. Technol.* 36, 3157-3164.
- Costanza-Robinson, M.S., Brusseau, M.L., 2002. Gas phase advection and dispersion in unsaturated porous media. *Water Resour. Res.* 38, 7-9.
- Crosson, E., 2008. A cavity ring-down analyzer for measuring atmospheric levels of methane, carbon dioxide, and water vapor. *Appl. Phys. B* 92, 403–408.
- Czepiel, P., Shorter, J., Mosher, B., Allwine, E., McManus, J., Harriss, R., Kolb, C., Lamb, B., 2003. The influence of atmospheric pressure on landfill methane emissions.
- Czepiel, P.M., Mosher, B., Harriss, R.C., Shorter, J.H., McManus, J.B., Kolb, C.E., Allwine, E., Lamb, B.K., 1996. Landfill methane emissions measured by enclosure and atmospheric tracer methods. *Journal of Geophysical Research: Atmospheres* 101, 16711-16719.
- Czepiel, P.M., Shorter, J.H., Mosher, B., Allwine, E., McManus, J.B., Harriss, R.C., Kolb, C.E., Lamb, B.K., 2003. The influence of atmospheric pressure on landfill methane emissions. *Waste Manage.* 23, 593-598.
- Dai, A., Deser, C., 1999. Diurnal and semidiurnal variations in global surface wind and divergence fields. *Journal of Geophysical Research: Atmospheres* 104, 31109-31125.
- De la Cruz, Florentino B, Green, R.B., Hater, G.R., Chanton, J.P., Thoma, E.D., Harvey, T.A., Barlaz, M.A., 2016. Comparison of field measurements to methane emissions models at a new landfill. *Environ. Sci. Technol.* 50, 9432-9441.
- De Visscher, A., 2013. Air Dispersion Modeling: Foundations and Applications. John Wiley & Sons.

- De Visscher, A., 2013. Air Dispersion Modeling: Foundations and Applications. John Wiley & Sons.
- De Visscher, A., Van Cleemput, O., 2003. Simulation model for gas diffusion and methane oxidation in landfill cover soils. *Waste Manage.* 23, 581-591.
- Deleersnijder, E., Campin, J., Delhez, E.J., 2001. The concept of age in marine modelling: I. theory and preliminary model results. *J. Mar. Syst.* 28, 229–267.
- Delkash, M., Zhou, B., Han, B., Chow, F.K., Rella, C.W., Imhoff, P.T., 2016. Short-term landfill methane emissions dependency on wind. *Waste Management* 55, 288-298.
- Delkash, M., Zhou, B., Han, B., Chow, F.K., Rella, C.W., Imhoff, P.T., 2016. Short-term landfill methane emissions dependency on wind. *Waste Manage.* 55, 288-298.
- EPA. (2019). U.S. Greenhouse Gas Emissions and Sinks: 1990–2017, U.S. Environmental Protection Agency, Washington, DC, USA.
- Feder, P.I., 1974. No title. Probability and Statistics for Engineers and Scientists.
- Flesch, T.K., Wilson, J.D., Harper, L.A., Crenna, B.P., Sharpe, R.R., 2004. Deducing ground-to-air emissions from observed trace gas concentrations: a field trial. *J. Appl. Meteorol.* 43, 487-502.
- Foster-Wittig, T.A., Thoma, E.D., Green, R.B., Hater, G.R., Swan, N.D., Chanton, J.P., 2015. Development of a mobile tracer correlation method for assessment of air emissions from landfills and other area sources. *Atmos. Environ.* 102, 323-330.
- Franzidis, J., Heroux, M., Nastev, M., Guy, C., 2008. Lateral migration and offsite surface emission of landfill gas at City of Montreal landfill site. *Waste Manage. Res.* 26, 121-131.
- Fredenslund, A.M., Rees-White, T.C., Beaven, R.P., Delre, A., Finlayson, A., Helmore, J., Allen, G., Scheutz, C., 2019. Validation and error assessment of the mobile tracer gas dispersion method for measurement of fugitive emissions from area sources. *Waste Manage.* 83, 68-78.
- Frey, M.M., Brough, N., France, J.L., Traulle, O., Anderson, P.S., King, M.D., Jones, A.E., Wolff, E.W., Savarino, J., 2012. The diurnal variability of atmospheric nitrogen oxides (NO and NO₂) above the Antarctic Plateau driven by atmospheric stability and snow emissions. *Atmospheric Chemistry & Physics Discussions* 12.
- Galle, B.O., Samuelsson, J., Svensson, B.H., Börjesson, G., 2001. Measurements of methane emissions from landfills using a time correlation tracer method based on FTIR absorption spectroscopy. *Environ. Sci. Technol.* 35, 21-25.

- Gebert, J., Gröngröft, A., 2006. Passive landfill gas emission – influence of atmospheric pressure and implications for the operation of methane oxidising biofilters. *Waste Manag.* 26, 245–251.
- Gebert, J., Gröngröft, A., 2006. Performance of a passively vented field-scale biofilter for the microbial oxidation of landfill methane. *Waste Manage.* 26, 399-407.
- Gebert, J., Rachor, I., Gröngröft, A., Pfeiffer, E., 2011. Temporal variability of soil gas composition in landfill covers. *Waste Management* 31, 935-945.
- Green, R.B., Hater, G.R., Thoma, E.D., DeWees, J., Rella, C.W., Crosson, E.R., Goldsmith, C.D., Swan, N., 2010. Methane emissions measured at two California landfills by OTM-10 and an acetylene tracer method. In: *Proceedings of the Global Waste Management Symposium*, pp. 3–6.
- Hall, R., Erdélyi, R., Hanna, E., Jones, J.M., Scaife, A.A., 2015. Drivers of North Atlantic polar front jet stream variability. *Int. J. Climatol.* 35, 1697-1720.
- Hargreaves, K., Fowler, D., Pitcairn, C., Aurela, M., 2001. Annual methane emission from finnish mires estimated from eddy covariance campaign measurements. *Theoretical and Applied Climatology* 70, 203-213.
- He, Y., McFarlane, N.A., Monahan, A.H., 2012. The influence of boundary layer processes on the diurnal variation of the climatological near-surface wind speed probability distribution over land. *J. Clim.* 25, 6441-6458.
- Intergovernmental Panel on Climate Change, 2006. 2006 IPCC guidelines for national greenhouse gas inventories. Hayama, Japan: IPCC.
<http://www.ipccnggip.iges.or.jp/public/2006gl/vol5.html>.
- Izumoto, S., Hamamoto, S., Kawamoto, K., Nagamori, M., Nishimura, T., 2018. Monitoring of methane emission from a landfill site in daily and hourly time scales using an automated gas sampling system. *Environmental Science and Pollution Research* 25, 24500-24506.
- Krzywinski, M., Altman, N., 2014. Visualizing samples with box plots. *Nature methods* 11, 119-120.
- Lapworth, A., 2005. The diurnal variation of the marine surface wind in an offshore flow. *Quarterly Journal of the Royal Meteorological Society: A journal of the atmospheric sciences, applied meteorology and physical oceanography* 131, 2367-2387.

- Laurila, T., Tuovinen, J., Lohila, A., Hatakka, J., Aurela, M., Thum, T., Pihlatie, M., Rinne, J., Vesala, T., 2005. Measuring methane emissions from a landfill using a cost-effective micrometeorological method. *Geophys. Res. Lett.* 32.
- Levintal, E., Dragila, M.I., Weisbrod, N., 2019. Impact of wind speed and soil permeability on aeration time in the upper vadose zone. *Agric. For. Meteorol.* 269, 294-304.
- Li, J., Green, R.B., Magnusson, D.A., Amen, J., Thoma, E.D., Foster-Wittig, T.A., McDermitt, D.K., Xu, L., Burba, G., 2015. Using eddy covariance to quantify methane emissions from a dynamic heterogeneous area. , 22-25.
- Lohila, A., Laurila, T., Tuovinen, J., Aurela, M., Hatakka, J., Thum, T., Pihlatie, M., Rinne, J., Vesala, T., 2007. Micrometeorological measurements of methane and carbon dioxide fluxes at a municipal landfill. *Environ. Sci. Technol.* 41, 2717-2722.
- Mahabadi, N. and Jang, J., 2014. Relative water and gas permeability for gas production from hydrate-bearing sediments. *Geochemistry, Geophysics, Geosystems* 15, 2346-2353.
- Maier, M., Schack-Kirchner, H., Aubinet, M., Goffin, S., Longdoz, B., Parent, F., 2012. Turbulence effect on gas transport in three contrasting forest soils. *Soil Sci. Soc. Am. J.* 76, 1518-1528.
- Massman, W., 1998. A review of the molecular diffusivities of H₂O, CO₂, CH₄, CO, O₃, SO₂, NH₃, N₂O, NO, and NO₂ in air, O₂ and N₂ near STP. *Atmospheric Environment* 32, 1111-1127.
- Matacchiera, F., Manes, C., Beaven, R.P., Rees-White, T.C., Boano, F., Mønster, J., Scheutz, C., 2019. AERMOD as a Gaussian dispersion model for planning tracer gas dispersion tests for landfill methane emission quantification. *Waste Manage.* 87, 924-936.
- McBain, M.C., Warland, J.S., McBride, R.A., Wagner-Riddle, C., 2005. Micrometeorological measurements of N₂O and CH₄ emissions from a municipal solid waste landfill. *Waste Manage. Res.* 23, 409-419.
- Metcalf, D.E., Farquhar, G.J., 1987. Modeling gas migration through unsaturated soils from waste disposal sites. *Water Air Soil Pollut.* 32, 247-259.
- Monin, A. and Obukhov, A., 1954. Basic laws of turbulent mixing in the surface layer of the atmosphere. *Contrib. Geophys. Inst. Acad. Sci. USSR* 151, e187.
- Mønster, J., Kjeldsen, P., Scheutz, C., 2019. Methodologies for measuring fugitive methane emissions from landfills—A review. *Waste Manage.* 87, 835-859.

- Mønster, J., Samuelsson, J., Kjeldsen, P., Scheutz, C., 2015. Quantification of methane emissions from 15 danish landfills using the mobile tracer dispersion method. *Waste Management* 35, 177-186.
- Mønster, J.G., Samuelsson, J., Kjeldsen, P., Rella, C.W., Scheutz, C., 2014. Quantifying methane emission from fugitive sources by combining tracer release and downwind measurements – a sensitivity analysis based on multiple field surveys. *Waste Manage.* 34, 1416–1428.
- Mukaka, M.M., 2012. A guide to appropriate use of correlation coefficient in medical research. *Malawi Medical Journal* 24, 69-71.
- Munyan, J., 2010. Delaware Solid Waste Authority, 1128 South Bradford Street,
- Park, J. and Shin, H., 2001. Surface emission of landfill gas from solid waste landfill. *Atmospheric Environment* 35, 3445-3451.
- Peterson, T.C., Parton, W.J., 1983. Diurnal variations of wind speeds at a shortgrass prairie site—a model. *Agricultural Meteorology* 28, 365-374.
- Pleim J, Ran L., 2011. Surface flux modeling for air quality applications. *Atmosphere* 2:271-302.
- Poulsen, T.G., 2018. Measuring horizontal pore gas velocity profiles in porous media in response to near-surface wind speed and gustiness. *Eur. J. Soil Sci.* 69, 997-1007.
- Poulsen, T.G., Moldrup, P., 2006. Evaluating effects of wind-induced pressure fluctuations on soil-atmosphere gas exchange at a landfill using stochastic modelling. *Waste Manage. Res.: J. Int. Solid Wastes Public Clean. Assoc., ISWA*
- Poulsen, T.G., Møldrup, P., 2006. Evaluating effects of wind-induced pressure fluctuations on soil-atmosphere gas exchange at a landfill using stochastic modelling. *Waste Manage. Res.* 24, 473-481.
- Pourbakhtiar, A., Papadakis, K., Poulsen, T., Bridge, J., Wilkinson, S., 2017. Effect of air turbulence on gas transport in soil; comparison of approaches. 68, 48-56.
- Rachor, I., Gebert, J., Gröngröft, A., Pfeiffer, E., 2013. Variability of methane emissions from an old landfill over different time-scales. *Eur. J. Soil Sci.* 64,
- Rawls, W.J., Brakensiek, D.L., Saxton, K.E., 1982. Estimation of soil water properties. *Trans. ASAE* 25, 1316-1320.

- Rees-White, T.C., Mønster, J., Beaven, R.P., Scheutz, C., 2019. Measuring methane emissions from a UK landfill using the tracer dispersion method and the influence of operational and environmental factors. *Waste Manage.* 87, 870-882.
- Scheehle, E., Godwin, D., Ottinger, D., DeAngelo, B., 2006. Global anthropogenic non-CO₂ greenhouse gas emissions: 1990–2020. Version: revised June.
- Scheutz, C., Kjeldsen, P., 2019. Guidelines for landfill gas emission monitoring using the tracer gas dispersion method. *Waste Manage.* 85, 351-360.
- Scheutz, C., Samuelsson, J., Fredenslund, A.M., Kjeldsen, P., 2011. Quantification of multiple methane emission sources at landfills using a double tracer technique.
- Seigneur, C., 2019. *Air Pollution: Concepts, Theory, and Applications*. Cambridge University Press.
- Spokas, K., Bogner, J., Chanton, J., 2011. A process-based inventory model for landfill CH₄ emissions inclusive of seasonal soil microclimate and CH₄ oxidation. *Journal of Geophysical Research: Biogeosciences* 116.
- Stern, J.C., Chanton, J., Abichou, T., Powelson, D., Yuan, L., Escoriza, S., Bogner, J.,
- Stull, R.B., 1988. *An Introduction to Boundary Layer Meteorology*. Springer Science & Business Media.
- Stull, R.B., 1988. *An Introduction to Boundary Layer Meteorology*. Springer Science & Business Media.
- Sun, W.Y., Chang, C.Z., 1986. Diffusion-model for a convective layer. 2. Plume released from a continuous point-source. *J. Clim. Appl. Meteorol.* 25 (10), 1454–
- Taylor D. M., 2017. *Atmospheric Dispersion Modeling to Inform a Landfill Methane Emissions Measurement Method*. PhD Dissertation, University of California, Berkeley.
- Taylor D.M., Chow F.K., Delkash M., Imhoff P.T., 2018. Atmospheric modeling to assess wind dependence in tracer dilution method measurements of landfill methane emissions. *Waste Management* 73, 197-209.
- Taylor, D.M., Chow, F.K., Delkash, M., Imhoff, P.T., 2016. Numerical simulations to assess the tracer dilution method for measurement of landfill methane emissions. *Waste Manage.* 56, 298-309.
- Teclé, D., Lee, J., Hasan, S., 2009. Quantitative analysis of physical and geotechnical factors affecting methane emission in municipal solid waste landfill. *Environmental Geology* 56, 1135-1143.

- Thien, S.J., 1979. A flow diagram for teaching texture-by-feel analysis. *Journal of Agronomic Education* 8, 54-55.
- Thorneloe, S.A., Reisdorph, A., Laur, M., Pelt, R., Bass, R.L., Burklin, C., 1999. The US Environmental Protection Agency's landfill gas emissions model (LandGEM). 4, 11-18.
- Von Hippel, P.T., 2005. Mean, median, and skew: Correcting a textbook rule. *Journal of statistics Education* 13.
- Wang, J., Xia, F., Bai, Y., Fang, C., Shen, D., He, R., 2011. Methane oxidation in landfill waste biocover soil: kinetics and sensitivity to ambient conditions. *Waste*
- Weitz, K.A., Thorneloe, S.A., Nishtala, S.R., Yarkosky, S., Zannes, M., 2002. The impact of municipal solid waste management on greenhouse gas emissions in the
- Wesely, M., Hicks, B., 1977. Some factors that affect the deposition rates of sulfur dioxide and similar gases on vegetation. *J. Air Pollut. Control Assoc.* 27, 1110-1116.
- Wille, C., Kutzbach, L., Sachs, T., Wagner, D., Pfeiffer, E., 2008. Methane emission from siberian arctic polygonal tundra: Eddy covariance measurements and modeling. *Global Change Biology* 14, 1395-1408.
- Wyngaard, J.C., 2010. *Turbulence in the Atmosphere*. Cambridge University Press.
- Xin, D., Hao, Y., Shimaoka, T., Nakayama, H., Chai, X., 2016. Site specific diel methane emission mechanisms in landfills: A field validated process based on vegetation and climate factors. *Environmental Pollution*
- Xu, L., Lin, X., Amen, J., Welding, K., McDermitt, D., 2014. Impact of changes in atmospheric pressure on landfill methane emission. *Global Biogeochemical Cycles* 28, 679-695.
- Xue, M., Droegemeier, K.K., Wong, V., 2000. The advanced regional prediction system (ARPS) – a multi-scale nonhydrostatic atmospheric simulation and prediction model. Part I: Model dynamics and verification. *Meteorol. Atmos. Phys.* 75, 161–193.
- Yeşiller, N., Hanson, J.L., Liu, W., 2005. Heat generation in municipal solid waste landfills. *Journal of Geotechnical and Geoenvironmental Engineering* 131, 1330-1344.

Appendix

A. SHORT-TERM METHANE EMISSIONS DEPENDENCY ON WIND

Calibration of the Sandtown TDM instrument

A prototype CH₄ and C₂H₂ analyzer, developed by Picarro, Inc. (Sunnyvale, CA), was used to monitor the concentrations of atmospheric CH₄ and C₂H₂ contained in the downwind plume from the landfill. This gas analyzer is based on an all-optical technique called cavity ring-down spectroscopy (CRDS).

The CRDS analyzer was calibrated by injecting five prepared gas mixtures that contain CH₄ over a range from 0 – 2.5 ppm. These bottles were calibrated using a second CRDS instrument that was calibrated at NOAA in 2007 against the World Meteorological Organization's artifact-based CH₄ scale. Because this calibration method relies on a spectroscopic transfer standard that is not directly traceable to primary standards, an independent gas bottle was obtained with traceability to NIST primary standards. The values in the header for each gas are the bottle concentrations and analytical uncertainties as specified by Spectra Gases (Stewartsville, New Jersey). The reported mean and standard deviation from the four single point calibrations are listed at the bottom of the table. The instrument readings are extremely stable, and since the mean of the measurements are well within the stated uncertainty of the bottle concentration, we elected not to adjust the instrument calibration to match the bottle.

The detection limits of the CRDS analyzer were determined in October, 2009, by injecting a gas bottle with about 1.8 ppm of CH₄ and zero C₂H₂ and measuring the standard deviation of the results over a period of approximately 30 minutes. The standard deviation of the CH₄ measurement was 0.8 ppb, and the standard deviation of the C₂H₂ measurement was 0.2 ppb, with a total measurement interval for both gases of 2 seconds. The limit of detection for a single measurement point was estimated to be equal to three times the standard deviation: 2.4 ppb for CH₄ and 0.6 ppb for C₂H₂.

Although the instrument was not calibrated in the field or after the field trial, tests with the CRDS analyzer configured for CH₄ and CO₂ measurement have demonstrated that CH₄ and CO₂ are typically very stable (better than two parts in one thousand of the reading) over weeks and months (Richardson et al. 2012). The instrument used in this study is based on the same technology (and in the case of CH₄ the same spectroscopy and analysis algorithms), and during proper operation should exhibit the same low-drift characteristics. To establish proper operation during field tests at the Sandtown Landfill, the cavity pressure and cavity temperature were measured and were within 0.1 Torr and 0.05 °C of their setpoint values of 70 Torr and 45 °C, respectively, indicating that the control systems were operating normally and that the sample temperature and pressure were set to the values used during calibration at the factory. Finally, the background values of CH₄ and CO₂ reported by the instrument when not in the landfill plume were 1.87 ppm and 1 ppb, respectively, which are within 0.1 ppm and 1 ppb of the well-mixed atmospheric values for those two compounds for the east coast of the United States .

Sensitivity Analyses of the Sandtown TDM Data

As The data filtering criterion $R^2 > 0.80$ was selected, since this goodness of fit criterion was recommended by Foster-Wittig et al. (2015). The second derivative of the normalized wind speed criterion was specified to be greater than 0.175 to remove data from regions where wind speeds changed rapidly, which created greater uncertainty in interpolated wind speeds necessary to match the times of CH₄ emissions measurements. A visual assessment of the wind data was used to select the 0.175 criterion. The sensitivity of the tracer dilution method results to these filtering criteria was investigated by adjusting the R^2 criterion between 0.70 and 0.90 and the second derivative of the normalized wind speed criterion between 0.10 and 0.25. VF1/CF1, CF1/3Pts and CF2/3Pts are insensitive to filtering criteria: all regressions show very weak correlation between emissions and wind speed. These results are consistent with the VF1 and CF1 simulations, where total landfill CH₄ emissions were not correlated with wind speed.

For simulation pair VF2/CF1, however, data collected at 2.5 m AGL are sensitive to filtering criteria: R^2 varies between 0.24 and 0.54 depending on the numerical values selected for filtering. Regardless of the filtering criteria specified, normalized CH₄ emissions are always positively correlated with normalized wind speed with the slope of the regression line ranging from 0.68 to 1.41. If $R^2 > 0.80$ and the second derivative criterion > 0.175 are used to filter data at 2.5 m AGL, the slope of the regression line is 0.84 ± 0.38 with the 95% confidence interval encompassing the known slope of 1.0 between landfill CH₄ emissions and wind speed as specified in the VF2 simulation. At 85 m AGL, VF2/CF1 data are relatively insensitive to filtering criteria over the range of parameters tested, with R^2 ranging from 0.49 to 0.56 and emission always positively correlated with

wind speed. When $R^2 > 0.80$ and second derivative criterion > 0.175 are used to filter these data, the slope of the regression line is 0.68 ± 0.26 with the 95% confidence interval coming closest to encompassing the known slope of 1.0 between emissions and wind speed when compared to all other filtering criteria. Based on this analysis, $R^2 > 0.80$ and the second derivative criterion > 0.175 are reasonable filtering criteria, since when applied to the simulation data they result in the best match between tracer dilution method results and known CH₄ emissions relationships with wind speed specified in the model simulations.

While data at 2.5 m AGL show similar correlation between emissions and wind speed for all filtering criteria tested, the correlation is negative when $R^2 > 0.70$ is used but positive for all other filtering criteria. The valid data are so few at 2.5 m AGL (see Figure 2.11) that the results at this elevation are sensitive data filtering. Conclusions about the relationship between CH₄ emissions and wind speed at 2.5 m AGL may not be significant because of the sparsity of data. At 85 m AGL, however, if data filtering is used the results are relatively insensitive to the numerical values specified for filtering: R^2 ranges from 0.49 to 0.55 and emissions are always positively correlated with wind speed for all criteria tested.

B. DIRNAL LANDFILL METHANE FLUX PATTERNS ACROSS DIFFERENT SEASONS AT A LANDFILL IN SOUTHEASTERN US

Gas transport in near-surface atmosphere

Methane transport from the subsurface in a landfill into the atmosphere highly depends on shear stress near the surface. Shear velocity is a measure describing near-surface shear stress and it is not a real wind speed (De Visscher, 2013). Shear velocity is defined in terms of the covariance between velocity fluctuations in the horizontal (u'), and vertical (w') directions ($u = \bar{u} + u'$; \bar{u} = mean wind speed):

$$u^* = \sqrt{\overline{w'u'}} \quad (\text{B.1})$$

Equation A.1 indicates that u^* changes with perturbations in the horizontal and vertical wind speed components. It has been shown that u' varies with mean horizontal wind speed (Calif et al., 2008; Stull, 1988; Wyngaard, 2010).

A measure of turbulence in the atmosphere is given by the velocity fluctuation terms (u' and w') (De Visscher, 2013). Turbulent kinetic energy (e) and turbulence intensity (i) are defined as

$$e = \frac{1}{2} (\overline{u'^2} + \overline{v'^2} + \overline{w'^2}) \quad (\text{B.2})$$

$$i = \frac{\frac{1}{3} \sqrt{\overline{u'^2 + v'^2 + w'^2}}}{\bar{u}} \quad (\text{B.3})$$

where u' is horizontal wind speed fluctuation $\left(\frac{m}{s}\right)$, v' the wind speed fluctuation in a direction orthogonal to the direction of u $\left(\frac{m}{s}\right)$, and w' the vertical wind speed fluctuation $\left(\frac{m}{s}\right)$.

The vertical wind profile near the ground is commonly approximated as a logarithmic profile under neutral atmospheric conditions and can be written as

$$u = \frac{u^*}{\hat{k}} \ln\left(\frac{z-d}{z_0}\right) \quad (\text{B.4})$$

where z is the height above the ground (m), z_0 is the surface roughness (m), \hat{k} the von Karman constant (-), and d the displacement height (m). The values of d , z and z_0 are site-specific and indicate that u and u^* are related to each other by a site-specific coefficient. For this landfill, the relationship between u^* and u measured at height 2.25 m is approximately $u^* = 0.1 u$ ($R^2 = 0.52$).

After methane moves through the topsoil and/or vegetation, methane transport in the near-surface boundary layer can be represented by a quasi-laminar boundary layer resistance (r_b) determined empirically as

$$r_b = \frac{5 v^{0.67}}{D_s^{0.67} u^*} \quad (\text{B.5})$$

where r_b ($s m^{-1}$) is the quasi-laminar boundary layer resistance, v is the gas kinematic viscosity $\left(\frac{m^2}{s}\right)$, and D_s the molecular diffusion coefficient $\left(\frac{m^2}{s}\right)$ (Wyngaard, 2010).

This parameter is intended to represent the resistance to methane diffusion from a stagnant air film on the ground surface, whose thickness ranges from a few millimeter

(typical conditions) to several meters (low wind conditions), depending on gas type and shear velocity (u^*) (Pleim and Ran, 2011; Wesley and Hicks, 1977).

Above the quasi-laminar boundary layer, methane encounters resistance in the aerodynamic layer. Resistance here is described by mass transfer from the quasi-laminar boundary layer into the atmosphere immediately above it (De Visscher, 2013). A vertical 1-D advective-diffusive equation describes methane transport through this layer

$$\frac{\partial c}{\partial t} + w \frac{\partial c}{\partial z} - \frac{\partial}{\partial z} \left(K_z \frac{\partial c}{\partial z} \right) = 0 \quad (\text{B.6})$$

where c is methane concentration ($\frac{g}{m^3}$), z the height above the ground (m), and K_z the vertical eddy diffusivity ($\frac{m^2}{s}$) that can be expressed as

$$K_z = \frac{\hat{k} z u^*}{\varphi} \quad (\text{B.7})$$

where \hat{k} is the von Karman constant (–) and φ is a similarity function that depends on atmospheric stability (–) (Seinfeld, 1986). Thus, aerodynamic resistance ($\frac{1}{K_z}$) depends on elevation, shear velocity, and atmospheric stability (eq. B.7) (Seinfeld, 1986). Since vertical wind speed in the aerodynamic resistance layer is typically small relative to turbulent diffusion (Sieigneur, 2019), the expression for steady-state total mass flux of methane through this layer is

$$Q_{CH_4}^{aero} = K_z \frac{\partial c}{\partial z} \quad (\text{B.8})$$

where $Q_{CH_4}^{aero}$ is the vertical methane flux due to turbulence in the aerodynamic resistance layer ($\frac{g}{s.m^2}$).

These resistances - soil resistance, vegetation and topsoil resistance (connected in parallel), quasi-laminar boundary layer resistance, and aerodynamic layer resistance - function in series (Fig. B.1). While the layer with greatest resistance dictates the overall methane flux, the situation is complicated if processes in one layer, for example turbulence in the aerodynamic layer, affect transport in other layers, such as transport through the soil and vegetation/topsoil.

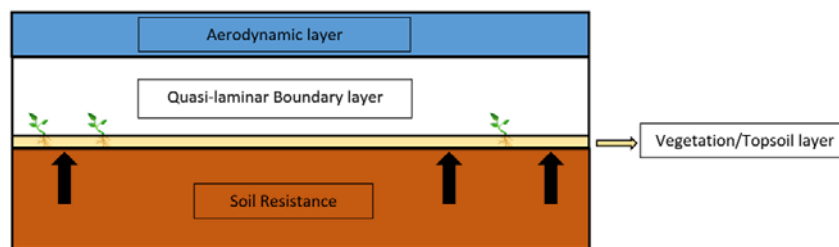


Figure B.1 Schematic of resistance layers that methane passes through from bottom of landfills into the atmosphere. Black arrows indicate methane emissions, which can move directly from topsoils into the atmosphere or go through plants. Scales are not considered in this schematic.

The CALMIM model estimates landfill methane emissions by assuming that resistance in the soil controls and molecular diffusion is the primary transport mechanism (Spokas et al., 2011). The only atmospheric influence on landfill methane emissions considered is temperature, where an increase in temperature increases flux by increasing the molecular diffusion coefficient, but decreases flux for temperatures less than 55°C by enhancing methane oxidation (Spokas and Bogner, 2011). However, several studies have demonstrated the impact of wind speed on methane flux when landfills are covered by daily and/or intermediate covers. Delkash et al. (2016) found that wind speed was positively correlated ($R^2 > 0.5$) with methane fluxes measured by the tracer dispersion method (TDM).

McBain et al. (2005) found an increase in wind speed led to an increase in methane flux measured by the EC method ($R^2 = 0.55$ for wind speed between 3 and 5 m s⁻¹). Pourbakhtiar et al. (2017) showed that even when there is no advective flow of bulk gas in soil, wind speed increases mixing of the soil gas. At the surface, the wind-induced mixing coefficient was as much as ~ 30 times greater than the molecular diffusion coefficient. More recently, Bahlmann et al. (2020) utilized numerical modeling and lab experiments to demonstrate that wind enhances multidimensional gas transport even in low permeability soils, and that this effect is enhanced for low density gases, like methane. They found that wind enhances subsurface gas transport and increases vertical concentration gradients, causing enhanced diffusion in soil.

To investigate wind impacts on mass transfer in the atmosphere near the surface, it is assumed that turbulence flux dominates molecular diffusion flux within the aerodynamic resistance layer of the atmosphere: $Q_{CH_4}^{aero} = cw$.

where w the vertical wind speed ($\frac{m}{s}$).

Averaging after decomposing them into mean and fluctuation terms

$$\overline{Q_{CH_4}^{aero}} = \bar{c} \bar{w} + \overline{c' w'} \quad (B.9)$$

where c' the methane concentration fluctuations ($\frac{g}{m^3}$), and overbars indicate averaging in time.

Assuming that mean vertical wind component near the surface is negligible ($\bar{w} = 0$)

$$\overline{Q_{CH_4}^{aero}} = \overline{c' w'} \quad (B.10)$$

Connection between eq. A.8 and A.10 is discussed in De Visscher (2013). Therefore, average gas flux $\overline{Q_{CH_4}^{aero}}$ depends on turbulence (w') within the aerodynamic resistance layer near the surface ground, where the mean vertical wind component is negligible.

Therefore, wind speed enhances the wind shear velocity near the ground surface that creates turbulence (Wyngaard, 2010), and this turbulence affects transport through soil usually increasing methane emissions from landfills especially with daily or intermediate covers.

Besides wind speed, another source of atmospheric turbulence is buoyancy. For example, solar radiation during daytime increases air temperature (T) near the surface more than at larger distances above the ground, which causes upward air movement by buoyancy (De Visscher, 2013). In this case, buoyancy creates upward w' (turbulence) near the surface that may affect soil gas/atmosphere gas exchange, just like wind-induced turbulence (Bahlmann et al., 2020). This may be the explanation for the positive correlation between short-term (up to one day) soil temperature (caused by air temperature) and landfill gas emissions previously reported (Tecele et al., 2009; McBain et al., 2005). Thus, both near-surface wind speed and upward atmospheric buoyancy due to rising air temperature may cause turbulence that enhances methane flux from landfill cover soils.

When the buoyant force acts upward, air temperature decreases with height above the ground and the atmospheric stability condition is unstable. In this case, upward or positive w' enhances the turbulence created by horizontal wind shear velocity. However, if the air temperature increases with height above the ground, buoyant forces resist upward

movement and the atmospheric stability condition is stable. Under this condition, buoyancy dampens the effects of wind-induced turbulence at the ground surface, decreasing soil gas/atmosphere mass transfer (De Visscher, 2013). If turbulence induced by upward buoyancy is not significant compared to the turbulence induced by wind shear, wind shear primarily affects soil gas/atmosphere mass transfer and the atmospheric stability condition is near neutral.

The Monin-Obukhov length (L) is a parameter commonly used to classify atmospheric stability (Monin and Obukhov, 1954). This length indicates the relative importance of the turbulence produced by shear velocity compared to the turbulence produced by buoyancy, and is defined by

$$L = -\frac{(u^*)^3 \theta_0}{\tilde{\kappa} g Q_0} \quad (\text{B.11})$$

where θ_0 is the mean potential temperature ($^{\circ}\text{K}$), and Q_0 is the surface potential temperature flux ($\frac{^{\circ}\text{K m}}{\text{s}}$). The parameters used to calculate L are determined from EC tower measurements, and discussion of these parameters is found elsewhere (Wyngaard, 2010). A cutoff Monin-Obukhov length (L_C) is needed to categorize the atmospheric stability conditions into unstable, stable, and neutral to investigate correlations between methane flux and meteorological parameters. The L_C depends on surface roughness and measurement height (Łobocki, 2003). For open terrain (e.g., landfills), where the measurement height was 2.25m (EC tower height), unstable and neutral atmospheric conditions have been separated at a height of 10 m (i. e., $-L_C = 10$ m) (Seigneur, 2019; Buske et al., 2012; Cañadillas et al., 2011). Thus, in this study, if $0 < -L < 10$ m, the

atmosphere was classified as unstable, if $|L| > 10$ m the atmosphere was neutral, and if $0 > -L > -10$ m, the atmosphere was classified as stable.

As illustrated in Fig. B.2, we hypothesize that buoyancy plays an important role in near-surface turbulence under unstable atmospheric conditions and therefore that air temperature would correlate with buoyancy; we also hypothesize that wind shear plays an important role in near-surface turbulence under neutral atmospheric conditions. As will be explained later, because the flux measuring instrument does not collect reliable data under stable atmospheric conditions, we do not analyze flux under stable atmospheric conditions. Therefore, the impacts of the atmospheric parameters on emissions will be separately investigated for unstable and neutral atmospheric conditions. Further description about atmospheric conditions and classification is provided in Section 3.3.

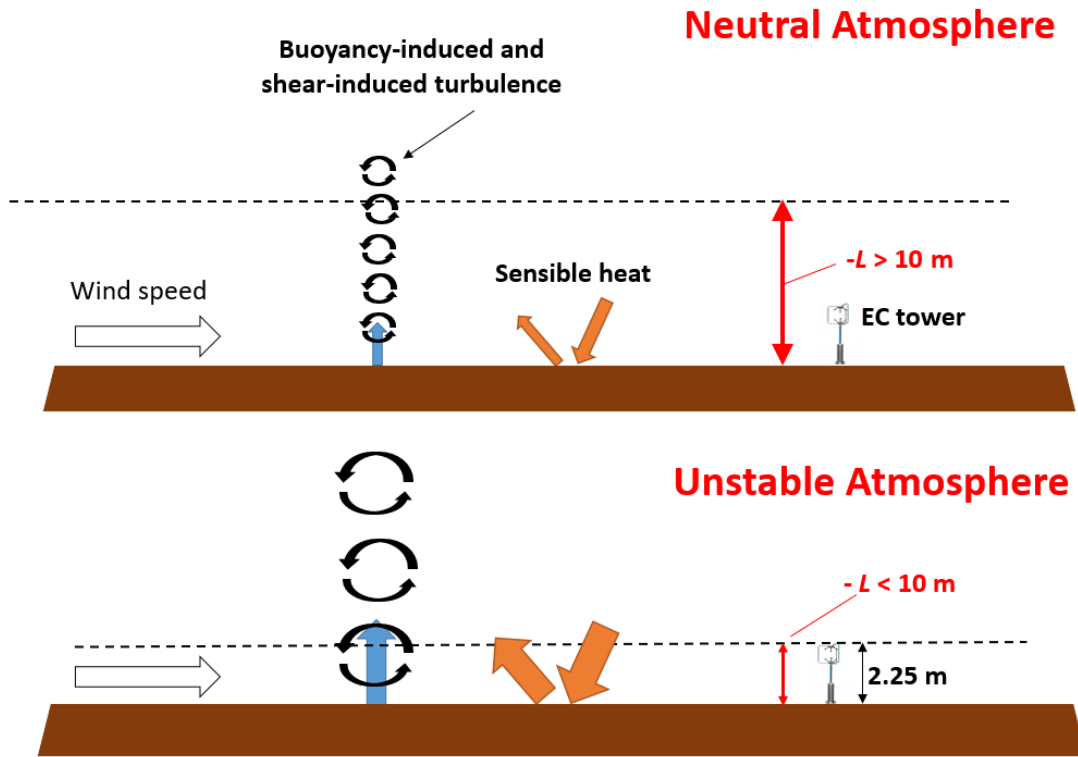


Figure B.2 Impacts of atmospheric stability on near surface gas fluxes. Top - neutral atmosphere, Bottom - unstable atmosphere. The orange arrow indicates sensible heat radiation, white arrow wind speed, blue arrow methane flux from surface, black vortex the turbulence. The dashed line is the Monin-Obukhov length L and the instrument on the right is the EC tower.

In addition to the effects of wind speed and atmospheric buoyancy on turbulence-enhanced methane diffusion through cover soil, gas pressure gradients between the soil and atmosphere are believed to contribute to methane flux through soil (Xu et al., 2014; Czepiel et al., 2003). This fluxes can be described by

$$Q_{CH_4}^P = \frac{k \rho X_{CH_4} \nabla P}{\mu} \quad (\text{B.12})$$

where $Q_{CH_4}^P$ is the pressure-induced vertical advective mass flux of methane $\left(\frac{kg}{s\ m^2}\right)$ through the landfill cover soil (soil resistance), k is the cover soil gas permeability (m^2), ρ is the landfill gas density $\left(\frac{g}{m^3}\right)$, μ is landfill gas dynamic viscosity $\left(\frac{g}{s\ m}\right)$, X_{CH_4} is the methane mole fraction ($-$), and ∇P is gas pressure gradient between the atmosphere and gas at the bottom of the landfill cover soil $\left(\frac{kg}{m\ s^2}\right)$. Equation B.12 indicates that a change in pressure gradient (∇P) changes methane emission. The gas pressure inside the landfill is controlled by gas generation and gas well operations, which are expected to change over time periods greater than one day. The atmospheric pressure, P_{atm} , on the other hand, changes over a period of a day or less.

Two different hypotheses are considered to describe the relationship between P_{atm} and methane flux. In the first, instantaneous P_{atm} is negatively correlated with methane flux (McBain et al., 2005; Czepiel et al., 2003). With this hypothesis, the gas pressure at the bottom of the landfill cover (P_{LC}) is assumed fixed and not affected by instantaneous P_{atm} . Under this hypothesis, short-term changes in the pressure gradient are only caused by changes in P_{atm} . Thus, if P_{atm} is lower at time t_1 and higher at time t_2 , landfill methane emissions are higher at time t_1 , regardless of pressure history.

In the second hypothesis, P_{LC} varies with the rate of change of P_{atm} . Lu (1999) presented an equation describing gas pressure inside a one-dimensional, vertical, unsaturated porous medium

$$\frac{\partial P}{\partial t} = \frac{kP}{\mu\varepsilon} \frac{\partial^2(P^2)}{\partial z^2} \quad (B.13)$$

where ε is the gas-filled porosity (-). According to eq. A.13, the soil gas pressure at any depth (z) depends on temporal atmospheric pressure variations ($\frac{\partial P}{\partial t}$) at the top boundary ($z = 0$) and soil physical properties (k and ε). An abrupt change in P_{atm} causes a lagged change in P_{LC} depending on soil permeability. Therefore, the history of P_{atm} affects present P_{LC} . This hypothesis asserts that the methane flux depends on $\frac{dP_{atm}}{dt}$ instead of instantaneous P_{atm} . Thus, methane fluxes decrease if $\left(\frac{dP_{atm}}{dt} > 0\right)$ and vice versa. Xu et al. (2014) found that methane flux increased 50% from a landfill when pressure gradients changed from positive $\left(\frac{dP_{atm}}{dt} > 0\right)$ to negative $\left(\frac{dP_{atm}}{dt} < 0\right)$.

To understand impacts of the time derivative of air pressure $\frac{dP_{atm}}{dt}$ on methane flux, the gas dispersive flux in the subsurface should be considered. The total dispersive methane flux is equal to the sum of mechanical mixing and molecular diffusion

$$Q_{CH_4}^D = -D_{total} \nabla c \quad (B.14)$$

where $Q_{CH_4}^D$ is the total dispersive methane flux $\left(\frac{kg}{s m^2}\right)$ through the landfill cover soil, D_{total} is summation of molecular diffusion (D_s) and mechanical mixing (D_m) $\left(\frac{m^2}{s}\right)$. The molecular diffusion coefficient in soil is obtained by multiplication of the diffusion coefficient in air (D_a) and tortuosity (Millington and Quirk, 1961). The mechanical mixing coefficient is obtained by multiplication of the dispersivity (α) and Darcy's flux (V) (Sharma and Poulsen, 2010).

$$D_{total} = D_s + D_m \quad (B.15)$$

$$D_s = D_a \tau; \quad \tau = \frac{\theta_a^{3.33}}{\varepsilon^2} \quad (\text{B.16})$$

$$D_m = \alpha V \quad (\text{B.17})$$

where τ is tortuosity (-), θ_a is gas-filled porosity, α is dispersivity (m) and V is the gas vertical velocity ($= \frac{k}{\varepsilon \mu} \frac{dP}{dz}$). Therefore, a change in air pressure would affect dispersive gas flux.

Decreases in atmospheric pressure will create vertical gradients in gas pressure in soil ($\frac{dP}{dz}$) that drive landfill gas upward. If the vertical pressure gradients and gas permeability are large enough, significant advective flux through the landfill cover soil might occur. For neutral stability conditions when the effects of buoyancy are reduced, there are strong negative correlations between $\frac{dP_{atm}}{dt}$ and methane flux in December and February compared to June: average $\left| \frac{95\% \text{ CI}}{\text{slope}} \right|$ for the correlation between $\frac{dP_{atm}}{dt}$ and flux are 0.68 and 0.45 in December and February, respectively, but 1.64 in June. The stronger negative correlation between $\frac{dP_{atm}}{dt}$ and flux in December and February is consistent with the wetter cover soils in these months. As soil moisture increases, the smallest pores fill first because of capillarity. While gas diffusion is a function of the total connected gas-filled pore space, gas advection preferentially occurs in the largest connected soil pores (Bear and Verruijt, 1987), which are the last to fill with water as soils moisten. Thus, as a soil wets the resistance to molecular diffusion will increase more relative to the resistance to gas advection, and the relative importance of gas advection will increase. Models for gas diffusion and advection in soil can be used to assess the resistance to methane

diffusion and landfill gas advection as a function of soil moisture. Although the volumetric water content of the landfill covers soils was only 21% (December) and 16% (February) wetter than in June, applying such models indicate that these moist conditions cause a ~ 50-62% decrease in gas diffusion but only a ~ 21-29% decrease in gas permeability in the winter months (December and February) compared to summer (June).

A second factor affecting the importance of pressure variations is the amplitude of P_{atm} variations during the three measurements periods. The largest peak-to-peak amplitudes of P_{atm} for June 2012, December 2012, and February 2013 periods were 2 kPa, 6 kPa, and 5 kPa, respectively. We associate this finding with the higher temperature difference between the polar and mid-altitude regions (location of this landfill) during winter compared to summer that causes stronger winds and correspondingly more significant P_{atm} variations at this landfill during winter (Hall et al., 2015). Xu et al. (2014) measured methane emissions using EC at a Nebraska US landfill in the second half of 2010 and reported maximum peak-to-peak amplitudes of P_{atm} of 3 kPa in the summer and 5 kPa in the winter. Xu et al. (2014) concluded that methane emissions were larger in winter when $\left| \frac{dP_{atm}}{dt} \right|$ was larger due to greater peak-to-peak amplitudes of P_{atm} . Thus, at the Nebraska US (Xu et al., 2014) and the Southeastern US landfill, the effect of $\frac{dP_{atm}}{dt}$ on methane flux was more significant in the winter than summer.

**C. DEPENDENCY OF THE TRACER DISPERSION METHOD ACCURACY
ON ENVIRONMENTAL PARAMETERS FOR LANDFILL GAS EMISSION
ESTIMATION**

Atmospheric Parameter Definition

Foster-Wittig et al. (2015) defined the ASI in terms of the TI and WDS as following.

According to this classification, the ASI=1 equals to an unstable atmospheric condition and the ASI=7 equals to a stable atmospheric condition.

Table C.1 Definition of ASI

<i>ASI class</i>	<i>TI</i>	<i>WDS</i>
1	> 0.205	> 0.7
2	$0.205 > TI > 0.180$	$0.7 > WDS > 0.6$
3	$0.180 > TI > 0.155$	$0.6 > WDS > 0.5$
4	$0.155 > TI > 0.130$	$0.5 > WDS > 0.4$
5	$0.130 > TI > 0.105$	$0.4 > WDS > 0.3$
6	$0.105 > TI > 0.080$	$0.3 > WDS > 0.2$
7	$0.080 > TI$	$> WDS$

Directional statistics:

$$\text{Assuming: } \overline{\sin X} = \frac{\sum_{i=1}^N \sin X_i}{N} \quad \text{and} \quad \overline{\cos X} = \frac{\sum_{i=1}^N \cos X_i}{N}$$

Where X_i is the measured wind direction and N is the number of data points.

$$\text{Circular wind direction standard deviation} = \sqrt{-2 * \ln(\overline{\sin X^2} + \overline{\cos X^2})}$$

Correlations between meteorological parameters

To study the relationship between the TDM filtering and meteorological parameters, it is important that the meteorological parameters behave independently. The correlations among the four meteorological parameters for the entire dataset (Case study IV) are shown in Table C.2. Since the *ASI* is correlated with wind speed (0.58), *WDS* (-0.39) and *TI* (-0.7), this parameter was removed from the parameter list. Although Table C.2 also indicates that *TI* is weakly correlated with *WDS* ($R = 0.19$), and with wind speed ($R = -0.41$), *TI* was kept in the analysis.

Table C.2 Correlation coefficients between the meteorological parameters.

Meteorological Parameter	Wind Speed	<i>WDS</i>	<i>TI</i>	<i>ASI</i>
Wind Speed	1	-0.11	-0.41	0.58
<i>WDS</i>	-0.11	1	0.19	-0.39
<i>TI</i>	-0.41	0.19	1	-0.7
<i>ASI</i>	0.58	-0.39	-0.7	1

Data Selection

This section presents the logic of data selection at this study. Numbers assigned to each classification can be interpreted as follows. Assume a string of three digits that represent wind speed, and WDS. That is, the first number represents wind speed, the second WDS, and the third TI. As explained in the manuscript, the meteorological parameters are categorized into two groups: above the average, and below the average. For each of the three digits, the number one (1) indicates that data for which the meteorological parameter is below the average of that data set is considered. The number two (2) indicates that data for which the meteorological parameter is above the average is considered. Number zero (0) indicates that there is no categorization for that meteorological parameter and that meteorological parameter is investigated in that correlation analysis.

The number of data points at each classification was determined. Moreover, the number of binned data groups formed in each classification was calculated. It is worthy to reiterate that the range of the groups for wind speeds, WDS, and TI were 0.5 m/s, 0.05, and 0.02, respectively, to create at least four sets of binned data in each plot. The two classifications with the highest number of data points and binned data were selected (classifications 011 and 201).

Table C.3 Results of Pearson correlations of Case I for different meteorological parameter classifications. The description about classification is found above. The selected classifications are highlighted.

Classification	Number of data points	Number of binned data
<u>011</u>	<u>39</u>	<u>7</u>
012	5	3
021	4	3
022	3	3
101	21	2
102	7	3
<u>201</u>	<u>27</u>	<u>7</u>
202	1	1
110	22	3
120	5	2
210	27	2
220	1	1

After selecting the classifications, the pairs of meteorological parameters and TDM filtering criterion that have absolute Pearson correlations greater than 0.3 were selected.

Table C.4 Pearson correlations between filtering parameter and the investigated meteorological parameter for the two selected classifications in Case study I: 011 corresponds to lower wind direction variations and turbulence intensity, and wind speed is the investigated parameter; 201 corresponds to higher wind speeds and lower turbulence intensity, and WDS is the investigated parameter. The selected pairs are highlighted.

Filtering parameter	Classification	
	011 (versus Wind Speed (m/s))	201 (versus WDS)
R^2	0.35	-0.32
σ_M	0.01	0.17
σ_A	-0.27	0.11
SN_M	0.07	-0.22
SN_M	0.40	-0.28
ERD	-0.24	0.28

Other Results of Statistical Analysis

This section presents Pearson correlations (R_1 in the manuscript) between each filtering criterion and each meteorological parameter not shown in the manuscript. The three digits on top of each table represent the meteorological conditions of the data. Description of these digits can be found above.

Case I

012

Filtering criterion	Wind Speed (m/s)
R^2	0.36
σ_M	-0.62
σ_A	-0.43
SN_M	-0.08
SN_A	-0.27
ERD	0.00

021

Filtering criterion	Wind Speed (m/s)
R^2	0.96
σ_M	0.47
σ_A	0.07
SN_M	1.00
SN_A	1.00
ERD	-0.87

022

Filtering criterion	Wind Speed (m/s)
R^2	-0.94
σ_M	-0.20
σ_A	-0.24
SN_M	-0.05
SN_A	0.21
ERD	0.48

101

Filtering criterion	WDS
R^2	-0.08
σ_M	0.22
σ_A	-0.07
SN_M	-0.09
SN_A	0.18
ERD	-0.20

102

Filtering criterion	WDS
R^2	0.63
σ_M	-0.77
σ_A	-0.45
SN_M	0.80
SN_A	-0.02
ERD	-0.50

110

Filtering criterion	Turbulent Intensity
R^2	-0.23
σ_M	0.68
σ_A	0.09
SN_M	-0.10
SN_A	0.57
ERD	-0.26

120

Filtering criterion	Turbulent Intensity
R^2	0.60
σ_M	0.23
σ_A	1.00
SN_M	-0.44
SN_A	-0.53
ERD	-0.95

162

Filtering criterion	Turbulent Intensity
R^2	-0.28
σ_M	0.13
σ_A	0.14
SN_M	-0.45
SN_A	-0.43
ERD	0.23

Case II

012

Filtering criterion	Wind Speed (m/s)
R^2	0.34
σ_M	-0.43
σ_A	-0.61
SN_M	-0.06
SN_A	-0.53
ERD	0.08

021

Filtering criterion	Wind Speed (m/s)
R^2	0.91
σ_M	-0.21
σ_A	-0.10
SN_M	0.87
SN_A	-0.29
ERD	-0.54

022

Filtering criterion	Wind Speed (m/s)
R^2	-0.37
σ_M	0.04
σ_A	-0.43
SN_M	-0.59
SN_A	-0.72
ERD	0.21

101

Filtering criterion	WDS
R^2	-0.30
σ_M	0.50
σ_A	-0.09
SN_M	-0.17
SN_A	0.58
ERD	0.30

102

Filtering criterion	WDS
R^2	0.37
σ_M	0.01
σ_A	0.05
SN_M	0.40
SN_A	0.60
ERD	0.10

110

Filtering criterion	Turbulent Intensity
R^2	-0.43
σ_M	0.24
σ_A	0.34
SN_M	-0.64
SN_A	0.28
ERD	0.44

120

Filtering criterion	Turbulent Intensity
R^2	-0.08
σ_M	0.34
σ_A	0.48
SN_M	-0.33
SN_A	0.47
ERD	0.06

210

Filtering criterion	Turbulent Intensity
R^2	-0.28
σ_M	0.14
σ_A	0.14
SN_M	-0.45
SN_A	-0.43
ERD	0.23

Case III

012

Filtering criterion	Wind Speed (m/s)
R^2	0.35
σ_M	-0.46
σ_A	-0.37
SN_M	0.14
SN_A	0.72
ERD	-0.52

021

Filtering criterion	Wind Speed (m/s)
R^2	0.63
σ_M	-0.17
σ_A	0.54
SN_M	0.42
SN_A	-0.08
ERD	-0.70

022

Filtering criterion	Wind Speed (m/s)
R^2	0.64
σ_M	-0.72
σ_A	-0.18
SN_M	0.26
SN_A	-0.13
ERD	-0.84

101

Filtering criterion	WDS
R^2	-0.10
σ_M	-0.19
σ_A	-0.35
SN_M	-0.30
SN_A	-0.45
ERD	0.55

102

Filtering criterion	WDS
R^2	-0.05
σ_M	-0.24
σ_A	-0.25
SN_M	0.22
SN_A	0.06
ERD	-0.26

110

Filtering criterion	Turbulent Intensity
R^2	-0.18
σ_M	-0.01
σ_A	0.47
SN_M	-0.31
SN_A	-0.76
ERD	0.65

120

Filtering criterion	Turbulent Intensity
R^2	-0.96
σ_M	0.91
σ_A	0.34
SN_M	-0.45
SN_A	0.18
ERD	0.16

210

Filtering criterion	Turbulent Intensity
R^2	0.16
σ_M	-0.69
σ_A	0.00
SN_M	-0.02
SN_A	-0.71
ERD	-0.60

Case IV

012

Filtering criterion	Wind Speed (m/s)
R^2	0.31
σ_M	-0.21
σ_A	-0.27
SN_M	0.26
SN_A	0.41
ERD	-0.16

021

Filtering criterion	Wind Speed (m/s)
R^2	0.15
σ_M	0.13
σ_A	-0.27
SN_M	-0.01
SN_A	-0.32
ERD	0.18

022

Filtering criterion	Wind Speed (m/s)
R^2	0.05
σ_M	-0.25
σ_A	-0.27
SN_M	0.32
SN_A	-0.29
ERD	-0.49

101

Filtering criterion	WDS
R^2	-0.21
σ_M	0.20
σ_A	-0.06
SN_M	-0.17
SN_A	0.36
ERD	-0.12

102

Filtering criterion	WDS
R^2	-0.32
σ_M	-0.22
σ_A	-0.04
SN_M	-0.31
SN_A	-0.14
ERD	-0.28

110

Filtering criterion	Turbulent Intensity
R^2	-0.03
σ_M	0.23
σ_A	0.00
SN_M	-0.16
SN_A	-0.05
ERD	-0.19

120

Filtering criterion	Turbulent Intensity
R^2	-0.17
σ_M	0.07
σ_A	0.18
SN_M	-0.11
SN_A	-0.45
ERD	-0.02

210

Filtering criterion	Turbulent Intensity
R^2	-0.08
σ_M	0.12
σ_A	0.02
SN_M	-0.13
SN_A	-0.06
ERD	-0.15

Required emissions from signal to noise ratio criterion

169

Fredenslund et al. (2019) conducted five controlled-field campaigns to evaluate the accuracy of the TDM. They found that a campaign whose controlled methane release was half of others (5.3 kg/hr compared to 10.9 kg/hr for four campaigns) had up to 18% error and associated this error to low methane emission release (i.e., low signal to noise ratio). Foster-Wittig et al. (2015) recognized a dataset with signal to noise ratio greater than 10 as a reliable dataset. Referring to eq. 4.5, the difference between background methane and tracer concentrations and peak concentrations should be at least 5 times greater than the maximum differences in background concentrations to meet this criterion. Field measurements at this landfill indicate that the h for methane defined in eq. 4.5 is about $(0.015 \pm 0.001SE \text{ ppm})$. For a given downwind road, minimum gas release rate and meteorological conditions should be considered to meet the signal to noise ratio criterion.

The following desktop tasks prior to field measurements are recommended to assure the downwind measurements suffice to have reliable data. Eq. C.1 describes approximate downwind gas concentrations from a fixed emission source and is taken from De Visscher (2013).

$$c = \frac{Q}{2\pi u s_y s_z} \exp\left(-\frac{1}{2} \frac{(y)^2}{s_y^2}\right) \left\{ \exp\left(-\frac{1}{2} \left[\frac{(z-h_s)^2}{s_z^2}\right]\right) + \exp\left(-\frac{1}{2} \left[\frac{(z+h_s)^2}{s_z^2}\right]\right) \right\} \quad (\text{C.1})$$

where Q is the gas release rate $\left(\frac{g}{s}\right)$; S_y and S_z are dispersion parameters in the horizontal and vertical direction, respectively (m); and h_s is the stack height (m). To simplify this equation for application to landfill-emitted gas plumes, we assume that the concentration peak occurs at the center of plume ($y=0$), and that the difference between height of

measurements ($z \sim 2$ m) and stack height ($h_s \sim 20$ m) is negligible compared to S_z for typical wind speeds. Assuming average downwind measurements 2 km from the landfill (Foster-Wittig et al., 2015), the daytime S_y is ~ 300 m and S_z is ~ 250 m when wind speed varies between 2 and 5 m/s (De Visscher, 2013). In this case, eq. 4.7 can be simplified to

$$c = \frac{Q}{2\pi u S_y S_z} \quad (\text{C.2})$$

To satisfy $SN_M > 10$, the field data indicate that at least 0.075 ppm methane should be detected at the downwind. For about 2 km downwind road and wind speed 3 m/s, eq. 4.8 indicates that 72 g/s methane emission is required to satisfy the SN_M criterion. Since most landfills emit methane at rates at least one order of magnitude larger, methane usually does not have a signal to noise ratio problem for 2 km downwind measurements.

However, these field measurements showed that the h for acetylene defined in eq. 4.5 is $(0.00080 \pm 0.0003 \text{ SE ppm})$. For acetylene, at least 5 times greater than the maximum differences in background concentration (0.00080 ppm) means detecting at least 0.0040 ppm acetylene downwind after background subtraction. Therefore, for about 2 km downwind road and wind speed 3 m/s, eq. 4.8 indicates that 6.2 g/s acetylene emission is required.

Impacts of atmospheric stability conditions on TDM data reliability

As the most relevant guideline about importance of meteorological parameters in reliability of TDM datasets, stable atmospheric conditions and high wind speed are

suggested (Foster-Wittig et al., 2015; Scheutz and Kjeldsen, 2019). To discuss these variables, their average wind speed and Monin Obukhov Length (L , an atmospheric stability indicator) for one week between June 19 and June 25, 2012 and one week between February 10 and February 17, 2013, are shown in Fig. C.1 for the Southeastern US landfill in this study. These weeks show different atmospheric and soil moisture conditions and can indicate emissions under different atmospheric and soil conditions. The definition of L is discussed in Chapter 3. Wind speed and L were estimated for each 30 minutes using data from an eddy covariance tower located on top of the landfill. Further explanation about this tower can be found in Chapter 3. These high frequency, 30-minute average data in Fig. C.1 indicate variations of wind speed and L during these weeks. According to surface roughness of the landfill and height of the measurements (2.25 m), if $0 < -L < 10m$ the atmosphere is unstable, if $0 < L < 10m$ the atmosphere is stable, and if $|L| > 10m$ the atmosphere is neutral (Łobocki, 2003; Seigneur, 2019). Figure C.1 indicates that wind speeds are higher in the daytime for this inland landfill. As mentioned earlier, wind speeds are higher in colder seasons because of the higher temperature difference between the polar and mid-altitude regions during winter. In addition, the atmosphere experiences more unstable conditions in the summer compared to winter. Therefore, higher wind speeds and less unstable atmospheric conditions make daytime measurements in winter the most favorable measurement period at this landfill for collecting accurate TDM data.

In summer, wind speeds are usually low and unstable atmospheric conditions occur more frequently. As discussed by Foster-Wittig et al. (2015), unstable atmospheric conditions have two important features significantly affecting the reliability of TDM data:

significant vertical air parcel transport and high wind direction variations. Vertical air transport causes lower methane and tracer gas concentrations at the ground that might negatively affect data reliability. Delkash et al. (2016) conducted field measurements at two heights 2.5 m and 85 m above the ground and found more reliable data at the higher elevation. Nevertheless, conducting stationary measurements is prone to error under unstable atmospheric conditions because of higher wind direction variations. As another practical solution, a closer downwind road to the landfill can improve data reliability, because a closer road gives less time for vertical plume movement. In general, Fig. C.1 shows that higher wind speeds coincide with more unstable atmosphere in summer at this Southeastern US landfill.

In conclusion, a site-specific consideration is required to have optimum number of reliable data that represents diurnal-average emissions. These site-specific considerations depends upon range of local wind speeds and atmospheric stability conditions throughout a typical day.

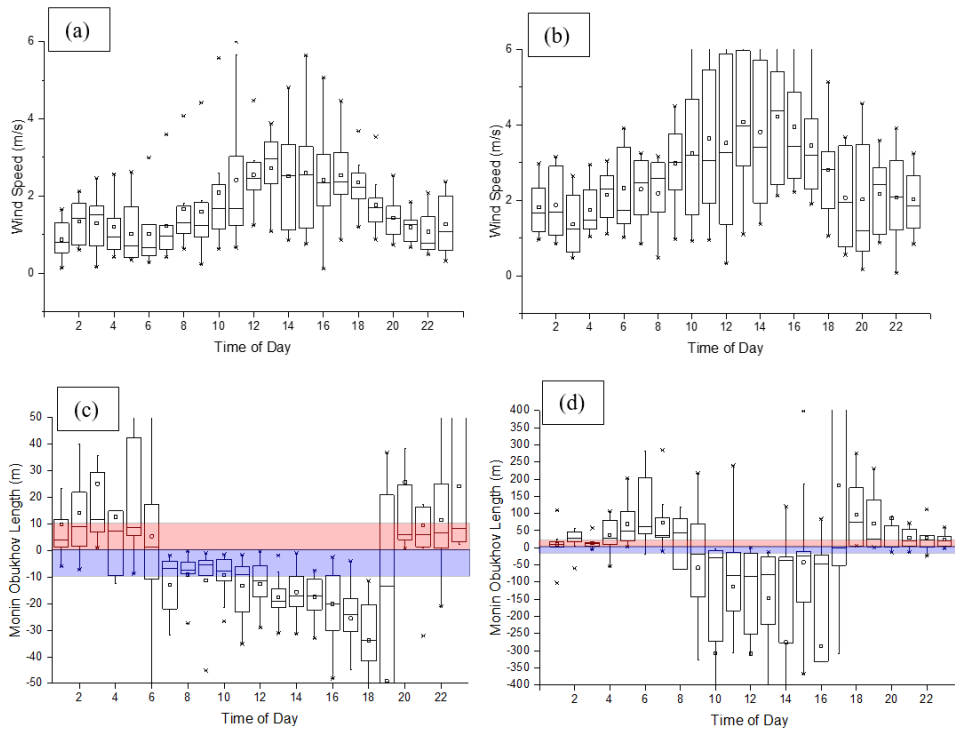


Figure C.1 Weekly averaged wind speeds a) the week in June 2012, and b) the week in February 2013. Weekly averaged Monin Obukhov Length, L for c) the week in June 2012, and d) the week in February 2013. The blue and red areas indicate unstable and stable atmospheric conditions, respectively. Other areas represent neutral atmospheric conditions.

D. PUBLICATION LIST

Chapter 2. Delkash, M., Zhou, B., Han, B., Chow, F.K., Rella, C.W., Imhoff, P.T., 2016. Short-term landfill methane emissions dependency on wind. *Waste Manage.* 55, 288-298.

Chapter 3. Delkash, M., Chow, F.K., Imhoff, P.T., (submission planned). Diurnal landfill methane flux patterns across different seasons at a landfill in Southeastern US. *Waste Manage.*

Chapter 4. Delkash, M., Legates D., Imhoff, P.T., (to be submitted). Dependency of the tracer dispersion method accuracy on environmental parameters. *Atmos. Environ.*

E. PRESENTATION LIST

1. P. T. Imhoff, M. Delkash, D. Taylor, F. K. Chow. Assessing the Impact of Atmospheric Conditions on Diurnal Methane Emission from Landfills. *9th ICLRS*, Japan, June 2016.

2. D. Taylor M. Delkash, F. K. Chow, P. T. Imhoff. Assessing the Accuracy of the Tracer Dilution Method with Atmospheric Dispersion Modeling. *9th ICLRS*, Japan, June 2016.

3. M. Delkash, D. M. Taylor, P. T. Imhoff, F. K. Chow. Addressing Some Practical Points in Employing the Tracer Dilution Method to Measure Methane Emissions from Landfills. *8th ICLRS*, Florida, October 2014.

4. D. M. Taylor, M. Delkash, F. K. Chow, P. T. Imhoff. Coupled land-atmosphere modeling of methane emissions with WRF. *8th ICLRS*, Florida, October 2014.

F. PERMISSION FROM PUBLISHERS

Chapter 2 is a version of the paper published in *Waste Management* by Elsevier. According to the Elsevier copyright policies, the authors can use their articles, in full or in part, for inclusion in a thesis or dissertation (provided that this is not to be published commercially). Please see the link below:

<https://www.elsevier.com/about/policies/copyright>

Chapter 3 is a version of the paper that will be submitted to *Waste Management* by Elsevier. According to the Elsevier copyright policies, the authors can use their articles, in full or in part, for inclusion in a thesis or dissertation (provided that this is not to be published commercially). Please see the link below:

<https://www.elsevier.com/about/policies/copyright>

Chapter 4 is a version of the paper that will be submitted to the *Atmospheric Environment* by Elsevier. According to the Elsevier copyright policies, the authors can use their articles, in full or in part, for inclusion in a thesis or dissertation (provided that this is not to be published commercially). Please see the link below:

<https://www.elsevier.com/about/policies/copyright>